UNIVERSITÀ
DEGLI STUDI
DI PADOVA

Sede Amministrativa: Università degli Studi di Padova
Dipartimento di Biologia

SCUOLA DI DOTTORATO DI RICERCA IN BIOSCIENZE E BIOTECNOLOGIE

INDIRIZZO BIOLOGIA CELLULARE

CICLO XXVIII

New insights into *S. cerevisiae* F-ATP synthase and its role in the mitochondrial permeability transition

Direttore della Scuola: Ch.mo Prof. Paolo Bernardi

Coordinatore dell'indirizzo: Ch.mo Prof. Paolo Bernardi

Supervisore: Ch.mo Prof. Paolo Bernardi

Dottorando: Michela Carraro

31 Dicembre 2015

“The important thing is to not stop questioning. Curiosity has its own reason for existence. One cannot help but be in awe when he contemplates the mysteries of eternity, of life, of the marvelous structure of reality. It is enough if one tries merely to comprehend a little of this mystery each day”

-Albert Einstein-

Table of contents

Summary/Sommario

Summary

The mitochondrial Permeability Transition Pore (PTP) has been characterized in mammals as a Ca^{2+}-activated channel whose opening allows solutes of molecular mass ≤ 1.5 kDa to equilibrate across the inner membrane, potentially causing matrix swelling, rupture of the outer membrane and release of pro-apoptotic factors. Together with Ca^{2+}, the onset of PTP opening is favored by oxidative stress, membrane depolarization and Pi; conversely, acidic pH, adenine nucleotides and Mg^{2+} are the major physiological desensitizers. So far, cyclosporin A and derived compounds that prevent the binding of the positive effector cyclophilin D, as well as new compounds identified by our laboratory, have been discovered to be potent antagonists of the channel. Whether or not the PTP is a conserved feature in yeast has long been debated. Several studies suggested that yeast mitochondria might present different independent permeability pathways with peculiar features and modulations, including an ATP-activated pathway that might play a role as an energy-dissipating mechanism. A high-conductance channel considered to be the yeast equivalent of the PTP (yPTP) is inhibited rather than activated by Pi and is insensitive to CsA, and due to the lack of a mitochondrial Ca^{2+} uniporter in yeast, its Ca^{2+} dependence has been difficult to assess. In our recent paper (see **Publication 1**), we confirmed the existence of Ca^{2+}-activated PTP in *S. cerevisiae*, as previously suggested by Shinohara and Coworkers, taking advantage of the Ca^{2+} ionophore ETH129, which allows the electrophoretic accumulation of added Ca^{2+}. We found that yPTP opening is strongly sensitized by the thiol reagents phenylarsine oxide, copper-*o*-phenantroline and diamide, which are effective PTP inducers in mammals, and that this effect could be reverted by reducing reagents. Our laboratory recently proposed that F-ATP synthase dimers are the crucial component of mammalian PTP (mPTP). We carried out a Blue-Native PAGE separation of yeast mitochondrial proteins with digitonin, identified F-ATP synthase dimers through an in-gel activity assay for ATP hydrolysis, and reconstituted them in planar lipid bilayer for electrophysiology experiments. Our data show that dimers of yeast F-ATP synthase form a Ca^{2+}- and oxidant-activated channel with "flickering" features resembling those of the mammalian PTP, although with a lower conductance of about 250-300 -pS. Like in mammals, activity of the channel was inhibited by ADP and Mg^{2+}. These findings provide evidence that the PTP-forming properties of F-ATP synthase have been conserved in evolution. To verify the role of F-ATP synthase dimer in yPTP formation, we analyzed knock-out mutants for subunits reported to be involved in dimerization of the enzyme. These subunits, localized in the lateral stalk, are subunit e (*TIM11*) and- subunit g (*ATP20*). *ΔTIM11, ΔATP20*, as well as double null mutants, did not display the presence of dimers when analyzed with a BN-PAGE. Furthermore, the Ca^{2+} retention capacity (CRC, a measure of the propensity to pore opening) of mitochondria devoid of subunits e and/or g displayed

an increased resistance to yPTP opening. BN-PAGE analysis after treatment with $CuCl_2$, which promotes the formation of disulfide bridges between adjacent Cys residues, demonstrated that some dimers formed upon thiol oxidation even in absence of "dimerization" subunits, which may explain why the yPTP could open at high Ca^{2+} concentration even in their absence. Very interestingly, these dimers show a channel conductance of about 30 -pS, which is remarkably decreased compared to that measured in wild-type strain. Further analysis in single KO mutant for e- and g subunits is under way in order to define the contribution of single subunits to channel conductance.

To identify the Cys residues affected by $CuCl_2$ treatment (which should be involved in dimer formation following oxidation), we carried out site-directed mutagenesis of each of the Cys residues of F-ATP synthase in the e- and g- null genetic background. There are eight Cys residues in the yeast enzyme (six in subunits encoded by nuclear DNA and two in subunits encoded by mitochondrial DNA). We found that Cys23 of subunit a (*ATP6*) is the target of oxidation, and mediates formation of a disulfide bridge between the two monomers thereby stabilizing the dimeric form. Another important finding was that the unique Cys of OSCP, the subunit located on top of the lateral stalk of F-ATP synthase, appears to mediate the effect of diamide on PTP activity, at least at low concentrations. Indeed, CRC analysis revealed that OSCP C100S mutant are less sensitive specifically to diamide, whereas the sensitivity to other oxidants is unaffected.

My results provide the first demonstration that yeast F-ATP synthase dimers form high conductance channels analogous to those formed by the mPTP and thus that channel formation is an evolutionarily conserved feature of F-ATP synthases. It is now possible to unravel the many open questions about structure and regulation of the PTP with the powerful methods of yeast genetics.

Sommario

Il poro di transizione della permeabilità (PTP) è stato caratterizzato nei mammiferi come un canale mitocondriale attivato dal Ca^{2+} la cui apertura permette ai soluti con un peso molecolare inferiore a 1.5 kDa di equilibrarsi attraverso la membrana, causando eventualmente il rigonfiamento della matrice, la rottura della membrana esterna e il rilascio di fattori pro-apoptotici. Oltre al Ca^{2+}, l'apertura del PTP è favorita, soprattutto, dallo stress ossidativo, dalla depolarizzazione della membrana interna e dal Pi; al contario, tra i principali "desensitizzatori" fisiologici troviamo i nucleotidi adeninici, il Mg^{2+} e un pH acido di matrice. Finora sono stati scoperti alcuni composti con un effetto antagonista al canale, come, per esempio, la ciclosporina A (CsA) e alcuni derivati, scoperti nel nostro laboratorio, che prevengono il legame della ciclofilina D, un potente induttore del poro. Se il PTP sia o meno una caratteristica mitocondriale conservata nel lievito è stato un quesito lungamente dibattuto. Diversi studi suggeriscono che i mitocondri di lievito presentano vari pathways indipendenti di permeabilità con caratteristiche e modulazione peculiari, includendo un pathway attivato dall'ATP, probabilmente atto a dissipare l'eccesso di energia. Inoltre, il PTP di lievito risulta essere inibito piuttosto che attivato dal Pi, insensibile alla CsA, mentre la dipendenza dal Ca^{2+} è stata difficile da verificare, data l'assenza di un uniporto mitocondriale del Ca^{2+}. Nell'articolo pubblicato recentemente (vedi **Pubblicazione 1**), abbiamo confermato l'esistenza di un PTP attivato da Ca^{2+} in *S.cerevisiae*, com'era stato suggerito in precedenza da Shinohara e collaboratori, utilizzando lo ionoforo del Ca^{2+}, ETH129, che permette l'accumulo elettroforetico del Ca^{2+} esogeno aggiunto durante esperimenti di capacità di retenzione del Ca^{2+} (CRC). I nostri dati mostrano che il PTP di lievito è fortemente sensibile a composti che agiscono sui tioli liberi come la phenylarsine oxide, copper-*o*-phenantroline e la diamide, riconosciuti attivatori del PTP mammifero, e che questo effetto può essere contrastato e ripristinato da agenti riducenti. Inoltre, abbiamo geneticamente dimostrato che *CPR3,* l'omologo di lievito della ciclofilina D di mammifero, non esercita alcun ruolo nella regolazione del PTP, spiegando quindi la mancata sensibilità del poro alla CsA. Nel 2013, il nostro laboratorio ha proposto un nuovo modello per il PTP di mammifero, attribuendo all'enzima F-ATP sintasi, nello specifico alla struttura dimerica, un ruolo chiave. Per verificare che questa caratteristica sia conservata anche nel lievito, abbiamo isolato dimeri attivi di F-ATP sintasi attraverso una Blue-Native PAGE e li abbiamo utlizzati in esperimenti di elettrofisiologia (planar lipid bilayer). I nostri dati dimostrano che i dimeri di F-ATP sintasi di lievito formano un canale attivato dal Ca^{2+} e da ossidanti, con un tipico comportamento di "flickering", molto simile a quello osservato nel poro di mammifero, anche se con un valore di conduttanza minore, di circa 250-300 -pS. Inoltre, l'attività del canale è inibita da ADP e Mg^{2+}, come riscontrato anche nel mammifero. Questi dati evidenziano che le

proprietà di formazione del PTP si sono conservate durante l'evoluzione. Per confermare ulteriormente questo ruolo dei dimeri, abbiamo analizzato mutanti deleti per due piccole subunità accessorie (e o *TIM11*, g o *ATP20*) coinvolte della dimerizzazione dell'enzima. I singoli mutanti come anche il doppio deleto, mostrano chiari difetti nella formazione di dimeri nella BN-PAGE e un incremento sensibile della CRC rispetto al controllo. Comunque, dopo trattamento con $CuCl_2$, che produce ponti disolfuro tra tioli vicini, è possibile rintracciare, nei mutanti, la formazione di dimeri, motivo per cui l'apertura del PTP non è completamente prevenuta. Da esperimenti preliminari di elettrofisiologia condotti con questi dimeri cross-linkati, appare evidente che la conduttanza del canale diminuisce drasticamente (circa 30 -pS) rispetto a quella misurata nel wild-type, supportando l'ipotesi che le subunità e, g possano essere proteine chiave nella formazione del PTP. Per identificare il residuo target del $CuCl_2$, che potrebbe avere un ruolo rilevante nella stabilizzazione del dimero nonché del canale, abbiamo condotto degli esperimenti di mutagenesi delle cisteine presenti nelle subunità dell'enzima in un background genetico di doppia delezione per e,g. Dall'analisi in gel nativo, abbiamo scoperto che il mutante per la cisteina 23 della subunità a (*ATP6*) non forma dimeri dopo trattamento con $CuCl_2$, indicando che il residuo in questione è effettivamente il target di questa ossidazione e che probabilmente media ponti disolfuro tra monomeri adiacenti, stabilizzando l'enzima. Un'altro importante risultato ottenuto dallo screening riguarda la cisteina di OSCP, una subunità del gambo laterale dell'F-ATP sintasi, che appare mediare l'effetto inducente della diamide sul poro. Infatti, i mutanti mancanti la cisteina 23 sono meno sensibili alla diamide, almeno a basse concentrazioni.

In conclusione, questi risultati rappresentano la prima dimostrazione che i dimeri di F-ATP sintasi di lievito formano un canale ad alta conduttanza analogo al PTP di mammifero e che quindi la formazione del canale è una proprietà conservata delle F-ATP sintasi. Cercheremo quindi di sbrogliare i tanti punti oscuri riguardo la struttura a la regolazione del PTP, sfruttando i potenti metodi di genetica disponibili nel lievito.

List of Publications

- **Michela Carraro, Valentina Giorgio, Justina Šileikytė, Geppo Sartori, Giovanna Lippe, Mario Zoratti, Ildiko Szabò and Paolo Bernardi.** Channel formation by yeast F-ATP synthase and the role of dimerization in the mitochondrial permeability transition. The Journal of Biological Chemistry (2014), vol. 289; p. 15980-15985.

- **Michela Carraro and Paolo Bernardi.** Calcium and reactive oxygen species in regulation of the mitochondrial permeability transition and of programmed cell death in yeast. Cell Calcium (2016), *in press*.

List of Figures

List of Abbreviations

ADP: adenosine diphosphate

ATP: adenosine triphosphate

ANT: adenine nucleotide transporter

Apaf-1: apoptotic protease activating factor-1

ATP: adenosine triphosphate

BH: Bcl-s homology

CsA: cyclosporin A

$Cu(OP)_2$: copper-*o*-phenanthroline

CyP D: cyclophilin D

Cyt *c*: cytochrome *c*

DIA: diamide

DISC: death-inducing signaling complex

ER: endoplasmic reticulum

ETC: electron transfer chain

FAD: flavin adenine dinucleotide

FADD: Fas-associated death domain

$FADH_2$: flavin adenine dinucleotide (reduced form)

FFA: free fatty acid

FMN: flavin mononucleotide

HCX: H^+/Ca^{2+} exchanger

HKII: hexokinase II

IAP: inhibitor of apoptosis protein

IMM: inner mitochondrial membrane

IMS: Intermembrane Space

LOHN: Leber hereditary optic neuropathy

LS: Leigh syndrome

LPS: lipopolysaccharide

MCU: mitochondrial Ca^{2+} uniporter

MELAS: mitochondrial encephalomyopathy, lactic acidosis and stroke-like episodes

MILS: maternally inherited Leigh syndrome

MLKL: mixed lineage kinase-domain like

mPTP: mammalian PTP

NAD: nicotinamide adenine dinucleotide

NADH: nicotinamide adenine dinucleotide (reduced form)

NARP: neuropathy, ataxia and retinitis pigmentosa

NCLX: Na^{+}/Ca^{2+} exchangers

NEM: N-ethylmaleimide

OMM: outer mitochondrial membrane

OXPHOS: oxidative phosphorylation

PBR: peripheral benzodiazepine receptor

PCD: programmed cell death

PDC: pyruvate dehydrogenase complex

PhAsO: phenylarsine oxide

Pi: inorganic phosphate

PiC: phosphate carrier

PMCA: plasma membrane Ca^{2+} -ATPase

PTP: Permeability Transition Pore

Q: ubiquinone

RC: respiratory chain

RIPK: receptor-interacting protein kinase 1

ROS: reactive oxygen species

RR: Ruthenium Red

SDH: succinate dehydrogenase

SERCA: sarco/endoplasmic reticulum Ca^{2+} -ATPase

TBH: t-butylhydroperoxide

TNF: tumor necrosis factor

TSPO: translocator protein

VDAC: voltage-dependent anion channel

yPTP: yeast PTP

1. Introduction

1.1 Mitochondria

Mitochondria are organelles found in the cytoplasm of almost every eukaryote. They derive from the endosymbiosis of ancestral proteobacteria into host cells that occurred more than 1.5 billion years ago[1]. Over time, they evolved strategies to adapt in the new context as well as to optimize the physiology of the hosts. The most prominent roles are the supply of energy in form of the high-energy molecule ATP through oxidative phosphorylation, the process that couples respiration to ATP synthesis; the control of cellular metabolism and redox-state, and the regulation of apoptosis and other forms of cell death[2]. Mitochondria are highly dynamics cellular components, constantly changing their shape in response to various external stimuli as well as to physiological processes[3,4].

1.1.1 Mitochondrial structure and dynamics

Mitochondria are 0.5-5 µm diameter organelles with a peculiar structure **(Figure 1)**. They are surrounded by two membranes that differ for protein and lipid composition as well as for functional roles: the outer membrane (OMM) and the inner membrane (IMM). These two lipid bilayers, in turn, define two different compartments: the matrix, containing essential enzymes (e.g. Krebs cycle and β-oxidation enzymes) and mitochondrial DNA, and the intermembrane space (IMS).

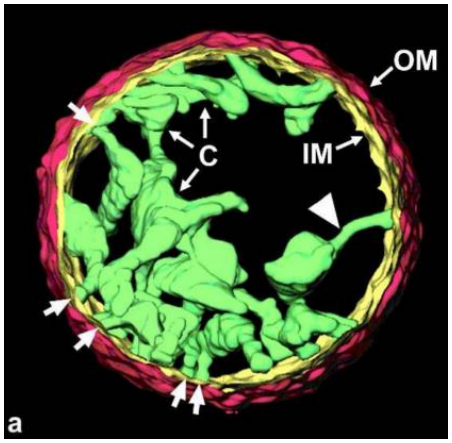

Figure 1. Electron tomography of mammalian mitochondria.
Morphology of an isolated rat liver mitochondrion. The outer membrane (OM), peripheral inner membrane (IM), and selected cristae (C) have been marked in red, yellow and green, respectively. Unlabeled arrows point connections between tubular cristae (C) and the IM. The diameter of the mitochondrion measured at the outer membrane is 1.5 µm; from[5].

Mitochondria possess their own genome with translation and assembly machineries, required for the correct production and folding of mitochondrial proteins. The genome (called mtDNA), which has

been fully sequenced in the early 1980s[6], is a 16.5 kb circular molecule, composed of two chains, the light and the heavy chains. Furthermore, it does not contain any introns and it appears not to be arranged within histonic complexes. mtDNA does not encode for the totality of mitochondrial components that, instead, is mainly transcribed from genomic DNA and then targeted toward this organelle through complex import systems. Among the products of mtDNA transcription, ribosomal and transport RNAs have been found as well as components of the oxidative phosphorylation system (discussed in the next chapter) such as subunits of the respiratory chain complexes and of the F-ATP synthase (subunit a and A6L)[7].

The OMM has the dual function of barrier, protecting mitochondria from external dangerous factors[8] and of exchange platform[9]. Indeed, due to its lipid composition and to the presence of a large aqueous channel (discussed later in the text), cations and small metabolites (up to 5 kDa) can diffuse between cytosol and the IMS. The OMM represents also the site of interaction with other cellular components such as the endoplasmic reticulum, ribosomes, nucleus and cytoskeleton filaments.

The IMM, in part composed of cardiopilin, is impermeable to ions and to most hydrophilic molecules, which are transported by a number of different transporters, exchangers and channels that reside in this bilayer. From electron microscopy images, it emerged that the structure of the IMM shows a tight organization into three main zones: the inner boundary membranes, the cristae junction and the cristae[10]. The first refers to contact sites between the two membrane layers (IMM and OMM) that contain specific enzymes and are involved in mitochondrial protein import as well as in lipid transfer[11]. Cristae are deep invaginations of the membrane toward the matrix space that can show different morphologies, e.g. tubular or balloon-shaped, and increase remarkably the overall surface of the IMM[12]. Depending on environmental cues, cristae can undergo an extensive structural remodeling, accompanied by changes in the overall abundance and tightening[13]. At the cristae bases, specific proteins arrange in the formation of junction structures, narrow openings that create sub-compartments in the IMS. The junction sites are thought to prevent free diffusion of cristae contents in the IMS as well as to control metabolite and protein transport[14].

The mitochondrial network reflects and responds to the energetic and metabolic demand of a cell. Two main mechanisms have evolved to allow quick cellular adaptation: mitochondrial fusion and fission[3]. As suggested by the name, fusion is the process by which mitochondria fuse creating a single functional organelle. This might be a crucial mechanism allowing maintenance of a healthy, homogeneous mitochondrial population, because—among other things—it permits mitochondrial content mixture, enabling protein complementation, mtDNA repair and distribution of metabolites and excess of superoxide species[15]. As a first step, fusion requires the cytoskeleton-dependent convergence of two mitochondria that, once close enough, start interacting via the dynamin-related

GTPase OMM proteins Mitofusin1 and -2. The formation of homo- or hetero-complexes favors the fusion of the two OMM that is followed by that of the IMM through the action of the OPA1 protein[16]. On the other hand, the fission process leads to formation of two or more daughter mitochondria from the division of one organelle[17]. The main effector is the cytosolic dynamin-related protein 1 that organizes into superstructures at the fission sites and initiates the fission process through its GTPase activity.

The IMM, hosting the complexes of the respiratory chain (RC) and the F-ATP synthase, is the site in which oxidative phosphorylation occurs. The IMM is a very good insulator, able to maintain a H^+ electrochemical gradient (ΔμH) of about 220 mV, generated by proton pumping driven by the RC. The gradient is composed of the membrane potential difference (ΔΨ) and the proton concentration difference (ΔpH) and provides the driving force (also called proton-motive force) for the synthesis of ATP and for ion and metabolite transport.

1.1.2 Mitochondrial oxidative phosphorylation and energy conservation

As already mentioned, mitochondria are the site where energy conservation and ATP production take place. The molecules fueling this process come from the stepwise oxidation of different carbon sources absorbed during food uptake, i.e. monosaccharides like glucose and free fatty acids (FFA) **(Figure 2)**. Glucose is partially oxidized in the cytosol by enzymes of glycolysis that yield two molecules of pyruvate, ATP and NADH. Then pyruvate completes its oxidation inside the matrix, where it is metabolized to Acetyl-CoA and finally converted to carbon dioxide by enzymes of the Krebs cycle. As resulting products, glucose oxidation generates ATP, the reduced electron carriers NADH and $FADH_2$ and CO_2 as waste. FFAs are, instead, metabolized by a stepwise process called β-oxidation occurring inside the matrix, whose products sustain the Krebs cycle and generate reduced electron carriers. The electron carrier molecules obtained following all these processes are then used as electron sources for the complexes of the mitochondrial RC[18].

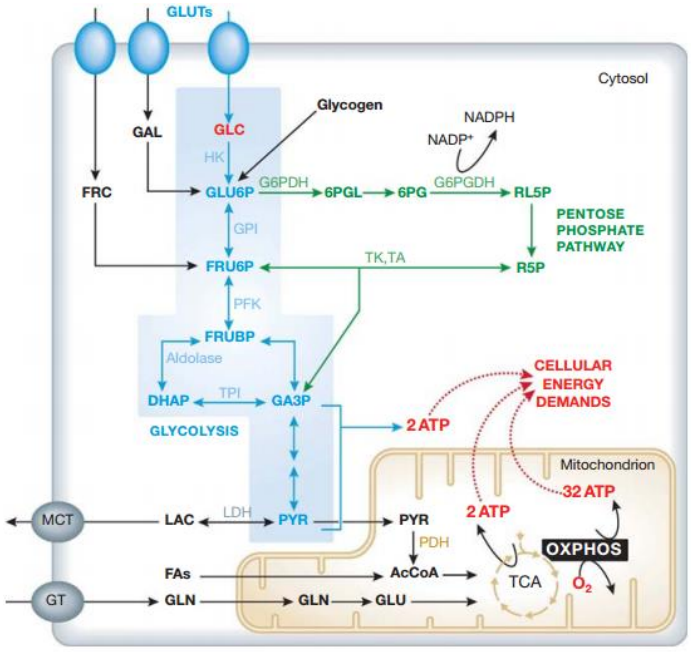

Figure 2. Pathways for cellular energy conservation.
Glucose is metabolized via glycolysis , with production of pyruvate, ATP and NADH. Pyruvate is then transported inside the mitochondrial matrix where it is converted to Acetyl-CoA, a primary substrate of the Krebs cycle. The Krebs cycle in turn generates reduced equivalents, substrates of the oxidative phosphorylation (OXPHOS) system that produces more than 30 ATP molecules per cycle via a specialized enzyme complex, the F-ATP synthase. Glycolysis also generates metabolites for the pentose phosphate pathway. Fatty acids are transported inside mitochondria, where they get stepwise oxidized, generating products sustaining Krebs cycle and therefore RC complexes; from [18].

The main function of the mitochondrial RC (also called electron transfer chain, ETC) is the translocation of electrons through its protein components from a donor (NADH and $FADH_2$) to an acceptor (oxygen) that is reduced to water, in a process matched by proton pumping across the IMM toward the IMS **(Figure 3)**. As discussed more in detail in the following paragraphs, significant differences exist between the ETC of mammals and that of the majority of yeast strains, including *S. cerevisiae*. In mammals, electron transfer occurs following two major pathways: the first starts from NADH as electron donor through the rotenone-sensitive NADH dehydrogenase or complex I, a redox-driven H^+ pump; the second starts from $FADH_2$, obtained upon oxidation of succinate. In yeast, NADH is oxidized by rotenone-insensitive NADH dehydrogenases that do not pump protons, while coupled electron transfer starts from $FADH_2$-coupled succinate oxidation[19].

As proposed by Peter Mitchell with the chemiosmotic theory[20], proton pumping leads to the formation of a large proton electrochemical gradient that drives the production of ATP, the primary source of energy in cells. This coupling process between oxidation of reduced equivalents and production of ATP is also referred to as oxidative phosphorylation (OXPHOS). The OXPHOS system consists of IMM-embedded complexes and two mobile electron carriers. Complexes I-IV contain

redox centers responsible for electrons transfer and are connected by two mobile redox-active molecule, ubiquinone and cytochrome *c* (cyt *c*), whereas complex V (or F-ATP synthase) is the enzyme responsible for ATP production.

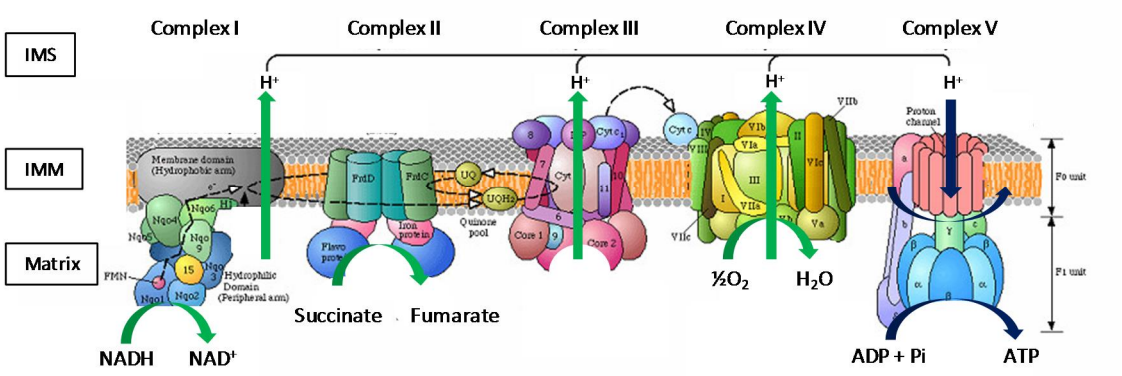

Figure 3. Schematic representation of the mammalian OXPHOS system composed of complex I-IV and the F-ATP synthase (complex V). Reactions through RC complexes that transfer electrons from reduced cofactors (NADH or $FADH_2$) to oxygen, finally yielding water, are marked with green curved arrows. Electron transfer is coupled with H^+ pumping from matrix to the IMS at the level of complex I-III and IV (marked with green straight arrows), generating an electrochemical gradient ($\Delta\mu H$) across the IMM. As a last step, protons reenter the matrix via the rotor domain of complex V (F-ATP synthase) (dark blue straight arrow), leading to its rotation (dark blue curved arrow) and thus driving the catalytic domain to synthesize ATP starting from ADP and Pi (bottom dark blue curved arrow); modified from [21].

1.1.2.1 Mammalian complex I

The first complex (**NADH-ubiquinone oxidoreductase**) is the largest of the RC, responsible for the oxidation of NADH to NAD^+ [22]. It functions by coupling the passage of two electrons from NADH to ubiquinone to the translocation of four protons across the membrane, contributing to the proton-motive force. Complex I is an L-shaped assembly formed by the hydrophilic (peripheral) arm, containing all the redox centers performing electron transfer, and the hydrophobic arm, embedded in the IMM, containing the proton-translocation machinery. The whole complex comprises more than 40 subunits and 14 evolutionary conserved redox components: flavin mononucleotide (FMN), eight iron-sulfur clusters and at least two bound ubiquinone species. How electron flux is connected with proton pumping is still a matter of debate, although it has been supposed to be associated with a long-range conformational change. Complex I can be pharmacologically inhibited by rotenone, a plant-derived compound able to inhibit the electron transfer between iron-sulfur centers and ubiquinone, leading to the production of reactive oxygen species (ROS). Indeed, complex I is one of the major contributors to the generation of ROS in mitochondria, especially superoxide anions, derived from a premature electron leakage to oxygen. Mutations in genes encoding for complex I

subunits, altering the normal activity, have been found in patients affected by several pathologies, e.g. Leigh syndrome, an early-onset, fatal neurodegenerative disorder and LOHN syndrome[23].

1.1.2.2 Yeast complex I

Yeast mitochondria lack an energy-conserving complex I, and instead contain three rotenone-insensitive NADH dehydrogenases distributed on both the external (Nde1 and Nde2) and the internal (Ndi1) surface of the IMM[24] **(Figure 4)**. These enzymes catalyze electron transfer from NADH to ubiquinone via FAD, the sole prostethic group, without proton translocation across the IMM[25], thereby not participating in the energy-conservation process. In particular, Nde1-2 are exposed to the the IMS side and oxidize cytosolic NADH, whereas Ndi1 is exposed to the matrix and oxidizes NADH generated by the Krebs cycle. Compared to mammalian complex I, NADH dehydrogenases are proteins of low molecular weight (up to 50 kDa), possessing a much simpler structure. From 3D studies, it emerged that Ndi1 form homodimers to create an amphiphilic domain structure, which anchors the protein to the membrane, and contains two separate binding sites for NADH and ubiquinone that can be possibly bound simultaneously[26].

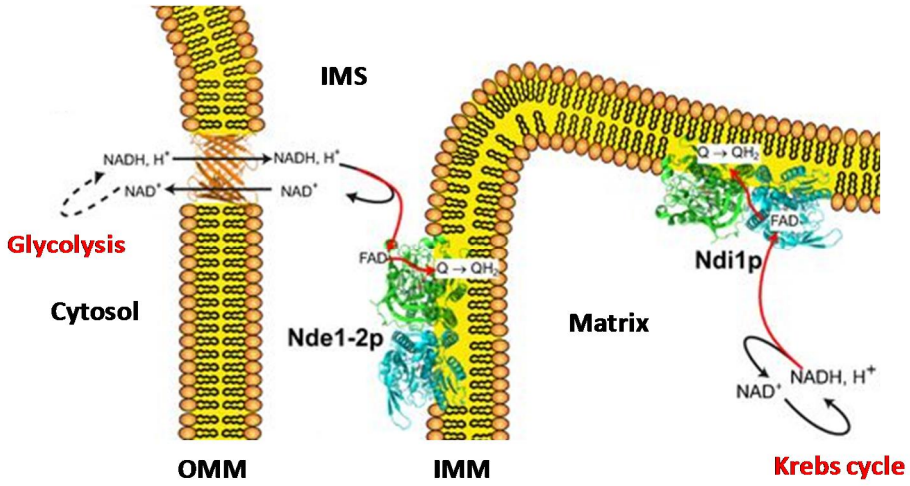

Figure 4. *S. cerevisiae* NADH dehydrogenases.
Yeast mitochondria possess non-proton-translocating NADH dehydrogenases at both the inner side (Ndi1p) and outer side (Nde1-2p) of the IMM. Ndi1p transfer electrons from NADH generated by the Krebs cycle to ubiquinone via FAD, whereas Nde1-2p from cytosolic NADH, generated by glycolysis; modified from[27].

1.1.2.3 Complex II

The second complex of the RC is **succinate dehydrogenase (SDH),** which is also part of the Krebs cycle. It organizes as a heterotetrameric complex composed of four subunits (SDHA, SDHB,

SDHC and SDHD). SDHA and SDHB contain the flavoprotein and the iron-sulfur protein, respectively, and protrude in the mitochondrial matrix, whereas SDHC and SDHD represent the hydrophobic regions, allowing membrane anchoring and the binding of ubiquinone. The catalyzed reaction is the oxidation of succinate to fumarate and the transfer of electrons from the generated $FADH_2$ to ubiquinone. Complex II represents a unique enzyme for many reasons. It does not pump protons across the IMM, therefore not contributing to generation of the proton-motive force, and it does not assemble into higher structures as the other complexes do, as I will discuss below. Mutations in SDH-encoding genes have been reported in many cancers and muscle disorders[28]. Indeed, the alteration of these genes often correlates with a loss of function of the complex that in turn results in two major outcomes: (i) accumulation of succinate in the cytosol, favoring the stabilization of hypoxia-inducible 1-α factor (HIF1α) transcription factor acting in cell transformation[29] and (ii) increased generation of ROS, also by reverse electron transport to complex I.

1.1.2.4 Complex III

Complex III (**cytochrome *b*-c_1 complex**) is a central enzyme of the electron transfer chain (ETC) that leads to the oxidation of reduced ubiquinone (QH_2) and the subsequent reduction of a mobile electron carrier, cytochrome *c*. Electron transfer is coupled to proton translocation across the IMM with a stoichiometry of four protons and two reduced cytochrome *c* molecules for each QH_2. The complex has many different subunits, among which cytochrome *b, c1* (containing *b* and-*c1* type hemes respectively) and Rieske iron sulfur (containing 2Fe-2S centers). The solved structure shows an obligatory homodimeric organization that apparently guarantees a higher electron transfer efficiency[30]. The overall reaction is commonly called Q-cycle and starts from the oxidation of QH_2 to ubiquinone. The two electrons are fed into two different pathways: one through the high-potential chain (Rieske and cytochrome *c1*) and the other through a low-potential chain (cytochrome *b*). The outcomes of the Q-cycle are the reduction of cytochrome *c*, which is a small hemeprotein located at the periphery of the IMM, and the net translocation of 4 H^+ across the membrane. Reduced cytochrome *c* can finally pass electrons to the cytochrome *c* oxidase complex, the last component of the ETC. Complex III can be fully inhibited by antimycin A, which disrupts the Q-cycle of the enzyme.

1.1.2.5 Complex IV

Complex IV (also called **cytochrome *c* oxidase)** functions as a dimer, in which each monomer contains two cytochromes and two copper atoms. The overall reaction consists of the acceptance of one electron at a time from cytochrome *c* and the passage of four at a time to oxygen, to form H_2O. This complex can be blocked by cyanide, which blocks respiration irrespective of the respiratory substrate used.

1.1.2.6 Complex V

The mitochondrial **F-ATP synthase** (or complex V) is the enzyme that catalyzes the synthesis of high-energy molecules of ATP from ADP and Pi, exploiting the proton gradient created by ETC as mechanical force. Since this enzyme is one of the main topics of my Thesis, I will describe its structure and properties in some detail in chapter 1.2.

1.1.2.7 Supercomplexes organization and ROS production

The supramolecular organization of the RC complexes was a major research topic in the 1970-80s, culminating with the introduction of the random collision model (RCM). Based on this theory, each complex has been considered as a single independent entity embedded in the IMM with ubiquinone and cytochrome *c* acting as mobile carriers, free to diffuse in the lipid membrane (reviewed in[31]). On the other hand, other studies have questioned this model, suggesting the existence of specific higher order units that might be preferentially associated in the IMM. Schägger and Coworkers, pioneers of the blue native gel electrophoresis technique, reported that, in presence of a mild detergent, complexes of RC are found to organize into supercomplexes in mammals[32,33]. For instance, free complex I accounts only for 14-16% of the total, whereas the largest part has been found associated with complex III. Moreover, interactions have been detected also between complex I-III and IV at variable copy number and stoichiometry, to form the so-called respirasome. On the other hand, the free fraction of complex IV is instead more than 80% and complex II is not found in association with any other complex. Together with the protein-protein interactions, the IMM lipid composition plays a key role in the correct assembly of the respirasome. For example, in patients affected by Barth syndrome -which alters normal cardiolipin remodeling-, the formation of supercomplexes is impaired[34]. In yeast, the organization of RC supercomplexes appears rather

different from that observed in mammals. The major supercomplexes seen consist of complex III (in the dimeric form) and IV with variable stoichiometry of complex IV to complex III, depending on the extraction conditions[35]. Recent data indicate that the three NADH dehydrogenases (Ndi1, Nde1 and Nde2) organize into a supercomplex, which has been suggested (i) to associate with other enzymes, such as the glycerol-3-phosphate dehydrogenase (Gut2) and D- and L-lactate dehydrogenases and (ii) to play a key role in NADH channeling in the yeast OXPHOS system[36].

In spite of these differences, it is now widely accepted that in all higher organisms the physiological meaning of the IMM organization of RC supercomplexes is to increase the efficiency of electron flux, which in turn would significantly prevent the generation of ROS[37,38].

Mitochondria represent a relevant source of ROS in eukaryotic cells. Depending on their concentration and site of production, mitochondrial ROS can be harmful or beneficial for cellular processes, enzyme regulation as well as gene expression. An excess in ROS levels could lead to damage, trigger apoptosis and is often related to the development of disorders and senescence (**Figure 5**)[39].

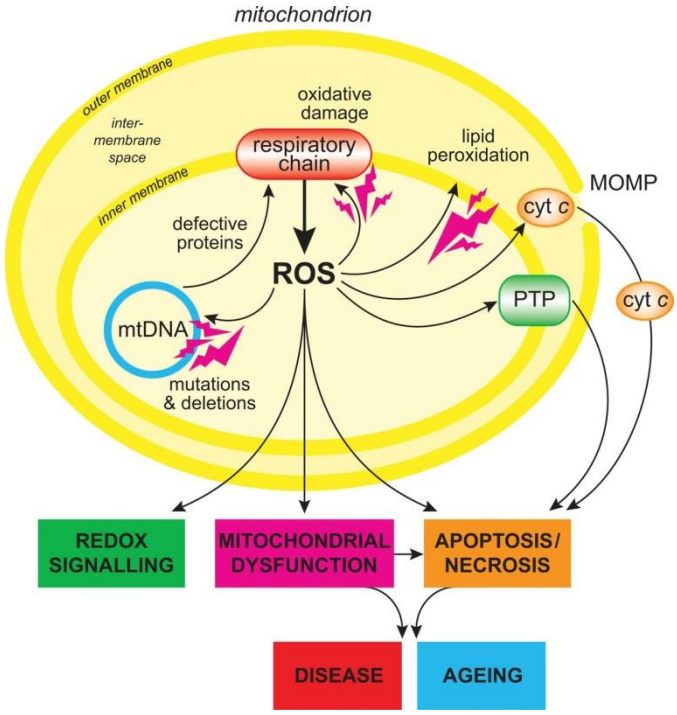

Figure 5. Downstream effects of mitochondrial ROS.
Mitochondrial ROS can lead to oxidative damage of mitochondrial proteins, membranes and DNA, impairing the ability of mitochondria to synthesize ATP and to correctly metabolize glucose intermediates and fatty acids. Mitochondrial oxidative damage can also increase the tendency of mitochondria to release intermembrane space proteins such as cyt *c* to the cytosol by mitochondrial outer membrane permeabilization and thereby activate the apoptosis initiation machinery. Consequently, it is not surprisingly that mitochondrial oxidative damage contributes to a wide range of pathologies. In addition, mitochondrial ROS may act as redox state modulator, reversibly affecting the activity of a range of enzyme in mitochondria, cytosol and nucleus; from[39].

As already mentioned, ROS are mainly produced in mammals by the electron leaks occurring within the RC at the level of complex I and complex III, although complex II has also been recently taken into account[40].

Among the events triggering ROS production, prominent causes are excess of reducing equivalents and hyperpolarization[41]. The superoxide anion ($O_2^{\bullet -}$) is the most common byproduct from one-electron reduction of O_2 and is rapidly converted into hydrogen peroxide (H_2O_2). This reaction occurs spontaneously but is much accelerated by superoxide dismutase (SOD). Because of its long half-life and ability to diffuse across membranes, H_2O_2 is a key signaling molecule, which exerts its effect mainly via reversibly oxidation of free thiol groups of Cys residues (S-oxidation) to sulfenic acid (-SOH). If ROS levels are high, further oxidation steps can occur with conversion of –SOH to sulfinic ($-SO_2H$) and sulfonic ($-SO_3H$) acids, leading to irreversible protein modification. Thus, protein Cys content appears to be a crucial player in controlling mitochondrial function and protein activity in response to local changes in redox environment. Indeed, the free Cys -SH groups exposed to solvent can be rapidly subjected to a range of redox-sensitive modifications, depending on their ability to become thiolate anions ($-S^-$). Each Cys residue has its own pKa value, influenced by the properties of surrounding residues and the aqueous environment; for instance, an alkaline locus or the proximity with charged residues substantially decrease the pKa, making it more reactive. Notably, Cys -SH can react with neighboring thiol groups to form disulfide bridges, thereby promoting reversible protein-protein interactions that likely disappear when the redox balance gets back to normal. Such modification is often involved in protein folding or complex formation, although it has been also associated with changes in protein function. For instance, this is the case of the F-ATP synthase exposed to an increased oxidative stress during heart failure[42]. Indeed, a disulfide bond generates between two subunits of the enzyme, α and γ, affecting its hydrolytic activity. This observation led to the suggestion that critical Cys residues might sense the redox state and consequently control ATP synthesis/hydrolysis. Moreover, the unique Cys residue of the α subunit has also been found to be S-glutathionylated in failing hearts. Primary S-oxidation modification (-SOH) can be followed by another modification, called S-glutathionylation, if the oxidized form of glutathione (GSSG), is available. This secondary modification is also considered as a protective mechanism that prevents further oxidation of Cys residue by H_2O_2. Intriguingly, S-glutathionylation of a protein can either proceed non-enzymatically or enzymatically, mainly via the action of the glutaredoxin (Grx), which uses glutathione as cofactor.

1.2 F-ATP synthase

F-ATP synthases are multisubunits enzyme integral components of energy-transducing membranes in bacteria, mitochondria and chloroplasts. They are close relatives of the V-ATPases, which use ATP hydrolysis-derived energy to generate H^+ gradients across membranes, and of archeal ATPase that synthesizes ATP in archea[43]. Here, I will focus on the mitochondrial F-ATP synthase that, together with its pivotal role in producing ATP, might have a key role in directly controlling cell death, as recently proposed by our laboratory[44].

1.2.1 F-ATP synthase structure

The structure of the catalytic part of the F-ATP synthase is highly conserved among species. I will present the structure of the bovine enzyme, highlighting relevant differences with the yeast complex. The bovine structure has been extensively characterized and crystals of almost all its extrinsic components have been defined with a resolution down to 1.9 Å. I will potentially highlight differences with the yeast complex. The whole enzyme is a membrane-bound protein assembly of about 30 subunits with a combined molecular mass of about 650 kDa[43,45,46]. It is organized into a soluble globular domain (F_1) that comprises the catalytic core, and a membrane intrinsic domain (F_o) joined together by central and peripheral stalks (**Figure 6**).

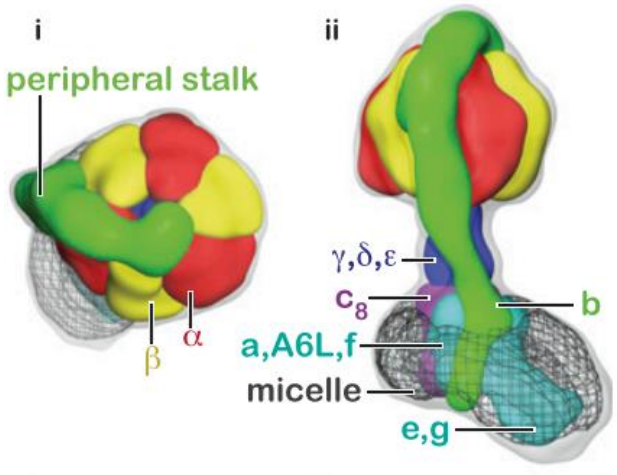

Figure 6. Structure of bovine F-ATP synthase.
View from the top (i) and from the lateral side (ii) of the enzyme. F_1 domain is represented as colored segments: catalytic α subunits and β subunits are in red and yellow, respectively, the peripheral stalk in green, the central stalk in blue (γ, δ, ε), the *c*-ring in purple and the other membrane-bound subunits (e, g, a, A6L, f) in light blue. In the F_1 region of the complex, the three α- and three β-subunits can be seen surrounding the γ-subunit, with the peripheral stalk running along an α/β-interface. A high density region containing subunit a, A6L and f would divide the peripheral stalk and the *c*-ring. At the intermembrane space side of the membrane region, a density that contains the e- and g-subunits can be seen running along the detergent micelle; from[46].

The **F_1 domain** catalyzes the synthesis of ATP from ADP and Pi. It has an orange-shape structure, composed of five globular proteins (subunits α, β, γ, δ and ε) that arrange with a specific stoichiometry: α_3, β_3, γ_1, δ_1 and ε_1. Three α-subunits and three β-subunits alternate in a spherical complex (pseudohexagon) around the γ-subunit (the central axis), that extends toward the membrane bound domain, representing the foot that connects the soluble part with the hydrophobic region of the enzyme. At the contact site with F_o, γ subunit associates with the δ- and ε subunits, two different but related proteins, forming the so-called central stalk. The peripheral stalk, instead, locates outside the catalytic core and appears to be a rigid rather than a flexible structure, acting as a stiff[47]. It is composed of several subunits: the oligomycin sensitivity conferring protein (OSCP), subunit b, d and F6. OSCP is essential for conferring the sensitivity to oligomycin, an antibiotic that fully inhibits the catalytic activity. It is composed by two domains: the N-terminal region that contacts one of the three α-subunits and the C-terminal region that binds subunit b and F6[48]. For the rest, subunits b, d and F6 seem to lie roughly parallel to each other. Many roles have been attributed to the peripheral stalk, among all the transient storage of elastic energy produced by enzyme rotation and the help to F_1 domain to resist the rotational torque of the central stalk[49].

The **F_o domain** counts a number of *c*-subunits, simple spanning proteins containing two transmembrane α-helixes, organized in a barrel-like structure within the membrane (also referred to as the *c*-ring) whose orifice is probably plugged by phospholipids[50]. This part of the enzyme, named also rotor, allows the re-entry of H^+ across the membrane, which gives rise to the clockwise rotation (if seen from the IMS) of the whole cylinder and sequentially of the central stalk that finally contacts the catalytic sites and promotes synthesis of ATP. The number of *c* units forming the ring varies among species, ranging from 8 (in *D. melanogaster* and *B. taurus*) to 15 (e.g. 10 in *E. coli* and *S. cerevisiae*). As a consequence, since each catalytic cycle generates three ATP molecules, a variation in the number of *c* subunits (and thus in the H^+ binding sites) among species leads to different H^+-to-ATP ratios (from 2.7 to 5) with a resulting difference in energy-conserving efficiency (inversely proportional to the *c*-ring size)[51]. The *c*-ring is strictly connected to another hydrophobic protein (subunit *a*) that likely provides a pathway for IMS H^+ to access specific residues of the *c*-ring and, after rotation, a preferential exit way[43]. Recently, the arrangement of the intrinsic region of subunit *a* of *Polytomella* F-ATP synthase has been defined by single-particle electron cryomicroscopy. Intriguingly, the structure showed four long horizontal α-helices arranged in two hairpins with an angle of about 70° to the *c*-ring helices. Moreover, the map suggests the formation of a solvent-accessible channel that extends from the mitochondrial matrix to a conserved Arg residue within subunit *a* that couples proton translocation to *c*-ring rotation[52].

Other supernumerary subunits have been found associated to the membrane bound part of the bovine enzyme such as subunit e, g, f, A6L, DAPIT (diabetes-associated protein in insulin-sensitive tissue) and 6.8 proteolipid, whose function is only partially understood[46,53]. Many reports proposed that subunits e and g could be implicated in the organization of higher structures of F-ATP synthase, e.g. dimers or oligomers within the IMM that are involved in the generation of the cristae shape.

The **e subunit** is a small single transmembrane α-helix protein anchored to the IMM by its N-terminal domain, whereas its C-terminus is exposed toward the IMS[54]. The amino acidic composition, overall structure and membrane orientation appear similar in the yeast and bovine proteins, except that the yeast C-terminus is longer. At the N-terminal part, in the middle of the membrane spanning-segment, this subunit shows a conserved "dimerization" GXXXG motif that seems to take contact with adjacent subunits as well as with subunit e of adjacent enzymes. In yeast, by cross-linking experiments it has been demonstrated that two subunits e of two monomers are close to each other and might interact via the "dimerization" motif[55].

Also **subunit g** is a single transmembrane α-helical protein and presents almost the same topology and orientation of subunit e, exposing the N-terminus in the matrix space and a short C-terminus in the IMS. The transmembrane segment contains the "dimerization" GXXXG motif and its ablation leads to a dramatic alteration and destabilization of dimeric and oligomeric structures[56,57]. Through cross-linking experiments of g mutants containing an exogenous Cys residue, a close proximity with subunit e within the membrane has been demonstrated.

1.2.2 F-ATP synthase catalytic activity

F-ATP synthase can work either by synthesizing or hydrolyzing ATP, depending on substrate availability and the $\Delta\mu H$, using Mg^{2+} as an essential cofactor. The catalytic mechanism of hydrolysis has been widely investigated through electron microscopy images and fluorescence technique and many X-ray crystals are available as well, whereas the synthesis is more difficult to assess because of the strict requirement of a proton gradient.

In the catalytic core, the three non catalytic α subunits and the three catalytic β subunits are very similar, presenting an N-terminal domain containing β strands, a central nucleotide binding domain and a C-terminus made of α-helixes. Each subunit contains a nucleotide binding site present approximately half way up the $\alpha_3\beta_3$ domain and another in the cleft between the α and β. The three binding sites in the β subunits carry out the ATP synthesis, participating in the steady state rotational catalysis, whereas the sites in the α subunits are non-catalytic and exchange bound nucleotide very

slowly. Recently, it has been proposed that the non catalytic sites can modulate the affinity for ADP in the neighboring catalytic sites[58]. Different conformations of the β subunits and their catalytic sites have been discovered and named based on the nucleotide bound: β_{TP} containing ATP, β_{DP} with ADP and β_E when the site is empty. While β_{TP} and β_{DP} can bind either ADP or ATP, β_E adopts radically a different conformation[59]. The conformational switch during catalysis is driven by the curvature of the γ subunit (**Figure 7**). Indeed, the γ subunit contains an asymmetric α-helical coiled coil domain and its rotation occurring during catalysis modulates the binding affinity of substrates and products for β subunit. Thus, as γ rotates during catalysis, each β subunit switches conformation depending on the face of γ it contacts. Using single particle experiments, Yasuda et al. showed that the γ subunit rotation tended to dwell at 120° intervals when in conditions of low ATP concentration[60]. Thus, each catalytic site would transit through the three conformations during a 360° rotation, and a different site would complete its cycle every 120° rotation, even if intermediate steps have been characterized as well[61]. This model implies that three ATP molecules are hydrolyzed or synthesized for each 360° rotation. Furthermore, because the direction of rotation is known, the order of the conformations is $\beta_E \rightarrow \beta_{TP} \rightarrow \beta_{DP}$ in hydrolysis (counter-clockwise rotation) and $\beta_E \rightarrow \beta_{DP} \rightarrow \beta_{TP}$ in the direction of synthesis (clockwise).

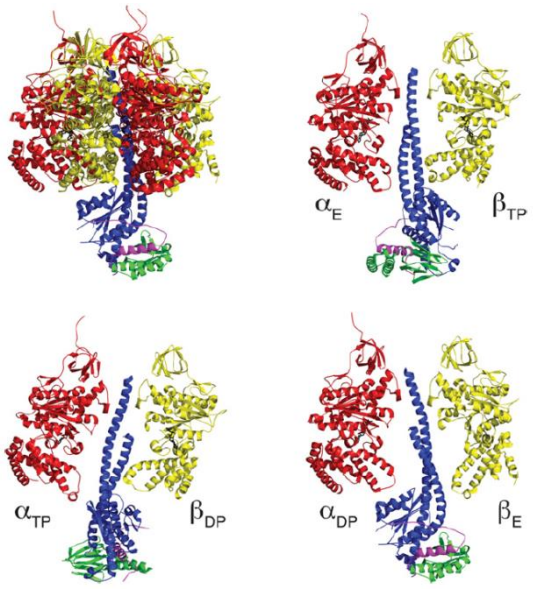

Figure 7. Bovine F-ATP synthase F_1 domain structure in the ground state during catalysis.
The subunits are depicted in ribbon representation. The α-, β-, γ-, δ- and ε-subunits are red, yellow, blue, green and purple respectively. Top left: the complete F_1 domain. γ subunit interacts with loop regions between the N- and C-terminal α-helices and with the c-subunits in the F_o membrane domain. Top right and bottom figures: representation of the three different conformations of the catalytic β subunits together with the central stalk (γ-, δ- and ε-subunits) and an α-subunit, for reference. Each of the three β-subunits has been obliged by the asymmetry of the α-helical coiled-coil region of the γ-subunit to adopt a different conformation, denoted β_{TP}, β_{DP} and β_E, with different affinities for nucleotides, the β_{TP}- and β_{DP}-subunits can each bind either ADP or ATP, and the βE-subunit is unable to bind any nucleotide. During the catalytic cycle of ATP synthesis or hydrolysis, the rotation of the central stalk takes each β-subunit through each of the three conformations. As the rotor turns, this action leads to the binding and entrapment of ADP and phosphate at the βE-site as it closes, ATP formation at the β_{DP}-site and ATP release from the β_{TP}-site as it opens and converts back into the β_E-site. Each 360° rotation of the central stalk (clockwise as viewed from beneath) leads to the formation of an ATP molecule from each of the three β-subunits; from[43].

1.2.3 F-ATP synthase regulation

When the proton-motive force across the IMM collapses (for example under hypoxic conditions or after addition of an uncoupler) and ATP is provided (for example by glycolysis) the F-ATP synthase switches its catalytic activity from ATP synthesis to ATP hydrolysis. Operation in "reverse" leads to proton pumping from the matrix to the IMS at the expense of ATP. Hydrolysis is regulated by an endogenous peptide, called IF_1 (inhibitory factor 1). Its function depends on the presence of ATP that favors its binding to the F_1 domain, blocking the catalysis process within the enzyme. First isolated from animal mitochondria[62], IF_1 was also found in plant[63] and in yeast mitochondria, here named INH1[64].

The bovine homologue is a small protein of 84 amino acids, keeping contact with F_1 α/β interfaces with a minimal consensus sequence (14-47 residues) in the N-terminus and blocking its rotary catalysis, likely by trapping ATP[65]. The active form is a dimeric association between coiled coil domains in the C-terminus of two monomers, leading to an accessible N-terminus, while the inactive structure keeps the inhibitory site masked within tetrameric and even higher oligomeric forms[66]. Intriguingly, the dimeric form is promoted by acidic pH values (below 6.5) and this seems to be correlated to a physiological defense of cells against ATP depletion in hypoxic conditions. Indeed, in absence of oxygen, glycolysis is up-regulated and this can lead to an overall decrease of pH values that in turn favors dimerization of IF_1 and the consequent inhibition of ATP hydrolysis. In keeping with this, increased IF_1 content has been documented in mitochondria of highly glycolytic lung, colon and breast carcinomas[67]. However, over-expression of IF_1 in cells with negligible IF_1 content also caused a reduction in ATP synthesis via F-ATP synthase and a consequent metabolic switch toward anaerobic glycolysis, suggesting that IF_1 may regulate cell metabolism also under normoxic conditions[68].

The yeast peptide INH1 is shorter (63 residues) than the bovine homologue, having a shorter C-terminal region[69]. Yeast contains also two stabilizing factors that favor the action of INH1, called STF1 and STF2. STF1 shares sequence similarity with INH1 and is potentially able to form coiled-coil structures, whereas STF2 sequence is unrelated to the other two.

1.2.4 F-ATP synthase organization in mitochondria

The overall arrangement of the mitochondrial F-ATP synthase *in vivo* is in form of oligomers that originate from the association of dimers, the "bulding blocks" of the enzyme. The existence of a supramolecular organization of F-ATP synthase in situ was first reported by Allen in *Paramecium*

multimicronucleatum. They observed that F-ATP synthase complexes formed a paired row around the outer curve of helical tubules[70]. It is now clear that yeast, mammalian and plant F-ATP synthase is organized in dimers associated to form long rows of oligomers located at the cristae ridges, and that this arrangement is essential to maintain a high local curvature and normal cristae morphology[46,71,72]. This overall structure is also observed in chloroplasts of algae[73] but not in bacteria. In yeast, the dimeric structure might be due to tight interactions between subunits e and g as well as k, another small subunit embedded to the F_o domain[74]. These three proteins, indeed, were found associated to the dimeric/oligomeric form and not to the monomeric one. Genetic ablation of these subunits prevented the formation of dimers/oligomers, resulting in abnormal anion-like cristae morphology, thus providing evidence about their role in the F-ATP synthase organization[71,74,75]. Cross-linking experiments revealed that subunits e and g can form either homo-dimers (e-e and g-g) or hetero-dimers through the GXXXG motif present in both proteins, as already mentioned. However, through *in vivo* FRET experiments, it has been shown that two subunits b are also in close proximity within the membrane, suggesting that the peripheral stalk participates in the connection between two neighboring monomers as well[76]. In support of this hypothesis, cross-links between subunit b - g and -e have been described, as well as abnormal cristae morphology in mutants lacking the first N-terminal transmembrane domain[77]. Furthermore, two other small proteins have been found to be close and interacting with each other within the dimeric interface, i.e. subunits k and h[75,78]. More recently, it has been proposed that the Cys residue of subunit *a* in position 23 contributes to keep the contacts between two monomers following formation of a disulfide bridge connecting two *c*-rings[79]. Thus, this complex scenario of membrane protein-protein interactions and extramembranous strengthening clearly attributes to e and g subunits a primary role in stabilizing dimers, but not an essential requirement for the catalytic activity.

While most studies have been carried out in yeast, the dimeric form of F-ATP synthase was also found in detergent extract of bovine heart mitochondria[35]. Notably, the bovine enzyme contains subunits e and g, but, differently from yeast F-ATP synthase, these subunits resulted to be present both in the monomeric and dimeric state of the enzyme.

Cutting-edge cryoelectron microscopy techniques allowed a more precise definition of the ultrastructural arrangement of F-ATP synthase in situ. The extensive analysis performed for mapping the dimeric form revealed a symmetrical V-shaped structure with an angle between the two monomers of approximately 90° in yeast (**Figure 8**). This preferential inclination of monomers induces a curvature of the lipid bilayer that has been postulated to be sufficient to drive the formation of long dimers rows able to give rise to the highly curved membrane ridges and lamellar cristae[71,80]. From these pioneering experiments, it emerged that dimers alone are perfectly adequate

to self-associate without the need for additional proteins or chaperones in an apparently low-energy requiring process. Furthermore, this particular arrangement of F-ATP synthase is conserved among species, being present in *S. cerevisiae* as well as in *B. taurus*, *Y. lipolytica* and *P. anserina*[81]. Physiological dimerization and oligomerization of the F-ATP synthase may provide several advantages such as stabilization of the enzyme structure during rotary catalysis and increased IMM surface area which is initiated by dimers.

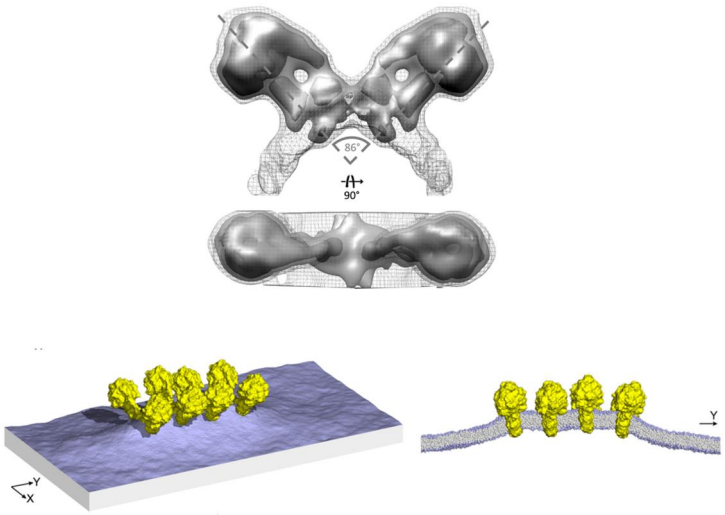

Figure 8. Membrane curvature induced by yeast F-ATP synthase dimers.
Upper images: Subtomogram average of the F-ATP synthase dimer from yeast mitochondria (viewed from the lateral side and from the bottom). Two F-ATP synthase monomers form a V-shaped dimer with an angle of 86° between their long axes. The central and peripheral stalks are clearly resolved. The dimer interface is located in the membrane between the two peripheral stalks. Lower images: perspective views of a simulated membrane patch with an F-ATP synthase dimer row distorting the planar lipid bilayer. The simulation is based on a coarse-grained representation of the dimer structure and its environment; from[71].

1.3 Mitochondrial Ca^{2+} homeostasis

In this chapter, I will present a short overview about mitochondrial Ca^{2+} homeostasis in mammals. The contribution of mitochondria to yeast Ca^{2+} homeostasis will be described more in detail in chapter 1.6.4.

Ca^{2+} is one of the most relevant second messengers involved in a variety of cellular processes and in signaling. Under resting conditions, its cytosolic concentration is strictly maintained at about 100 nM. An elevation of intracellular Ca^{2+} levels is, indeed, the triggering event leading to the initiation of downstream cascades. The [Ca^{2+}] rise can be highly localized and follow well defined spatial and temporal patterns. This can be achieved by the existence of specialized compartments able to store Ca^{2+} ions via efficient transport systems, channels and pumps and to release it upon stimulation. The control of intracellular [Ca^{2+}] occurs at different levels, from the plasma membrane that contains Ca^{2+}-ATPases (PMCA), pumping Ca^{2+} outside the cell, and Na^{+}/Ca^{2+} exchangers (NCLX), to the most important intracellular Ca^{2+} store, the ER, with its Ca^{2+}-ATPases (called SERCA in muscle cells)[82]. Upon stimulation, Ca^{2+} can be locally released and sensed by Ca^{2+}-dependent enzymes or target proteins containing a Ca^{2+} binding domain that in turn induce specific cellular responses[83].

Mammalian mitochondria were the first organelle to be associated with Ca^{2+} handling and their ability to store Ca^{2+} in an energy-dependent process was first unraveled using isolated energized rat kidney mitochondria in the late 1960s[84]. Moreover, in later studies the pivotal role of this cation in regulating gene expression, mitochondrial functions and enzyme activity such as the NADH-linked dehydrogenases has been further demonstrated[85]. Thus, mitochondria represent key players in control of Ca^{2+} homeostasis, being involved in a wide range of physiological processes such as buffering of free cytosolic Ca^{2+}, excitation-contraction coupling and apoptosis.

Under basal conditions, mitochondrial Ca^{2+} concentration is about 50–100 nM, i.e. similar to that in the cytosol, but it can reach values >100 µM upon strong cell stimulation[86,87]. Unlike other organelles, in which ATP hydrolysis drives the Ca^{2+} uptake, mitochondrial Ca^{2+} accumulation does not need ATP, but rather relies on a channel, the mitochondrial Ca^{2+} uniporter (MCU)[88,89]. Another difference compared to other compartments concerns the Ca^{2+} efflux pathway that in mitochondria is mainly due to exchangers instead of release channels. This unique toolkit allows the maintenance of a low matrix Ca^{2+} concentration in resting cells and a rapid Ca^{2+} accumulation by the organelle when cytosolic Ca^{2+} is elevated. Moreover, mitochondria have been found to be located in proximity to Ca^{2+} release channels in the ER and in the plasma membrane, where a microdomain of elevated Ca^{2+} level (10-20 µM) is generated under certain stimuli. These microdomains have the key function of maximizing the efficiency of Ca^{2+} signal, by ensuring mitochondria to quickly respond acting as local

buffers[90]. Mitochondrial Ca^{2+} equilibration with the electrochemical gradient (influx in energized mitochondria) is mediated by a gated channel, the MCU, a highly selective, low conductance channel. The MCU has been found in most eukaryotes, but is missing in budding yeast. Although the molecular nature of the MCU has been recognized relatively recently, its major features had been thoroughly characterized in the past decades. Indeed, mitochondrial Ca^{2+} uptake had been shown to be specifically inhibited by Ruthenium Red (RR) and lanthanides, and activated by various natural modulator including ADP, polyamines and Ca^{2+} itself[91]. In 2011, two groups independently identified a 40 kDa protein, ubiquitously expressed in all mammalian tissues and eukaryotes but not in yeast, that contains two transmembrane domains forming a gated channel (possibly through oligomerization of more units)[88,89]. Most intriguingly, De Stefani et al., demonstrated that in lipid bilayer-reconstituted MCU displayed a Ca^{2+} channel with a conductance matching that found in previous electrophysiological recordings, fully sensitive to RR and other inhibitors[92].

Ca^{2+} influx via the MCU is an electrophoretic process, driven by the Ca^{2+} electrochemical gradient ($\Delta\mu Ca^{2+}$), leading to membrane depolarization. In turn, this stimulates H^+ pumping activity of the RC and leads to matrix alkalinization, which lowers the $\Delta\Psi$ and inhibits further Ca^{2+} uptake[93]. The uptake of substantial amounts of Ca^{2+} could be achieved by buffering matrix pH to allow $\Delta\Psi$ regeneration, and matrix Ca^{2+} to keep the concentration gradient[94]. The buffering of matrix pH is mainly due to the action of the phosphate carrier (discussed below) that allows the re-entry of H^+ together with inorganic phosphate, or to the diffusion of CO_2 that re-generates bicarbonate and H^+ in the matrix. Concerning Ca^{2+} buffering, it normally occurs via the formation of Ca^{2+}/Pi complexes that precipitates and decreases the amount of free matrix Ca^{2+} [95]. Matrix [Ca^{2+}] is also controlled by efflux pathways that, together with MCU, govern the kinetic steady state of the cation. Indeed, if Ca^{2+} accumulation was allowed to reach thermodynamic equilibrium with a $\Delta\Psi$ of -180 mV (negative inside), according to the Nernst equation and for a cytosolic Ca^{2+} concentration of 0.1-1.0 μM, the matrix cation concentration level should be between 0.1 and 1 M, i.e. 1,000,000-fold higher than that measured inside the matrix. The solution of this paradox came from the observation that a slow efflux of Ca^{2+} takes place, whose activity prevents attainment of electrochemical equilibrium[96] (**Figure 9**). Two main release pathways have been described: the H^+/Ca^{2+} (HCX) and the Na^+/Ca^{2+} (NCLX) exchangers, that both drive the extrusion of matrix Ca^{2+} depending on H^+ and Na^+ concentration gradients[97,98]. While the molecular identity of the NCLX has been recently identified with the discovery of the related gene[98], much less is known about the HCX that has been only characterized by functional studies. However, the predicted stoichiometry for these two exchangers would be 1 Ca^{2+} for 3 H^+/Na^+, i.e. Ca^{2+} exit would be favored by the membrane potential. Another process proposed to be involved in the regulation of mitochondrial Ca^{2+} level is the transient opening of the Permeability

Transition Pore (PTP), an unselective IMM channel that appears to play a key role in controlling *in vivo* Ca^{2+} homeostasis[99] and that I will describe more in detail in next sections.

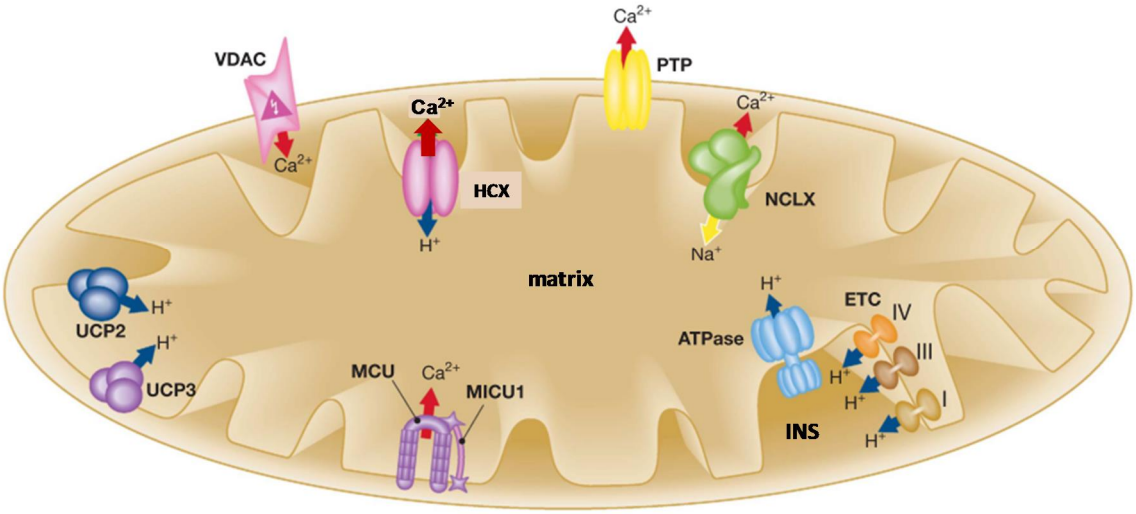

Figure 9. Schematic representation of the mitochondrial Ca^{2+} transport mechanisms.
Ion fluxes are indicated by arrows. Red arrow, Ca^{2+}; blue arrow, H^+; green arrow, K^+; yellow arrow, Na^+. ETC: electron transport chain; NCLX, Na^+/Ca^{2+}exchanger; HCX: H^+/Ca^{2+} exchanger; PTP, permeability transition pore; UCP2/3, uncoupling protein 2/3; VDAC, voltage-dependent anion channel; IMS: intermembrane space; MCU: mitochondrial Ca^{2+} uniporter; MICU1: mitochondrial Ca^{2+} uptake 1; modified from[100].

1.4 Mitochondria-dependent apoptosis

The term apoptosis refers to the programmed cell death process that has been described and characterized in almost all higher eukaryotic cells[101]. Differently from necrosis, which is characterized by loss of membrane integrity and induces uncontrolled release of cellular factors leading to inflammation, the onset of apoptosis involves a tightly regulated cascade of intracellular events. The discovery of the existence of specific mediators and regulators[102] strengthened the idea that this process might be controlled at different levels: by genome, cellular homeostasis and environmental conditions. Indeed, apoptosis is essential for normal development, body growth, defense against intracellular pathogens as well as for removal of damaged or transformed cells[103,104]. Thus, the alteration of this process correlates with the onset of many pathologies, e.g. degenerative diseases when apoptosis occurs indiscriminately, or cancers when the pathway is inhibited[105]. Morphological changes appreciable during apoptosis are membrane blebbing, cell shrinkage, nuclear fragmentation, chromatin condensation and DNA fragmentation[106]. Notably, the formation of apoptotic bodies during membrane blebbing allows the retention of all cellular factors, preventing the generation of an inflammatory site and thus the alteration of surrounding cells.

Many triggering mechanisms have been found beyond apoptosis initiation in mammals. Indeed, depending on the nature of the stimuli, two different pathways have been described: (i) the **intrinsic pathway** is mainly induced by oxygen radicals, hypoxia and DNA damage and proceeds via mitochondria signaling, and (ii) the **extrinsic pathway** is mediated by the binding of the so-called death ligands to the cognate death receptors (**Figure 10**). There is a clear cross-talk between these two pathways, which makes mitochondria primary actors also in the extrinsic pathway.

1.4.1 Intrinsic pathway

The first molecular evidence that apoptosis plays a role in tumorigenesis derived from the discovery that Bcl-2, an apoptosis inhibitor, is overexpressed in human follicular B-cell lymphomas[107]. Subsequently, a set of proteins involved in the control and execution of apoptosis have been identified and classified in three major groups: the anti and the pro-apoptotic proteins containing one or more Bcl-s homology (BH) domains; and the initiators that possess only a short motif called the BH3 domain. The **anti-apoptotic** proteins like, Bcl-2 and Bcl-xL, are associated with the OMM and cooperate in maintaining its integrity. The apoptosis **initiators** like Bad, Bid, Bim, Puma and Noxa act, instead, as sentinels over many cellular processes; normally they are in the inactive form and undergo activation only in the presence of death stimuli. Once this happens, these initiators induce

the activation of **pro-apoptotic** factors like Bax and Bak that are organized in heterodimers together with Bcl-2 and Bcl-xL at the OMM. Following a conformational change, these can be released by the anti-apoptotic factors and generate oligomers that likely form a channel in the OMM, breaching its integrity favoring the release of cyt *c*. Released cyt *c* can bind the apoptotic protease activating factor-1 (Apaf-1), changing its conformation and leading the formation of the apoptosome, a wheel-shaped homo-heptameric Apaf-1 complex[108]. Here, the protease binds and cleaves initiator procaspase-9 (inactive form), converting it in its active form, that in turn allows the activation of other effector caspases like caspase-3, -6 and -7 (cysteine-aspartic proteases).

1.4.2 Extrinsic pathway

Proteins triggering the extrinsic pathway are ligands of the so-called death receptors (TNF, RAS or TRAIL) present in the plasma membrane of particular cell types. The signaling cascade starts with the binding of a ligand to its receptor that promotes a conformational change of its intracellular region, in turn leading to the recruitment of a variety of adaptor proteins and thus the formation of the death-inducing signaling complex (DISC). Finally, this complex causes the cleavage of procaspase-8 that becomes active and able to proteolytically process effector caspases (3, -6 and -7) which trigger cell death events. At the same time, active caspase 8 can also cleave Bid in its truncated form tBid that is able to translocate to the mitochondria and induce the initiation of the intrinsic pathway by favoring OMM rupture and release of pro-apoptotic factors[109].

Thus, the extrinsic and intrinsic pathways are not separate mechanisms but rather cooperate to eventually turn on the same final common pathway for cell demise.

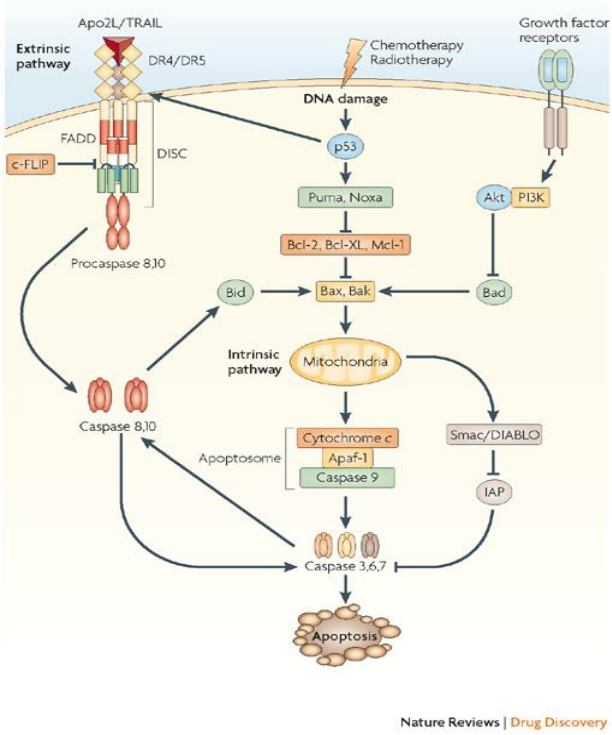

Figure 10. Apoptosis pathways.

Intrinsic pathway: cellular stress activates the intrinsic pathway by upregulating Puma and Noxa, which in turn activate Bax and Bak. Bax and Bak permeabilize the outer mitochondrial membrane, resulting in release of cyt *c*, which binds to the adaptor Apaf-1 to recruit the initiator procaspase 9 into a signalling complex termed the apoptosome. Activated caspase 9 then cleaves and activates the effector caspases 3, 6 and 7 to trigger apoptosis. The mitochondrial protein Smac/DIABLO augments apoptosis by binding inhibitor of apoptosis proteins (IAP) and reversing their grip on several caspases. Extrinsic pathway: cytotoxic immune cells produce pro-apoptotic ligands such as Apo2L/TRAIL that bind specific membrane receptors, allowing the recruitment of the adaptor protein Fas-associated death domain (FADD) and the initiator caspases 8 and 10 as pro-caspases, forming a death-inducing signalling complex (DISC). This triggers activation of caspase cascade. Although the extrinsic and intrinsic pathways can function separately, they often interact. Extrinsic-pathway activation leads to caspase 8-mediated processing of Bid; truncated Bid subsequently stimulates Bax and Bak to engage the intrinsic pathway; from[110].

1.4.3 Necroptosis

As already mentioned, necrosis is a form of cell death considered to be an uncontrolled event occurring in response to physicochemical insults. However, recent genetic evidence[111,112] and the discovery of specific chemical inhibitor[113] pointed at the existence of a regulated mechanism related to necrosis. Indeed, "regulated necrosis" was defined as a genetically controlled process that results in cellular leakage, characterized by cytoplasmic granulation as well as organelle swelling. Necroptosis is the object of intense scrutiny, and its molecular definition is constantly improving[114]. Principal mediators of this pathway are the receptor-interacting protein kinase 1 (RIPK1) and RIPK3 crucial kinases in TNF (tumor necrosis factor)-induced regulated necrosis. Upon stimulation with TNF, TNF receptor 1 (TNFR1), recruits RIPK1 through adaptor proteins, which undergo polyubiquitylation and the formation of IKK (inhibitor of NF-kB) complex that activates the NF-kB transcription factor. Once the polyubiquitylation is removed, RIPK1 can dissociate from the plasma membrane and initiate

two distinct cell death pathways, depending on whether caspase 8 is in its active/inactive form. Indeed, when caspase 8 is active, apoptosis occurs through the canonical pathway, whereas when inactive, RIPK1 and RIPK3 associates in microfilament-like complexes and undergo auto- and trans-phophorylation, recruiting the mixed lineage kinase-domain like (MLKL) that finally initiates necroptosis. A number of different stimuli can trigger necroptosis, e.g. ROS, UV, thapsigargin, ischemia reperfusion injury, TNFR and bacterial lipopolysaccharides. Many initiator mechanisms are shared with other pathways and converge to mediator events such as depletion of ATP, Ca^{2+} overload, dysregulation of the redox status, activation of phospholipases[114].

Many pieces of evidence point at the involvement of PTP opening as mediator of necroptosis in certain conditions, for example during ischemia reperfusion injury[114]. Of note, CyP D knock-out mice showed a degree of protection from neurological and cardiological damages following ischemic injury[115], and the derived fibroblasts were unaffected by necroptosis induced by ER-dependent Ca^{2+} release and/or from oxidative stress[116]. Furthermore, preventing the PTP from opening by pharmacologically inhibiting CyP D might provide a certain degree of protection to patients following myocardial infarction[117].

1.5 Permeability Transition Pore

The mitochondrial permeability transition (PT) has been described in mammals as an increased permeability of the inner mitochondrial membrane (IMM) to ions and solutes with molecular masses up to 1500 Da in response to Ca^{2+} and other stimuli[118–120]. Initially considered an *in vitro* artifact, its importance has been reevaluated after the discovery that the release of mitochondrial intermembrane proteins is a key event in the commitment and execution of cell death[121]. Over the last 20 years, the PT has been shown to play a role in a number of diseases e.g. ischemia-reperfusion, many types of cancer and several forms of muscular dystrophy (reviewed in[122]). In this chapter, I will present the major features of the mammalian PTP (mPTP), which have been thoroughly characterized over the years, whereas I will discuss the debated properties of *S. cerevisiae* permeability transitions in section 1.6.5.

1.5.1 Brief history

Onset of the PT has been shown to require matrix Ca^{2+}, which is an essential permissive agent, and at least one of a large number of "inducers"[123]. Haworth and Hunter, who coined the term *permeability transition*, proposed that this phenomenon was attributable to the opening of a channel, the so called permeability transition pore (PTP), providing a potentially reversible and tightly regulated mechanism for the PT[124].

This concept was not immediately accepted by the scientific community, and for many years this process was considered more an *in vitro* artifact than a physiological pathway. Indeed, a widespread skepticism stemmed from acceptance of the chemiosmotic theory of Peter Mitchell, who identified the mechanism of energy conservation occurring in energy-transducing membranes and laid the foundations of modern bioenergetics. As a matter of fact, the presence of a large channel that allows solutes and ions to equilibrate across the membrane appeared to contradict the need for maintenance of the proton gradient to allow the synthesis of ATP. Another controversial aspect of the PT concerned its molecular nature, since the estimated radius of the putative channel at about 1.4 nm appeared too large to be attributable to a protein and rather suggested onset discontinuities in the lipid bilayer[125].

Strong evidence for the existence of a specific protein mediating the PT came from the key discovery that cyclosporin (Cs) A can inhibit or delay the onset of pore opening[126]. This compound targets and inhibits the cyclophilins, peptidyl-prolyl *cis-trans* isomerases acting as chaperones. The PTP-inhibitory

effects depend on inhibition of matrix cyclophilin (CyP) D as discussed later[127]. Thus, the effect of CsA provided an indication that a CyP D interacting protein or set of proteins was responsible for PTP formation and offered the possibility to test occurrence of its opening in a variety of cells and living organisms.

Subsequent studies strengthened the hypothesis that the PTP has a role in pathophysiology and highlighted its major contribution to cell death[128]. Indeed, the equilibration of ions and solutes (below 1500 Da) consequent to prolonged PTP opening leads to influx of water into the matrix, increasing the mitochondrial volume. Matrix swelling causes widening of cristae junctions and consequent cristae unfolding, which, in turn, may be followed by rupture of the OMM. As a result, the large fraction of cyt *c* residing within the intracristal compartments can be released into the cytosol together with other proapoptotic factors, triggering the cell death cascade. However, onset of PTP opening is not only associated with this dramatic event, but may be part of a more complex scenario in the control of Ca^{2+} homeostasis[99,129]. Indeed, the consequences of the PT depend on the number, open time and conductance of individual pores, and on whether PTP opening is synchronized in the mitochondrial population. Measurements of transient and reversible openings have been possible through patch clamp analysis and fluorescence microscopy, which revealed the occurrence of asynchronous cycles of depolarization-repolarization likely associated with Ca^{2+} release events[130].

1.5.2 PTP regulation

Classical studies in isolated mitochondria from mammalian tissues allowed a through characterization of the functional properties and regulation of the putative channel. The transition between the “open” and “closed” state (and viceversa) occurs under certain conditions and in presence of many different physiological factors, ions and exogenous compounds as well[123]. These PTP effectors can be classified into *inducers*, which increase the propensity of the pore to open and *inhibitors* that, on the contrary, decrease the open probability.

As already mentioned, **Ca^{2+}** is a “permissive factor”, which is necessary but may not be sufficient to trigger a PT while all other factors either sensitize (inducers) or desensitize (inhibitors) the pore[129]. Importantly, all other divalent cations e.g. Mg^{2+}, Sr^{2+} and Mn^{2+}have a desensitizing effect and likely compete for the same binding site of Ca^{2+} [131]. Another accessible site for divalent cations is exposed to the intermembrane space and mediates PTP desensitization with all tested Me^{2+}, including Ca^{2+} itself.

Among the physiological modulators of the PTP, **matrix pH** plays a major role. Experiments performed with de-energized mitochondria showed a bell-shape dependence on matrix pH with an optimum for PTP opening at pH 7.4 and a marked desensitization at both basic and acidic pH values. The inhibition occurring at below pH 7.4 is mediated by the reversible protonation of a critical His residue that could be prevented by the addition of diethylpyrocarbonate, specifically promoting reversible carbethoxylation of the residue[132]. However, in respiring-mitochondria an external acidic pH may also affect the pore indirectly through the uptake of **Pi** (via the phosphate carrier, as described below) leading to PTP induction rather than inhibition given that Pi is one of the most effective inducers in mammalian mitochondria[133]. As already discussed, increasing concentrations of Pi decrease matrix free Ca^{2+}, yet Pi in mammalian mitochondria is an inducer of the PTP, probably because it favors binding of **cyclophilin D** to the F-ATP synthase and favoring its transition to the PTP, as we I will discuss in later paragraphs.

The membrane potential (**ΔΨ**) is another upstream key factor for regulation of the pore, which indeed displays a remarkable voltage-dependence. Collapse of the ΔΨ favors pore opening, whereas a high inside-negative ΔΨ tends to stabilize it in the closed conformation[134]. A specific ΔΨ sensor comprising Arg residues has been proposed to mediate the conformational change required for pore opening, as suggested by the modulation of the PTP voltage dependence by Arg-selective reagents[135].

The PTP is modulated by **oxidation-reduction** events. Indeed, at least two sites have been described: the "P" site, which is apparently affected by the redox state of the pyridine nucleotide pool, and the "S" site, which comprises an oxidation-reduction-sensitive dithiol and may be modulated by glutathione[136]. This second site can be activated by reaction with dithiol reagents such as arsenite or phenylarsine oxide (PhAsO), whereas other compounds like diamide (DIA) and t-butylhydroperoxide (TBH) can affect both sites, either by depleting the pyridine nucleotide pool or by oxidizing critical Cys residues. The effect of this oxidation is reversible and can be prevented by low concentrations of N-ethylmaleimide (NEM), monobromobimane or other thiol-selective reagents.

1.5.3 PTP structure: early models

Several hypotheses have been put forward over the last decades concerning the molecular structure of the pore. The resulting models, mostly based on pharmacological and biochemical approaches, postulated the existence of a multiprotein channel composed by several mitochondrial proteins. Initially, prominent candidates were the IMM adenine nucleotide translocator (ANT) and

the OMM voltage-dependent anion channel (VDAC) and the peripheral benzodiazepine receptor (PBR) today called mitochondrial 18-kDa translocator protein (TSPO)[137] together with putative regulators hexokinase (HK) II, PiC and CyP D (**Figure 11**).

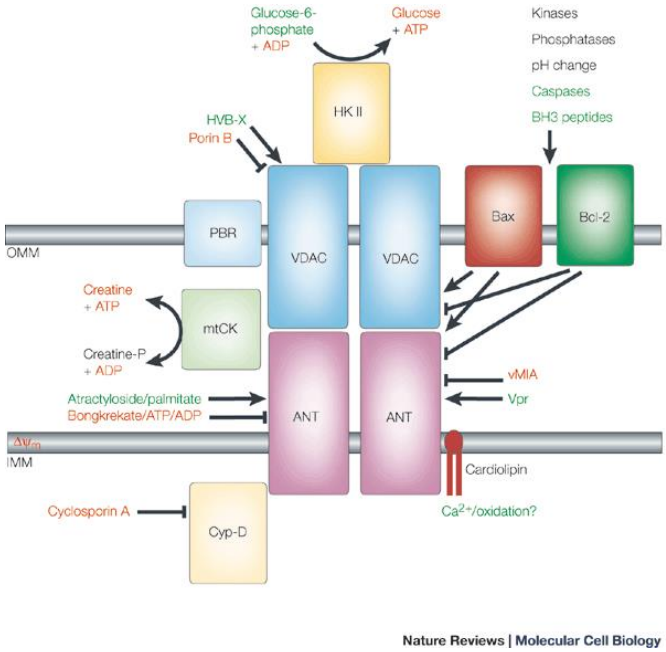

Figure 11. The PTP old model.
Putative model for the PTP. ANT, adenine nucleotide translocator; VDAC, voltage-dependent anion channel; PBR, peripheral benzodiazepine receptor; HK, hexokinase; mtCK, mitochondrial creatine kinase; from[137].

1.5.3.1 Peripheral benzodiazepine receptor

TSPO has traditionally been considered as a key player in cholesterol and porphyrin trafficking between cytosol and mitochondria, a role that has been recently questioned by genetic inactivation studies[138,139]. A first indication that TSPO might belong to the PTP complex came from the effect of specific TSPO ligands in modulation of the PTP channel activity[140]. In spite of these intriguing data, analysis of TSPO conditional knock-out mice showed the PTP onset is unaffected and indistinguishable from that of wild-type mice[141]. Today, it appears reasonable to conclude that the effect of benzodiazepines on the pore is rather mediated through their interaction with the F-ATP synthase, which is inhibited by several ligands of the TSPO[142].

1.5.3.2 Voltage-dependent anion channel (porin)

VDAC (also known as mitochondrial porin) is an OMM protein, expressed in three isoforms (VDAC1, -2 and -3) that acts as a gatekeeper for entry and exit of mitochondrial metabolites up to 5000 Da, thereby controlling mitochondrial diffusion of metabolites[143]. The findings supporting its inclusion in the PTP model were (i) that purified VDAC1 forms a channel in lipid bilayer with a conductance similar to that of the PTP[144]; (ii) that VDAC appears to preferentially localize at the contact sites with the IMM, creating a "contact site"[145]; and that (iii) VDAC has been found to co-purify with ANT and TSPO, other two putative pore components[146]. However, the characterization of VDAC1$^{-/-}$ mice (VDAC1 is the major protein isoform) revealed that the PTP still forms and retains identical properties compared to those of wild-type mice[147]. Moreover, studies carried out with cells lacking all of the three isoforms revealed no major alterations in channel formation and regulation, strengthening the conclusion that VDAC is not a component of the PTP[148].

1.5.3.3 Adenine nucleotide translocator

ANT is the most abundant IMM protein, expressed in several isoforms, whose primary function is the exchange of ATP and ADP, which in energized mitochondria catalyzes the efflux of ATP supplying the substrate and removing the product. Evidence for its contribution to PTP formation came from pore inhibition by adenine nucleotides and from its peculiar sensitivity to the ANT inhibitors atractylate and bongkrekate, which act as PTP inducer and inhibitor, respectively[149]. Another indication that ANT may be a component of the PTP came from the observation that bovine ANT reconstituted in liposomes displays a high-conductance channel activity responsive to Ca^{2+} but insensitive to CsA[150]. However, mitochondria from conditional knock-out individuals for both mouse isoforms (ANT1 and ANT2) still display oxidant-and CsA-sensitive PTP opening that requires a higher matrix Ca^{2+} threshold and is insensitive to ADP and atractylate[151]. Thus, experimental data based on genetic manipulation of this protein suggest that ANT may be involved in the regulation of the pore but certainly not be a core component of the channel.

1.5.3.4 Hexokinase KII

Hexokinase (HK) II catalyzes the first, rate-limiting step of glucose metabolism by converting glucose into glucose-6 phosphate. The enzyme has been found attached to the OMM, docked to

VDAC, and considered to have an important role to keep its integrity, preventing the release of pro-apoptotic factors. It was originally thought to be a key regulator of the PTP because of its interaction with VDAC and because its detachment from the OMM induced PTP opening and cell death in tumor cell models[152] and in cardiomyocytes. However, it remains still unclear how the interaction of HK II with the OMM may affect the PTP[153].

1.5.3.5 Phosphate carrier

The phosphate carrier (PiC) belongs to the family of mitochondrial carriers and is responsible for the transport of Pi across the IMM, which is critical for the synthesis of ATP as well as for Ca^{2+} uptake. PiC has been suggested to be an inner-membrane component of the PTP because it can form channels in lipid membranes[154]. Moreover, PiC has been reported to have a CsA-sensitive CyP D binding site and to be modified by oxidative stress and PhAsO consistently with their effect on PTP opening[155]. Moreover, from additional biochemical studies, it emerged that inhibitors of the pore such as NEM and Ub_0[156] are able to block the activity of this carrier. However, considering the relationship between Pi and Ca^{2+} transport, whether these compounds inhibit the PTP directly or via an overall alteration of matrix Ca^{2+} remains hard to be sorted out. Only the genetic manipulation of PiC might shed light on its contribution in PTP formation. Recently, the very first knock-out of PiC has been carried out in a mouse model with an inducible cardiomyocyte-specific system[157]. Resulting data showed that cardiac mitochondria depleted of PiC were still able to undergo the PT, although with an overall desensitization to Ca^{2+}. This strongly indicates that PiC is not an essential component of the PTP but may rather act as a regulator.

1.5.3.6 Cyclophilin D

The peptidyl-prolyl-*cis-trans* isomerase (PPIase) CyP D is a mitochondrial member of the cyclophilin family, PPIases that assist in protein folding. CyP D is encoded by the *Ppif* gene[158]. The enzymatic activity of CyPs is inhibited by cyclosporine A (CsA), an immunosuppressant drug. After binding cytosolic CyP A, the CsA-CyP A complex binds to, and inhibits the phosphatase activity of calcineurin (calcium-calmodulin-activated serine/threonine-specific protein phosphatase), thus preventing the transcription of genes involved in cell growth[159]. The first evidence that CyP D is involved in the control of PTP opening came from the fact that CsA prevents mitochondrial Ca^{2+}-

induced Ca^{2+} release[160] and swelling[126,145] at concentrations very similar to those required for the inhibition of the CyP D PPIase activity[161]. Very intriguingly, CyP D has also been demonstrated to bind the anti-apoptotic protein Bcl2 in a CsA-sensitive manner, linking this protein directly to the cell death pathway likely via the PTP[162]. Together with CsA, other CyP targeting drugs have been successfully tested in pharmacological experiments to prevent PTP opening such as NIM-811[163] and Debio-025[164]. However, the most convincing demonstration that CyP D plays a role in PTP modulation was obtained from the genetic ablation of the *Ppif* gene (which encodes CyP D). Isolated mitochondria from *Ppif*$^{-/-}$ mice still showed the formation of the PTP with the same properties of the wild-type species, consistent with the fact that CyP D is a PTP modulator rather than a structural component[165,166]. The only difference was that PTP opening in CyP D null mitochondria required about twice the Ca^{2+} load of wild-type mitochondria, much like the after treatment of the latter with CsA. As expected, there was no effect of CsA in CyP D null mitochondria confirming beyond reasonable doubt that the effect of the drug is mediated by CyP D. Further studies carried out by Basso et al. showed that the effects of CyP D ablation and CsA treatment on the pore were dependent on the presence of Pi[167]. In mitochondria lacking CyP D, low (submillimolar) concentrations of Pi inhibit pore opening, suggesting the presence of an additional inhibitory binding site for the anion.

A finding that turned out to be crucial for the PTP field was published in 2009, when Giorgio et al. discovered that CyP D interacts with the lateral stalk of F-ATP synthase[168]. The binding required Pi and led to a decrease of F-ATPase activity of about 30%, while treatment with CsA displaced CyP D from its binding site and fully restored the enzymatic activity. Following this finding, in 2013, the same Authors were able to show (i) that F-ATP synthase purified from bovine heart mitochondria forms Ca^{2+}-activated, high-conductance channels with many features of the PTP and (ii) that CyP D interacts with OSCP in a region overlapping with helices 3 and 4, which is the same binding region of Bz423, a pore agonist that also binds TSPO[48].

1.5.4 New insights on PTP structure: Channel formation by F-ATP synthase

In the last three years, research in the field has made major steps forward in understanding and defining the molecular nature of the PTP.

In 2013, our group was the first to provide evidence that dimers of F-ATP synthase from bovine mitochondria form the PTP[44]. The direct demonstration was that gel-purified dimers inserted in lipid bilayer form a channel, with a conductance of 500-pS, in response to Ca^{2+}, PhAsO and Bz-423. Remarkably, the channel activity could be fully inhibited by Mg^{2+}/ADP and by the F-ATP synthase

inhibitor AMP-PNP (a non-hydrolyzable ATP analog). Furthermore, the measured conductance closely matched that defined by electrophysiological analysis of the PTP[169,170], basal conductance being about one-half of the "full-conductance" pore. Notably, the dimer preparation was devoid of any VDAC or ANT. Another important aspect is the fact that the monomeric form of the enzyme was not able to create a channel in spite of the same overall subunit composition, suggesting that the pore may form at the interface between two monomers. The proposed model[171] (**Figure 12**) suggests that the transition between close/open states of the channel is promoted by CyP D binding to OSCP, which would cause a conformational change of the enzyme increasing the accessibility of Me^{2+} to catalytic site. In the presence of adequate matrix [Ca^{2+}], Ca^{2+} occupancy would cause a conformational change triggering the PT[122]. The accessibility of Ca^{2+} binding site would be increased also by thiol oxidation and counteracted by thiol reduction. Ions and solutes permeation would then occur at the interface between the two monomers.

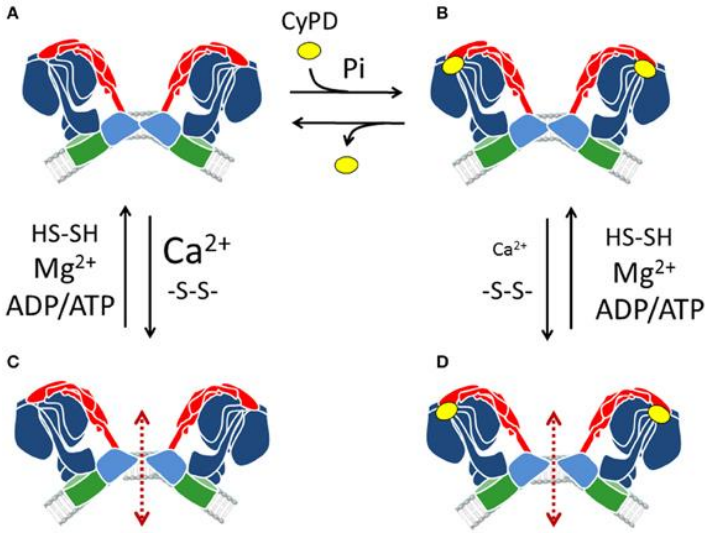

Figure 12. Transition between close/open states of F-ATP synthase dimers as PTP.
F-ATP synthase dimers (A) can undergo PTP formation when Ca^{2+} rather thanMg^{2+} is bound, possibly at the catalytic sites, in a reversible process favored by thiol oxidation (C). Binding of CyP D, which is favored by Pi (B) would increase the accessibility of the metal binding sites, allowing PTP formation at lowerCa^{2+} concentrations (as depicted here by a smaller face type)(D).Adenine nucleotides counteract PTP formation in synergy with Mg^{2+}. Red arrows denote the hypothetical pathway for solute diffusion between two F_O subunits; from[171].

The precise site of channel formation within the F-ATP synthase is still a matter of debate. Recently, Jonas and co-workers provided evidence that liposomes-reconstituted *c*-ring displayed Ca^{2+}-activated currents with properties similar to those described for purified dimers[172]. They suggested that channel opening requires displacement of F_1, whereas its closure is mediated by CsA, suggesting a binding site for CyP D in the *c* subunit, as well as by β subunit alone, but this proposal appears not to explain regulation by most PTP effectors that are unlikely to be accommodated by the *c* subunit[122].

1.5.5 Evolutionary conservation of the PTP among species

Other than in mammals, occurrence of the PT has been demonstrated in, fish, amphibians, in the fruit fly *Drosophila melanogaster*, and in plants, suggesting that this pathway has been evolutionary conserved[173]. Until recently, it was not clear whether the mitochondrial permeability changes detected in all these organisms could be ascribed to the same molecular entity. Studies carried out in zebrafish (*Danio rerio*) revealed the existence of a permeability transition stimulated by oxidative stress and requiring matrix Ca^{2+} that has all the regulatory features defined for the PTP in mammals[174]. Another model organism in which mitochondrial Ca^{2+} homeostasis and PT has been studied in detail in our laboratory is *Drosophila melanogaster*. Here, Ca^{2+} is rapidly transported within mitochondria through a RR-sensitive mechanism, whereas the release is mediated via a Ca^{2+} induced pathway insensitive to RR and CsA, but inhibited by Mg^{2+} and Pi[175]. Ca^{2+} release is matched by depolarization but, at variance from the case of the PTP, is not accompanied by increased in mitochondrial permeability to solutes, including K^{+} and Cl^{-}. It had been suggested that the "PTP" of *D. melanogaster* may have a smaller size[175] and that lack of inhibition by CsA is due to the lack of a mitochondrial CyP D as expression of the human species sensitized the *Drosophila* pore to Ca^{2+}, suggesting that (i) the contribution of CyP D to pore regulation would have appeared later during evolution, although (ii) the molecular identity of the channel has been conserved among species. Notably, in the fruit fly Pi acts as an inhibitor rather than an activator (as is instead the case in mammals), probably because of the lack of CyP D. Further studies in asolectin-incorporated F-ATP synthase dimers from *D. melanogaster* showed that they generate a Ca^{2+}-and -oxidant activated channel with a conductance of a mere 53 -pS, which is much smaller than the 500 -pS of the mammalian PTP)[176]. This result supports the evolutionary conservation of the pore and perfectly matches the predictions of previous studies on the mitochondrial Ca^{2+}-induced Ca^{2+} release of *D. melanogaster* mitochondria[175]. The occurrence and properties of the yeast PTP are covered in detail below.

1.6 *Saccharomyces cerevisiae* as model organism

The budding yeast *S. cerevisiae* is a widely used unicellular eukaryotic organism also used as a model system in a variety of research fields. Yeast is inexpensive, easy to grow and manipulate, and the first eukaryote whose genome was completely sequenced. Thus, a wide array of molecular and post-genomic techniques is available, explaining why yeast is a forerunner in large-scale screening approaches e.g. whole genome deletion and over-expression libraries[177,178]. Moreover, many signaling pathways are conserved between yeast and mammals, providing an often useful system for the dissection of molecular mechanisms relevant to the physiology and pathophysiology of mammals and often to onset of human pathologies.

1.6.1 Yest life cycle

S. cerevisiae cells grow rapidly, doubling every 100 min or so through a budding process whereby a mother cell gives rise to an ellipsoidal daughter cell, made entirely by new cell surface material (at variance from fission, in which the mother cell divides into two daughter cells) (**Figure 13**)[179]. Therefore, the daughter cell is initially smaller than the mother and must increase its size before proceeding with the duplication of chromosomes and further division. In stress conditions, or in starvation, yeast cells can transiently arrest in G1 and stop proliferating until the environment changes and nutrients become available again. Another factor that can induce this transient block in G1 phase is the mating process. Yeast exists in three different cell types, detectable during cell cycle phases. The haploid form has two mating types (a and α) that efficiently mate with one another when they are close enough. Indeed, they secrete specific pheromones (a and α factors), small peptides that bind corresponding surface receptors and activate a signaling cascade required for the mating preparation. These pheromones promote cell cycle arrest in G1, synchronizing cells in the same phase, and synthesis of proteins involved in the mating. As a result the mating process, accompanied by cell and nuclear fusion, gives rise to a diploid cell, the third specialized cell, which contains one nucleus. This zygote has its own distinctive shape and generates daughter diploid cells through mitosis. At variance from the haploid cells, the diploid is not able to mate with any mating type but instead it can undergo meiosis (also named sporulation) to produce four haploid cells (spore) that are wrapped up into a specialized compartment called ascus. One requirement for the initiation of sporulation is the complete starvation from both nitrogen and carbon sources.

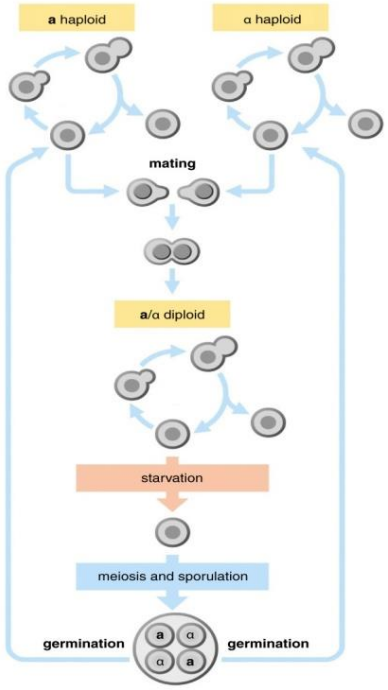

Figure 13. The life cycle of a unicellular yeast.
The budding yeast *Saccharomyces cerevisiae* is an example of a sexual unicellular yeast, with haploid cells of two mating types, a and α, that mate when pheromone produced by each cell is recognized by pheromone receptors expressed on the opposite cell type. This event stimulates fusion of the two cells to produce an a/α diploid cell that grows vegetatively when nutrients are plentiful, but upon starvation undergoes meiosis to produce four haploid spores that can remain dormant until conditions improve; from[236].

1.6.2 Cell growth and metabolism

As already mentioned, *S. cerevisiae* can be easily kept in culture both in agar plates and in liquid medium under a variety of conditions that allow modulation of its physiological response. Generally, yeast growth curve can be subdivided in 4 major phases that can be followed by measuring the optic density of the culture at 600 nm[180] (**Figure 14**).

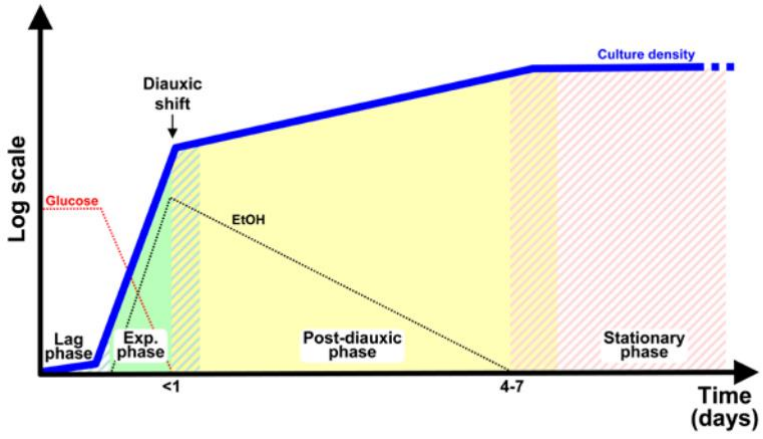

Figure 14. Growth phases of yeast cell.
Yeast growth can be divided into 4 phases. Lag phase: period of slow proliferation in which cells adapt to the new growth condition. Exponential phase: high-rate proliferative period, supported by fermenting glucose to ethanol (EtOH). Upon nutrient depletion, cells transiently arrest growth to adjust metabolism from fermentation to respiration (diauxic shift). Post-diauxic phase: cells proliferate slower by consuming the EtOH produced during the preceding phase. Stationary phase: upon EtOH depletion, cells stop to grow and start to die; from[180].

Once cells are inoculated in fresh medium, containing all nutrients and the carbon source, they exhibit an initial period of slow proliferation called the **lag phase**. Then, a rapid metabolic change occurs and cells start proliferate at very high rate by fermenting glucose to ethanol (**exponential phase**). Indeed, despite the presence of oxygen, glucose is preferentially processed by alcoholic fermentation, rather than being fully oxidized to water and carbon dioxide through the TCA cycle. This mechanism may have evolved as a defense system because, although being a less efficient energy-conserving process, fermentation can proceed at much faster rates, allowing yeast to consume quickly all available sugar at the expenses of other competitive organisms. Moreover, the ethanol generated could cause an overall toxic environment for other organisms, thus favoring the survival of yeast cells.

Upon nutrient exhaustion, yeast cells transiently stop growing and adjust their metabolism switching from fermentation to the respiratory mode (diauxic shift). Cells then start to proliferate again, albeit at a slower rate, by consuming all the ethanol accumulated in the medium, which provides reducing equivalents to the RC (**post-diauxic phase**). When ethanol is exhausted, cells enter into a non-proliferating, quiescent state (**stationary phase**) characterized by decreased rates of transcription and protein synthesis, severely reduced expression of genes encoding for ribosomal proteins and increased transcription of stress-responsive genes, accumulation of storage carbohydrates, condensation of chromosomes and onset of autophagy.

1.6.3 Yeast as model for mitochondrial diseases

Mitochondrial diseases include a wide, heterogeneous group of disorders caused by an overall dysfunction of the mitochondrial respiratory chain or F-ATP synthase, due to mutations of genes encoded by either nuclear or mitochondrial (mt) DNA[181]. Concerning mtDNA, many mutations have been found in genes encoding for subunits of complex I, III and IV as well as in two subunits of F-ATP synthase (subunit a and A6L) and in ribosomal/transfer RNA genes. Notably, each cell contains thousands of mtDNA copies that can be identical (condition of homoplasmy). However, individuals with mitochondrial disorders resulting from mutations of mtDNA can harbor a mixture of mutant and wild-type mtDNA within each cell (condition of heteroplasmy). For a disease to manifest, the mutated form must exceed a critical threshold that varies depending on the mutation. These factors can explain the enormous variability of clinical manifestations of mtDNA diseases, which depend on the percentage of mutated mtDNA, which is different among individuals and tissues as well. Indeed, while some mitochondrial disorders only affect a single organ (e.g., the eye in Leber hereditary optic neuropathy, LHON), many involve multiple organ systems and often present themselves with

prominent neurologic and myopathic features. Many individuals with a mutation of mtDNA display a cluster of clinical features that fall into a discrete clinical syndrome, such as mitochondrial encephalomyopathy with lactic acidosis and stroke-like episodes (MELAS), neurogenic weakness with ataxia and retinitis pigmentosa (NARP) and Leigh syndrome (LS). On the other hand, nuclear DNA mutations have been found in genes encoding for proteins involved in mtDNA maintenance and also in subunits of RC or assembly factors.

S. cerevisiae contains roughly 1,000 mitochondrial proteins and almost all mtDNA genes are conserved between yeast and humans. One relevant difference is at the level of complex I, which in most yeast strains is a non-proton-translocating NADH dehydrogenase (Ndi1p) with the electron acceptor site at the inner side of the IMM and two additional NADH dehydrogenases (Nde1p, Nde2p) on the external side of the IMM. They deliver electrons at the level of ubiquinone, and from this point the respiratory chain and OXPHOS system of *S. cerevisiae* is similar to the mammalian system[182]. Yeast mitochondria are the major source of ATP when cells are grown in a non-fermentable carbon source (e.g. glycerol), condition when mitochondrial function is strictly required for cell proliferation. However, as already mentioned, yeast is able to proliferate through fermentation (in the presence of glucose) without mitochondrial activity and consequently, all mutations of the mitochondrial genome can be studied without cell lethality. This property makes yeast a formidable tool and a model for studying mitochondrial diseases. Indeed, pathogenic mutations that lead to mitochondrial dysfunction are able to be maintained in yeast as long as a fermentable carbon source is available. Furthermore, mutants with dysfunctional mitochondria are unable to grow (or grow very slowly with a phenotype also called *petite*) in media without a fermentable carbon source. Additionally, mtDNA can be inserted through transformation into a specific strain lacking mtDNA (the ρ_0 strain). This allows a defined mutation identified in patients to be studied in the context of a unique host nuclear genetic background, singularly or even in combination with other mutations. Unlike mammalian cells, yeast become homoplasmic within a few generations, thus overcoming the problems of heteroplasmy typical of mammalian cells.

Only three F-ATP synthase subunits are encoded by the mitochondrial genome, Atp6, Atp8, and Atp9, all of which are components of F_o sector. Mutations in *ATP6* present with a range of phenotypes, from severe infantile maternally inherited Leigh syndrome (MILS), to adult onset NARP[183]. Pathogenic mutations have been modeled in yeast to better understand the mechanism of F-ATP synthase dysfunction. The *ATP6 L183R* mutant decreases ATP synthesis by 90%, and decreases COX content by 95%. Despite the functional defect, F-ATP synthase assembles properly, indicating that the defect is catalytic in nature. When the same residue was mutated to Pro, ATP synthesis was only reduced by 40–50%, and COX abundance was decreased. BN-PAGE analysis showed an increased abundance of

ATP synthase subcomplexes, indicating that the stability of the F-ATP synthase is reduced when this mutation is present.

1.6.4 Ca^{2+} homeostasis in yeast

As already mentioned, Ca^{2+} ions are fundamental key regulators of a wide variety of processes in eukaryotic cells. Its signaling pathway is triggered by activation of either ion channels or G protein-coupled receptors that are upstream to kinase cascades. The physiological role of Ca^{2+} signaling ranges from the modulation of enzymes and components of cytoskeleton to that of ion channel permeability, making it particularly relevant in cellular processes e.g. muscle contraction, neuronal transmission and cell-cycle progression. In yeast, in addition to cell growth, Ca^{2+} controls mating between MATa and MATα cells that secrete specific pheromones able to increase its cytosolic concentration, leading to cellular changes required for agglutination[184]. Moreover, a key role of Ca^{2+} signaling has been attributed in the response of yeast cells to an alkaline environment[185] as well as to the hypotonic shock through the activation of MAP kinases[186]. Thus, cytosolic free Ca^{2+} concentration in yeast cells should be finely regulated and maintained at low levels (50-200 nM)[187], through its storage in several compartments e.g. vacuole, endoplasmic reticulum (ER), Golgi apparatus and likely by mitochondria as we will discuss later (**Figure 15**). Extracellular Ca^{2+} influx is mainly due to the plasma membrane voltage-gated Ca^{2+} channel, also referred as Cch1/Mid1 complex, that activates upon several stimuli e.g. depolarization, hypotonic shock and pheromone stimulation[184,188]. Once entered inside the cytosol, Ca^{2+} ions can bind the sensor calmodulin, creating a complex able to induce phosphatase calcineurin, promoting the activation of specific set of genes required for cell proliferation and for the response to pheromone[189]. On the other hand, intracellular Ca^{2+} is rapidly sequestered by vacuole, which is the major store, through the Ca^{2+} ATPase Pmc1[189] and the high capacity, low-affinity Ca^{2+}/H^{+} exchanger Vcx1[190]that might link Ca^{2+} homeostasis with the regulation of intracellular pH. Furthermore, the contribution of ER/Golgi as alternative Ca^{2+} storage have been recently described by D'hooge et al., that analyzed the importance of this transport system following specific stimuli[191].

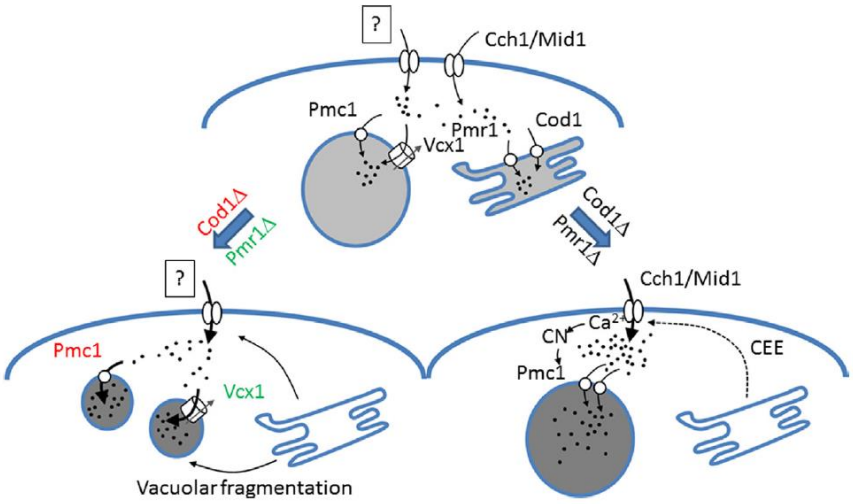

Figure 15. Ca^{2+} homeostasis in *S. cerevisiae*.
Upper scheme: In wt yeast extracellular Ca^{2+} enters the cytosol through Cch1/Mid1 channel complex and an unknown transporter. Cytosolic [Ca^{2+}] is sequestered by vacuole through Vcx1 and Pmc1 and by ER/Golgi via Pmr1 and Cod1. To account for increased Ca^{2+} influx in Pmr1 or Cod1 cells, two compensatory mechanisms have been proposed. Right lower scheme: Plasma membrane Cch1/Mid1 channels become activated resulting in increased levels of cytosolic Ca^{2+}, activation of calcineurin (CN), a CN-induced compensatory increase in expression of Pmc1 and hence increased vacuolar Ca^{2+} uptake. Left lower scheme: yeast cells activate a mechanism that enhances Ca^{2+} influx through not-yet identified plasma membrane Ca^{2+} transporter, which in turn stimulates vacuolar Ca^{2+} uptake and induces vacuolar fragmentation or vice versa; from[192].

1.6.4.1 Mitochondrial Ca^{2+} in *S. cerevisiae*

In mammals, mitochondria play a crucial role in cytosolic Ca^{2+} homeostasis through an array of transport systems. Yeast mitochondria do not possess an MCU complex[193] and therefore their potential role in Ca^{2+} homeostasis is usually not given much consideration. However, also in yeast the Ca^{2+} electrochemical gradient favors Ca^{2+} accumulation with the same predicted equilibrium distribution as that of mammalian mitochondria. To quote the original conclusions of Carafoli and Lehninger "We consider it likely that all mitochondria, whatever the cell type, possess the electrochemical capacity for moving Ca^{2+} across the membrane. This capacity cannot be expressed, however, unless a pathway for trans-membrane movement of Ca^{2+} is available, either through the occurrence of a specific Ca^{2+} carrier system or through simple physical permeability of the mitochondrial membrane to Ca^{2+}" [194]. The emergent hypothesis is that the driving force is so large that Ca^{2+} uptake could be relevant even if it occurred through a leak pathway rather than through a specific transport system. Consistently (i) *S. cerevisae* mitochondria have a Ca^{2+} content of 8-9 ng atoms/mg protein, which is close to that of rat liver mitochondria[194], and (ii) electrophoretic Ca^{2+} uptake coupled to H^{+} ejection can be easily measured in isolated *S. cerevisiae* and *C. utilis* mitochondria when the cation is added at concentrations of 1-10 mM[195]. It is of note that respiration-driven uptake is observed with Ca^{2+}, Sr^{2+} and Mn^{2+} but not with Mg^{2+}, suggesting that cation

accumulation could be taking place through a low-affinity system whose discrimination for the transported species is strikingly similar to that of the MCU[87]. It is also interesting to recall that yeast mitochondria are endowed with a very effective $2H^+/Ca^{2+}$ antiporter activated by fatty acids that mediates mitochondrial Ca^{2+} release[196]. Like in mammals, the antiporter could prevent excessive mitochondrial Ca^{2+} accumulation but also allows rapid mobilization of the matrix Ca^{2+} pool following activation of phospholipases and perhaps other relevant pathophysiological stimuli.

In contrast to the general assumption that yeast mitochondria lack a specific Ca^{2+} transport system machinery, a high-capacity Ca^{2+} uptake system driven by the membrane potential and stimulated by polyamines and ADP has been described in the yeast *E. magnusii*[197,198]. Rather than acting as an inhibitor, and at variance from the mammalian MCU, ruthenium red affected Ca^{2+} transport only marginally or even stimulated it under specific conditions[199]. Taken together, these findings suggest that a specific Ca^{2+} transport system may exist also in yeast mitochondria, and that this putative system could be expressed at varying levels in different yeast strains. This might explained more recent studies on the role of Ca^{2+} in regulating mitochondrial functionality as well as initiation of mitochondrial-dependent cell death. For instance, Gordon Lindsay and Coworkers observed a clear effect of Ca^{2+} ions on the activity of the pyruvate dehydrogenase complex (PDC)[200], responsible for the conversion of pyruvate to acetyl-CoA. From data obtained with isolated mitochondria, it emerged that the activity of PDC, previously inhibited with ATP, could be restored in a Ca^{2+}-dependent manner, suggesting that mitochondrial Ca^{2+} fraction plays a key role in controlling cellular metabolism. Moreover, occurrence of Ca^{2+} uptake in *S. cerevisiae* mitochondria (if over-threshold) might be linked with apoptosis initiation via the activation of the PT pathway, as occurs in mammals.

1.6.5 Permeability transitions in *S. cerevisiae*

Several studies suggested that yeast mitochondria might present different independent permeability pathways with peculiar features and modulations. From electrophysiological analysis, the presence of a number of channels with different conductances and possibly unique cellular functions emerged. In a very first work of Szabò et al. the patch-clamp technique applied to *S. cerevisiae* mitochondria led to the discovery of a multiple conductance channel (from 100 to 600 -pS), that was insensitive to CsA and ADP, two major negative regulators of mPTP[201]. Conflicting results came from data obtained from Lohret and Kinnally, who in yeast mitoplasts measured a large channel characterized by multiple substates (predominantly with transitions of 300-500 -pS) with a peak of conductance of 1-1.5 -nS, comparable to that found in mammalian mitoplasts[202,203].

1.6.5.1 Respiration and ATP-induced pathways

The first evidence that yeast mitochondria may possess a PTP-like high conductance channel was obtained in studies of Pi transport in an industrial baker's yeast strain, Yeast Foam[204]. Mitochondria suspended in a K^+-based medium showed respiration-dependent large-amplitude swelling insensitive to mersalyl (and thus independent of the Pi carrier) and fully inhibited by antimycin A. Subsequent studies demonstrated that a similar pathway was also present in laboratory yeast strains, where it allowed solute permeation with a cutoff of about 1.5 kDa[205,206]. The characterization and interpretation of the permeability transition in yeast became even more complicated with the observation that the addition of exogenous ATP to isolated mitochondria causes a large-amplitude swelling[207–210]. Prieto and Coworkers postulated the existence of an energy-dissipating mechanism, which might play a role in scavenging excess reducing equivalents and keeping the redox balance during aerobic growth[207]. Indeed, they showed that near physiological cytosolic concentrations of ATP induce a proton-permeability pathway in mitochondria, which uncouples respiration from ATP synthesis, finally causing matrix swelling. In this system, Pi acts as negative modulator of the effect of ATP, probably by competing with the nucleotide at an external site of the channel since its effect is not prevented by mersalyl.

1.6.5.2 The yeast permeability transition

In 1997, Jung et al. solved many controversies about the existence of the yPTP, by demonstrating that respiratory substrates or exogenous ATP induce mitochondrial swelling, which is prevented by ADP but not by CsA[206]. At variance from the mammalian PTP, the "yPTP" (i) was unaffected by matrix Ca^{2+} even when uptake of the cation was made possible by the ionophore ETH129; (ii) was insensitive to Mg^{2+} and ADP; (iii) was insensitive to CsA in spite of the presence of a CsA-sensitive matrix CyP[211]; and (iv) was inhibited rather than induced by Pi[206,212]. A PT could be detected in strains lacking VDAC or the ANT, both of which were considered to be essential components of the PTP in mammals, but the demonstration of a CsA-sensitive PTP in mammalian mitochondria lacking ANT and VDACs has refuted the paradigm that these proteins are essential for the PT (reviewed in[213]). Many apparent discrepancies with the mammalian PTP have been resolved in recent years, although interpretation of the experiments can be complicated by the occurrence of multiple permeability pathways in yeast mitochondria. The Ca^{2+}-dependence of the yeast PTP was demonstrated beyond doubt in protocols where Ca^{2+} uptake was permitted by addition of the

ionophore ETH129 and the concentration of Pi was optimized to prevent its inhibitory effect on the pore, which would otherwise mask the inducing effects of Ca^{2+} itself[214]. An open issue was the insensitivity to CsA together with the effect of Pi, which in yeast acts an inhibitor rather than an activator. This issue could be explained by the fact that (i) the effect of CsA is limited to the presence of its target (CyP D) and (ii) Pi becomes a PTP inhibitor in CyP D KO mitochondria[167]. Finally, it is now clear that PTP opening can occur in the absence of CyP D also in mammalian mitochondria, as demonstrated both after genetic ablation of CyP D[165,166] and in cells and tissues where CyP D is expressed at low levels[215], conditions under which pore opening is obviously insensitive to CsA.

Table I summarizes the features of the PTP in *S. cerevisiae, D. melanogaster* and *M. musculus* as determined in isolated mitochondria. Conserved general features are (i) the requirement for matrix Ca^{2+} and facilitation by oxidants; and (ii) inhibition by Mg^{2+} (which competes with Ca^{2+} for a matrix binding site) and adenine nucleotides. The main difference concerns the involvement of CyP D in PTP regulation that in turn confers the sensitivity to CsA and determines the role Pi.
In summary, the key features of the PTP may have appeared early in evolution and their potential role in yeast programmed cell death can be addressed with the powerful tools of genetics.

Table I. Features of the PTP in *M. musculus*, *D. melanogaster* and *S. cerevisiae*.

Specie	PTP	Effect of Ca^{2+}	Matrix CyP	Effect of CsA	Effect of Pi	Effect of oxidants
M. musculus	YES	YES	YES	YES	ACTIVATION	ACTIVATION
D. melanogaster	YES	YES	NO	NO	INHIBITION	ACTIVATION
S. cerevisiae	YES	YES*(ETH129)	YES	NO	INHIBITION	UNKNOWN

1.6.6 Programmed cell death in yeast: Ca^{2+} and ROS contribution

Occurrence of programmed cell death (PCD) in yeast and its role in population dynamics and aging is increasingly understood[216,217]. Remarkably, many of the signaling events of the mammalian intrinsic (mitochondrial) pathway to apoptosis are present in yeast[218]. These include increase of intracellular [Ca^{2+}] and reactive oxygen species (ROS), which are causally involved in yeast PCD induced by oxidative stress itself[219], acetic acid[220], pheromone or amiodarone[221,222], ethanol[223], osmotic[224] and ER stress[225]. As in mammals, increased intracellular [Ca^{2+}] precedes the surge of ROS levels, cristae remodeling, mitochondrial depolarization, ATP depletion, matrix swelling and outer

membrane permeabilization eventually leading to release of cyt *c* and other proapoptotic proteins[216–218] through the opening of an unselective channel. In yeast, the link between increased intracellular [Ca^{2+}]/ROS and outer mitochondrial membrane (OMM) permeabilization remains puzzling. It is remarkable that the mechanistic basis for these changes has not been fully clarified yet, and it is legitimate to wonder whether the striking analogies with the matching consequences of PTP opening in mammals are just a coincidence.

An important advance linking yeast PCD to the Bcl-2 inhibitable Bax/Bak pathway for OMM permeabilization to cyt *c* was the identification of Ybh3, a yeast protein possessing a functional Bcl-2 homology domain 3[226]. Upon treatment with lethal stimuli, Ybh3 translocates to mitochondria and triggers apoptosis that is accompanied by mitochondrial depolarization and release of cyt *c* and other proapoptotic proteins in a process that involves the Pi carrier Mir1 and the core subunit of ubiqinol-cytochrome *c* oxidoreductase Cor1. The mechanism(s) through which Ybh3 translocation causes the mitochondrial changes and intermembrane protein release, and whether the PTP could have been involved, remains unclear particularly because the site of integration of Ybh3—whether the IMM or the OMM—was not defined. It is interesting, however, that the stimulus used to trigger apoptosis was acetic acid, which causes increased ROS production[220] and may therefore require a functional respiratory chain and thus Cor1. The requirement for Mir1, on the other hand, may depend on the Pi-requirement for mitochondrial Ca^{2+} uptake which is stimulated up to 8-fold by Pi [195]. In this respect, it is very intriguing that cell death induced by acetic acid was greatly reduced in ρ_0 cells (where no mitochondrial respiration hence ROS production takes place) and in *ATP10* mutants (which cannot assemble the F-ATP synthase)[220]. One of the most relevant studies on the involvement of mitochondria in yeast PCD was performed using the pheromone α factor or amiodarone, agents known to induce an increase of cytosolic [Ca^{2+}] and cell death with superimposable features[222]. Cell death occurred by apoptosis and required a functional respiratory chain, as ρ_0 cells were extremely resistant; and was linked to ROS formation, as it could be protected by antioxidants and by the protonophore FCCP. Amiodarone had complex effects on respiration in intact yeast cells, but consistently increased mitochondrial respiration and ROS production which preceded mitochondrial depolarization. The Authors suggest that the increased respiration was caused by Ca^{2+}-dependent stimulation of NADH dehydrogenase from the intermembrane space, sequentially causing an increase of membrane potential and of ROS production, followed by inner membrane permeabilization and cell death[222]. The involvement of Ca^{2+} in the mitochondrial-dependent apoptotic pathway has been elucidated also by the work of Kajiwara and Coworkers[225]. They investigated the impact of sphingolipid metabolism in yeast cell death, since ceramide (a sphingolipid metabolite) is a second messenger acting during apoptosis initiation. The hypothesized mechanism

proposed that accumulation of sphingolipid precursors in the ER causes an overall stress of the organelle and the consequent release of sequestered Ca^{2+} via Mid1/Cch1 channels. Increased cytosolic [Ca^{2+}] level in turn leads to ROS production, mitochondrial damage and release of proapoptotic factors.

We suspect that ROS-dependent depolarization in this and other paradigms was caused by PTP opening induced by oxidative stress and that this event could be a final common pathway in a variety of forms of yeast PCD (recently reviewed by Carraro and Bernardi, *paper in press,* see **Publication 2**).

1.7 Aim of the work

Considering the role of the PTP in Ca^{2+} homeostasis and cell death initiation, it is important to unravel the many open questions concerning its molecular structure and modulation. The goal of my PhD project was the definition and characterization of the *S. cerevisiae* PTP, to test the role of F-ATP synthase in channel formation and to begin a molecular dissection of the structural bases for the transition of this enzyme from an energy-conserving into an energy-dissipating device.

2. Materials and Methods

2.1 Biological Samples

2.1.1 Yeast strains and mutants generation

The *S. cerevisiae* strains BY4743 (4741/4742), as well as the mutants *ΔCPR3* (MATa, *his3Δ1, leu2Δ0, met5Δ0, ura3Δ0*), *ΔTIM11* (MATa, *his3Δ1, leu2Δ0, met5Δ0, ura3Δ0*) and *ΔATP20* (MATα, *his3Δ1, leu2Δ0, lys2Δ0, ura3Δ0*) were purchased from Thermo Scientific. Deletions were obtained through the substitution of genes with the KanMX cassette.

ΔTIM11ΔATP20 mutants were obtained by mating the *ΔTIM11* and *ΔATP20* strains and selecting the formed diploid by growth on SD (0.67% nitrogen base w/o amino acids, 2% dextrose) selective medium, containing the required nutritional supplements except methionine and lysine. Diploids were then induced to sporulate in 1% potassium acetate agar medium. Obtained tetrads were dissected and haploids were analyzed with semi-quantitative polymerase chain reaction (PCR) to detect null mutants for *TIM11* and *ATP20* genes.

Briefly, haploids were suspended in 20 mM NaOH, then incubated 10 min at 95°C and centrifuged 3 min at 13,000 x *g*. The surnatant contained genomic DNA that was added to the 25 µl PCR mixture as following:

- 12.5 µl GoTaq® Green Master Mix
- 10 µM FOR primer
- 10 µM REV primer
- 1 µl genomic DNA

The protocol used is described in **Table II**.

Cycle step	temperature	time	cycles
denaturation	95°C	2 min	1
denaturation	95°C	30 sec	
annealing	58°C	30 sec	35
extention	72°C	2 min	
final extention	72°C	5 min	1

The "wild-type" yeast strain MR6 (MATa ade2-1 his3-11, 15 trp1-1 leu2-3,112 ura3-1 CAN1 arg8::HIS3) and the derived mutant *ATP6 C23S ΔTIM11* was kindly provided by the laboratory of Dr. Roza Kucharczyk (University of Warsaw). *ATP1 C203S, ATP5 C100S* and *ATP4Δ1TM* mutants in *ΔTIM11ΔATP20* genetic background were generated by a stepwise procedure, i.e. knocking-out of

the target gene and complementing its function with the vector-expressed mutated form, as described in details in following paragraphs.

2.1.1.1 Gene deletion

Deletion of *ATP1*, *ATP4* and *ATP5* genes has been carried out by substituting the genomic sequence with the **His cassette** contained in the pFA6a-His3MX6 vector (**Figure 16**). The selection cassette was amplified by PCR, using specific primers for the vector, carrying at the 5' a sequence homologous to the immediately upstream and downstream sequences of target genes (45 bp). The following table (**Table III**) reports primers used for the so-called "inactivation" PCR.

Table III: Sequences of primers used for the "inactivation PCR". At 5' primers contain sequences (about 45 bp marked in black) homologous to the sequences of target genes immediately upstream the ATG codon (Delta 5) and downstream the TAA codon (Delta 3). At 3' primers contain sequences specific for pFA6a-HISMX6 vector (marked in light blue), allowing the amplification of HIS cassette.

Primer name	Sequence
ATP1 Delta 5	5'- CAAGAACAGTAACAAAATAAATAAAAAAAACACGCACATATAATACAGCTGAAGCTTCGTACGC
ATP1 Delta 3	5'- TTTTTGAGACGTACCTTATATTCATTTTTATTTTTTTAGTTCACAGCATAGGCCACTAGTGGATCTG
ATP5 Delta 5	5'- AACCGATTAGCAAGTTACCGCATTATTTTTAAACCGTGGACAATCCAGCTGAAGCTTCGTACGC
ATP5 Delta 3	5'- AAGTAACATCAAACGAGTTGAGCATATCCAACTATATTATTAACGGCATAGGCCACTAGTGGATCTG
ATP4 Delta 5	5'- AAGACTGACGAGAATTCAGTACCTCCTAAGTGCGCAAGAGATAAACAGCTGAAGCTTCGTACGC
ATP4 Delta 3	5'- CTTTTCTTTC ATTCTTGTCG CAGTTACTGT TGTGATTACT TCAATGCATAGGCCACTAGTGGATCTG

PCRs were performed in a 25 µl reaction mixture containing:

- 50 ng pFA6a-HISMX6 vector
- 5 µl 5X Colorless GoTaq® Flexi Buffer (Promega)
- 25 mM $MgCl_2$
- 10 mM dNTPs
- 10 µM FOR primer
- 10 µM REV primer
- 0.25 µl GoTaq® Flexi DNA Polymerase (Promega)
- H_20 (up to 25 µl)

The protocol used is described in **Table IV**

Cycle step	temperature	time	cycles
denaturation	95°C	2 min	1
denaturation	95°C	30 sec	
annealing	58°C	45 sec	35
extention	72°C	90 sec	
final extention	72°C	2 min	1

The obtained PCR products (1403 bp) were loaded into 2% agarose gel and checked with an electrophoretic run. Then, they were used for yeast high efficiency transformation that allows the substitution of target genes through homologous recombination events, following a modified version of the protocol described by[227].

Briefly, *ΔTIM11ΔATP20* diploids were inoculated in 5 ml YP medium containing 2% glucose (for each transformation), and incubated overnight on a rotator shaker (180 rpm) at 30°C. The next day the titer of cell culture was determined by measuring the OD at 600 nm. For a more efficient transformation, cell culture OD should be about 0.5-0.6 (7-8 x 10^6 cells ml^{-1}) that reflects a log phase of growth. Cells were harvested by centrifugation 3,000 x *g* for 5 min, washed once with sterile H_2O, pelleted again and finally suspended in 1 ml sterile H_2O. After a high speed centrifugation (30 sec at 13,000 x *g*), cells were suspended in 100 mM LiAc solution and incubated 15 min at 30°C, to start the permeabilization process. Cells were then pelleted again and added to 360 µl mixture containing:

- 240 µl PEG 3350 (50% (w/v))
- 36 µl LiAc (1 M)
- 20 µg/ml DNA carrier (previously boiled 5 min and kept immediately on ice)
- 10 µl PCR product
- Sterile H_2O

After vigorous vortexing, cells were incubated 30 min at 30°C and subsequently 20 min at 42°C (heat-shock). Then, cells were pelleted and added to YP medium containing 2% glucose for 3 hours growth in agitation (180 rpm). Finally, cells were centrifuged again, washed once with H_2O sterile and plated for 2/3 days at 30°C in SD selection medium containing all nutrients except His. Three or four of obtained clones were selected and checked for the presence of the deletion using a semi-quantitative PCR (previously described) and appropriate primers.

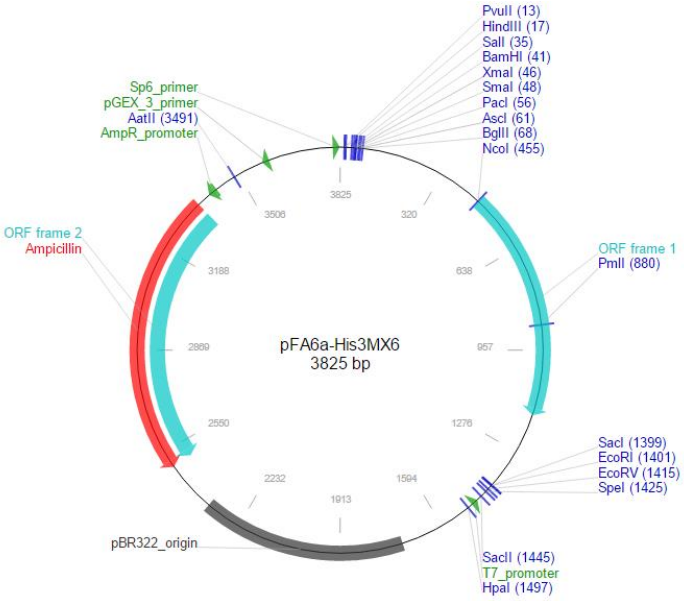

Figure 16. pFA6a-HIS3MX6 vector (3825 bp).

2.1.1.2 Gene cloning

BY4743 yeast genomic DNA was extracted with a standard protocol. 2 ml BY4743 culture (grown overnight at 30°C) was centrifuged 5 min at 13,000 x *g* and the pellet was suspended in 200 µl Lysis buffer containing 100 mMNaCl, 10 mMTris-HCl, 1 mM EDTA, 1% (w/v) SDS, 2% TritonX-100, pH 8, supplemented with 200 µl acid-washed glass beads. Then, further 200 µl SEVAG solution (containing Phenol, Clorophorm and Isoamyl alcohol, pH 8 at the ratio 25:24:1, respectively) were added and the pellet was mixed vigorously for 30 sec. A volume of 200 µl of TE buffer (10 mM Tris-HCl and 1 mM EDTA, pH 8) was added to cells that were vortexed and centrifuged 5 min at 13,000 x *g*. The supernatant was collected, vortexed with 1 ml EtOH 100% and incubated at -20°C for 2/3 h. After centrifugation at 13,500 x *g* for 20 min, the supernatant was discarded and the pellet suspended in EtOH 70%. After a further centrifugation at 13,500 x *g* for 10 min, pellet was dried at 65°C. Finally, DNA was diluted in 100 µl sterile H_2O, supplemented with RNAse and incubated 10 min at 37°C.

For *ATP1*, *ATP4* and *ATP5* genes cloning, the centromeric vector pFL38 (carrying the URA cassette) has been properly digested at the polylinker site with KpnI and BamHI restriction enzymes (**Figure 17**). Briefly, an appropriate amount of pFL38 was incubated with the two restriction enzymes in 1X NEB1 buffer, supplemented with 1 X BSA. Incubation steps were: 2h at 37°C and 20 min at 65°C. To check the efficiency and the quality of the digestion, the cut vector was evaluated through a 2% gel

agarose. For "cloning PCRs", specific primers have been designed for amplifying also promoter and terminal sequences (**Table V**): the FOR primers carried at the 5' a 45 bp length sequence homologous to the polylinker region of the vector containing KpnI restriction sites and a tail of 20 bp homologous to the DNA sequence 250/350 bp upstream the target gene, whereas the REV primer carried at 5' the recognition site of BamHI and a tail of 20 bp homologous to 150/250 bp downstream of target genes. The cut with the restriction enzymes was thought to maintain the reading frame of the coding sequence.

Table V: Sequences of primers used for the "cloning PCR". At 5', primers contain sequences (about 45 bp marked in light blue) of pFL38 polylinker region containing the BamHI (REV) (in red) or KpnI (FOR) (in purple) restriction sites. At 3', primers contain around 20 bp homologous to genomic region 250/350 bp upstream (FOR) or 150/250 bp downstream (REV) the target genes.

Primer name	Sequence
Atp1 (-350bp) FOR	5'- CACGACGTTGTAAAACGACGGCCAGTGAATTCGAGCTCGGTACCCCAATTCACTTTCTGAATAAG
Atp1 (+150 bp) REV	5'- TTACGCCAAGCTTGCATGCCTGCAGGTCGACTCTAGAGGATCCCCGGGTTATTGTTTGGCTGCAC
ATP5 (-350 bp) FOR	5'- CACGACGTTGTAAAACGACGGCCAGTGAATTCGAGCTCGGTACCCTGCCGTCGTCATAAAGTGGAC
ATP5 (+250 bp) REV	5'- TTACGCCAAGCTTGCATGCCTGCAGGTCGACTCTAGAGGATCCCCGTTTGCCTGGATACACGAAC
ATP4 (-250 bp) FOR	5'- CACGACGTTGTAAAACGACGGCCAGTGAATTCGAGCTCGGTACCCCTCTTCACCGCTCATTCGGA
ATP4 (+150 bp) REV	5'- TTACGCCAAGCTTGCATGCCTGCAGGTCGACTCTAGAGGATCCCCCAAACTGAACTCATAAGGCG

The PCRs were performed in 25 µl reaction mixture containing:

- 5 µl 5X KAPA High-Fidelity Mix (Kapa Biosystem)
- 0.75 µl dNTPs
- 10 µM FOR primer
- 10 µM REV primer
- 1 µl genomic DNA
- 0.5 µl KAPA High-Fidelity DNA Polymerase

The protocol used is described in **Table VI**

Cycle step	temperature	time	cycles
denaturation	95°C	2 min	1
denaturation	98°C	20 sec	
annealing	60°C	30 sec	35
extention	72°C	3 min	
final extention	72°C	3 min	1

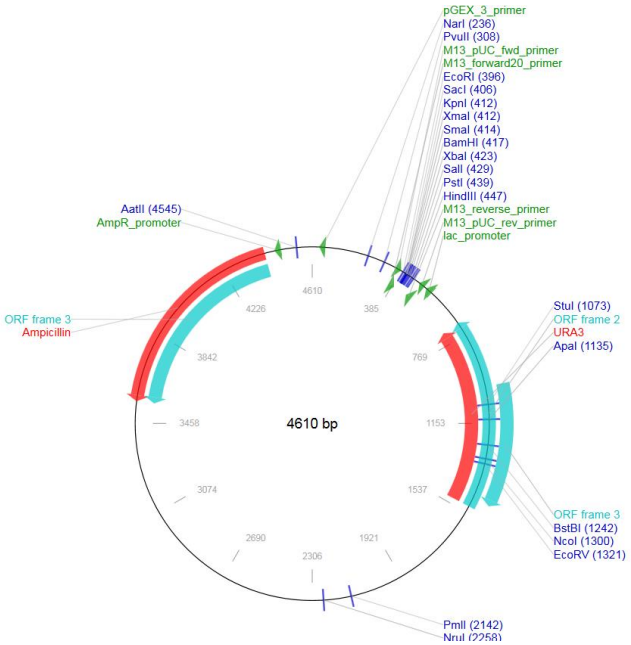

Figure 17. pFL38 vector map (4810 bp).

Obtained PCR products were checked for the proper size with a 2% agarose gel.

2.1.1.3 One-step transformation

The ligation within the previously digested pFL38s was performed by taking advantage of the homologous recombination machinery of yeast. W303 (standard wild-type) strain was cultured overnight and the next day cells were pelleted. Thawed DNA carrier together with PCR product and digested vector were added directly to cells that were immediately suspended in a transformation solution composed of 50% (w/v) PEG 3350, 100 mM LiAc and 100 mM DTT. After vortexing, cells were incubated for 30 min at 45°C (heat shock) and then centrifuged at 13,000 x *g* for 5 min. The supernatant was discarded and the pellet washed with sterile H_2O. Cells were finally plated in a SD agar medium containing all nutrients except uracil, and let growing for 2/3 days. The vector was then extracted from yeast colonies with a PureLink®Quick Plasmid MiniPrepkit, according to the manufacturer's instructions, and successively used to transform OneShot TOP_{10} *E. coli* cells (Invitrogen). Positive clones were used for a further purification of the vectors that were fully sequenced by BMR Genomics.

2.1.1.4 Site-direct mutagenesis

Cys residues mutants: the *ATP1* Cys243 and the *ATP5* Cys100 were substituted with the Ser residue (from TGT to TCT codon), through a "mutagenesis" PCR, using appropriate primers (**Table VII**), according to the manufacturer's instructions (QuikChange II XL Site-Directed Mutagenesis Kit). Vectors were then sequenced to assess the point mutations of the insert and to control for unwanted further modifications in the sequence (BMR Genomics).

Deletion mutant: the first transmembrane domain (186-243 bp) of ATP4 has been deleted using the In-Fusion HD Cloning Plus kit, according to the manufacturer's instructions. This protocol combines the potency of In-Fusion HD enzyme with the inverse PCR. During inverse PCR, primers are oriented in opposite directions on the target vector and allow the amplification of adjacent sequences (**Figure 18**). Primers should have a 15-bp overlaps that do not include the bases to be deleted (**Table VII**).

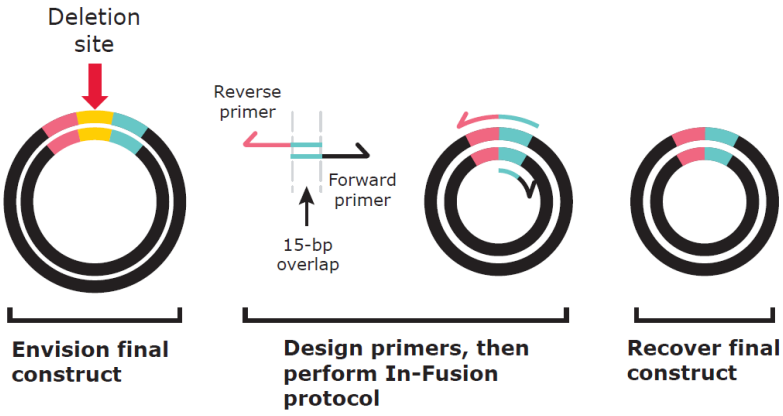

Figure 18. In-Fusion primer design for deletion mutagenesis. Primers are designed to eliminate a section of the original vector.Deletion site is marked in yellow; the binding site for the reverse primer (pink and turquoise) spans the deletion. The binding site for the forward primer (turkoise and black) is located on the cloning vector backbone. There is no gap between the pink and turquoise regions in the actual primer sequence; the deleted nucleotides are not included in either of the primers.

Table VII. Primers used for mutagenesis PCR. In yellow, single nucleotide substitution to allow the substitution from TGT (Cys) to TCT (Ser) codon.

Primer name	sequence
ATP1Mut FOR	5'-GAAACTTTACTCTGTTTACGTTGC
ATP1Mut REV	5'-GCAACGTAAACAGAGTAAAGTTTC
ATP5Mut FOR	5'-CAGACTGGGATCTTTTGAAAAAATTGCG
ATP5Mut REV	5'-CGCAATTTTTTCAAAAGATCCCAGTCTG
ATP4del FOR	5'- AATGAATTGTACGTTATCAACGATGAAAGTATTTTATTGC
ATP4del REV	5'- AACGTACAATTCATTATTATTACCTGGAATGGCATTGATG

2.1.1.5 Diploids sporulation and haploids selection

ΔTIM11ΔATP20 diploids, presenting the further deletion of *ATP1* or *ATP4* or *ATP5*, were transformed with pFL38 vectors carrying the mentioned genes, as described in the protocol for the one-step transformation. Resulting clones were grown in 2% potassium acetate medium and induce to sporulate. Thus, the diploid cells gave rise to 4 haploids daughter contained into an ascus structure that was dissected at microspcope. Haploids were then plated in selection agar media (SD-HIS, SD-URA, SD+G418) and selected for the presence of correct deletions and the vector.

2.1.2 Yeast culture and mitochondria isolation

Yeast cells were cultured aerobically in 50 ml of 1% yeast extract, 1% bacto-polypeptone (YP) medium containing 2% glucose at 30°C. When it reached an optical density of 2 at 600 nm, the culture was added to 800 ml of YP medium supplemented with 2% galactose and incubated for 20 h at 30°C under rotation at 180 rpm, yielding about 4.0 g of yeast cells. Yeast mitochondria were isolated as described (Yamada 2009) with the following modifications. Briefly, cells were washed, incubated for 15 min at 37°C in a 0.1 M Tris-SO_4 buffer (pH 9.4) supplemented with 10 mM dithiothreitol (DTT) and washed once with 1.2 M Sorbitol, 20 mM Pi pH 7.4. Yeast cells were then suspended in the same buffer and incubated for 45 min at 30°C with 0.4 mg/g of cells of zymolyase 100T to form spheroplasts. The latter were washed once with sorbitol buffer and homogenized in 0.6 M Mannitol, 10 mM Tris-HCl, pH 7.4 and 0.1 mM EDTA-Tris with a Potter-Homogenizer. The homogenate was centrifuged for 5 min at 2,000 x *g*, the supernatant was collected and centrifuged for 10 min at 12,000 x *g*. The resulting mitochondrial pellet was suspended in mannitol buffer and protein concentration was determined from the A_{280} of SDS-solubilized mitochondria[205].

2.1.3 Mouse Liver Mitochondria (MLM) isolation

B6J mouse liver was excised and immediately immersed in ice-cold 250 mM Sucrose, 10 mM Tris-MOPS, 100 µM EGTA, pH 7.4 medium. After sample trituration with appropriate tools, it was homogenized with a Potter-Homogenizer until no visible debris were present. The homogenate was centrifuged for 10 min at 688 x *g* and the supernatant (containing mitochondria) was centrifuged at 6,005 x *g* for 10 min. The pellet was then resuspended in the buffer and centrifuged again at 9,383 x *g* for 5 min. The pellet was resuspended in about 300 µl of the same buffer and its protein content quantified with Biuret method.

2.1.4 HEK293T cell culture and permeabilization

HEK293T cells were cultured in standard DMEM medium supplemented with 10% fetal serum bovine and 1% Penycilin/Streptomycin cocktail. Depending on the desired culture size, cells were kept in 75 or 150 cm^2 T flasks. Cells were incubated at 37°C in a CO_2 incubator and split every 3-4 days at 1:4 to 1:10 dilutions. HEK293T cells were permeabilized as described below. Briefly, trypsin-treated cells were suspended in 250 mM Sucrose, 10 mM Tris-MOPS, 100 µM EGTA, pH 7.4 (B1) buffer and counted with Burker's chamber. Cells were then centrifuged at 2,500 x *g* for 5 min, suspended in 250 mM Sucrose, 10 mM Tris-MOPS, 1 mM EGTA, pH 7.4 (B2) at 20 x 10^6 cells/ml and incubated with 100 µM digitonin on ice for about 10 minutes. Permeabilization was stopped by the addition of 20 ml of B1 and cells were centrifuged, washed with B1 and centrifuged again. Finally, permeabilized cells were suspended at 5 x 10^6 cells/ml in 250 mM Sucrose, 10 mM Tris-MOPS, pH 7.4 buffer supplemented with 5 mM Glutamate/2.5 mM Pyruvate, and 0.5 µM Calcium Green-5N for CRC experiments. Further additions were as indicated in the Figure legends.

2.2 Mitochondrial bioenergetics parameters

2.2.1 Measurement of oxygen consumption

Mitochondrial oxygen consumption was measured with a Clark electrode (Yellow Springs Instruments, OH, USA), equipped with magnetic stirring and thermostatic control maintained at 25°C. Additions were made through a port in the frosted glass sealing of the 2 ml chamber. Isolated yeast mitochondria were incubated in 250 mM Sucrose, 10 mM Tris-MOPS, 2 mM Pi, 10 µM EGTA, pH 7.4 medium at the final concentration of 0.5 mg/ml. NADH (purchased by Roche) was used as respiratory substrate and added at the final concentration of 1 mM. Here, a slow oxygen consumption is visible because of the proton leak across the membrane (**state 2 or 4**). A limited amount of ADP is then added to allow the F-ATP synthase to synthesize ATP, which is coupled to the reentry of H^+ across the enzyme. This leads to partial dissipation of the proton-motive force and thus to the stimulation of the RC resulting in increased oxygen consumption (**state 3**). When all ADP has been transformed into ATP respiration slows down to the basal rate (**state 4**). A parameter that can be extrapolated is the respiratory control ratio (ADP-stimulated over basal), a measure of respiratory coupling. The subsequent addition of an uncoupler (like FCCP) leads to the complete dissipation of the proton-motive force (**state 3u**) and therefore to the maximal O_2 consumption (until the O_2 concentration falls to zero) (**Figure 19**).

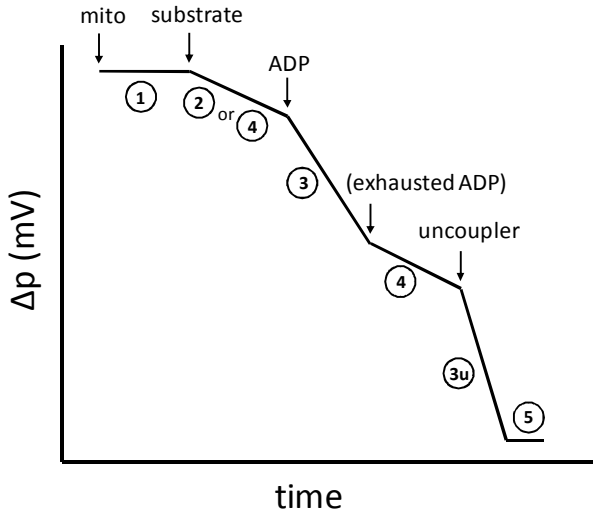

Figure 19. Schematic representation of a Clark oxygen electrode trace.
Oxygen consumption (expressed as decrease in oxygen tension) in isolated coupled mitochondria following additions of the respiratory substrate, ADP and an uncoupler. State 1: no respiratory substrate added; State 2/4: basal respiration (in absence of ADP or in presence of oligomycin, an inhibitor of the F-ATP synthase); State 3: ADP stimulated coupled respiration; State 3u: maximal respiration caused by proton leak across the IMM induced by an uncoupler (like FCCP).

2.2.2 Measurement of membrane potential

Mitochondrial membrane potential (ΔΨ) was evaluated using the lipophilic positively charged fluorescent probe Rhodamine$_{123}$, measured with a Fluoroskan Ascent FL (Thermo Electron) 96-well plate reader. Excitation and emission wavelengths were 503 and 523 nm, respectively. This probe accumulates within energized mitochondria because of the inside-negative ΔΨ, resulting in the quenching of the signal. Yeast mitochondria (0.5 mg/ml) were suspended in 250 mM Sucrose, 10 mM Tris-MOPS, 2 mM Pi, 10 µM EGTA, 0.15 µM Rhodamine$_{123}$ at the pH specified in the figure legends). After a short incubation (to reach the stabilization of the signal), the respiratory substrate was added (1 mM NADH) that allows membrane polarization with the consequent matrix accumulation of Rhodamine$_{123}$ (decrease in fluorescence). Once the signal reaches a plateau value (F), the further addition of an uncoupler (2 µM FCCP) dissipates ΔΨ and causes the release of the probe in the external medium, increasing the fluorescence signal (F*) (**Figure 20**). The membrane potential ΔΨ was estimated according to the Nernst equation using Rhodamine$_{123}$ fluorescence after the addition of NADH (F) and of FCCP (F*) as endpoints (ΔF = F*- F).

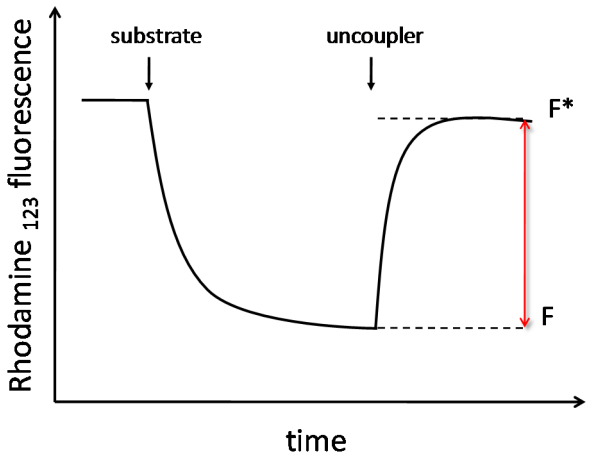

Figure 20. Measurement of mitochondrial membrane potential (ΔΨ) using the Rhodamine$_{123}$ fluorescent probe.
Example illustrating a typical trace of Rhodamine$_{123}$ fluorescence in isolated mitochondria, following indicated additions. The membrane potential ΔΨ was estimated according to the Nernst equation using F and F* as endpoints.

2.2.3 Measurement of mitochondrial Ca^{2+} Retention Capacity (CRC)

The mitochondrial CRC-assay was used to assess pore opening as well as changes in its sensitivity to Ca^{2+} in isolated mitochondria/permeabilized cells. The minimal Ca^{2+} threshold required to induce opening of the pore can be determined by adding a train of Ca^{2+} pulses of known concentration at short intervals. The onset of PTP opening is marked by a sudden release of accumulated matrix Ca^{2+}. Extramitochondrial $Ca^{2+}$was measured with Calcium Green-5N (Molecular Probes) fluorescence using a Fluoroskan Ascent FL (Thermo Electron) plate reader, equipped with a plate shaker. Excitation and emission wavelengths were 485 and 538 nm, respectively. Calcium Green-5N is a Ca^{2+} sensitive dye not able to cross the mitochondrial inner membrane that emits a fluorescent signal upon Ca^{2+} binding. Thus, adding a Ca^{2+} pulse induces a peak of fluorescence that is followed by a decrease as Ca^{2+} is taken up by mitochondria. When a threshold accumulation of matrix Ca^{2+} is reached, the PTP opens and releases the accumulated cation in the external medium, causing an increase of Calcium Green-5N fluorescence (**Figure 21**).

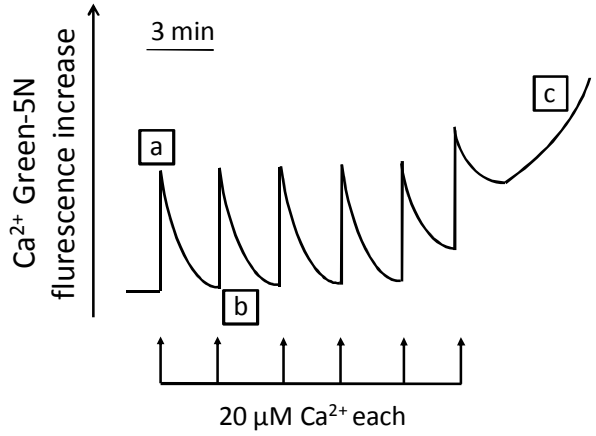

Figure 21. Ca^{2+} Retention Capacity (CRC) assay.
Extramitochondrial Ca^{2+} was measured with the Calcium Green-5N fluorescent probe. a) Addition of a known concentration Ca^{2+} pulse leads to a sudden increase in fluorescence value because of the binding with the dye. b) Energized mitochondria take up available cations, resulting in a decrease of the signal (the dye is membrane impermeable). c) Once reached a certain matrix Ca^{2+} threshold, the PTP opens leading to cations release and to a quick increase in fluorescence.

Yeast: The incubation medium contained 250 mM Sucrose, 10 mM Tris-MOPS, 10 µM EGTA, pH 7.4 (and Pi-Tris as indicated in the Figure legends), supplemented with 1 mM NADH, 0.5 mg/ml bovine serum albumin, 5 µM ETH129 (Ca^{2+} ionophore) and 1 µM Calcium Green-5N. A concentration of 0.5 mg/ml mitochondria was used in each CRC experiment. Further additions were made as indicated in the Figure legends.

Mouse liver mitochondria: Mitochondria (1 mg/ml) were incubated in a medium containing 250 mM Sucrose, 10 mM Tris-MOPS, 10 µM EGTA, pH 7.4 (and Pi-Tris as indicated in the Figure legends), supplemented with 5 mM Glutamate/2.5 mM Malate and 0.5 µM Calcium Green-5N. Further additions are indicated in the Figure legends.

HEK293T cells: Permeabilized cells were suspended at 5 x 10^6 cells/ml in 250 mM Sucrose, 10 mM Tris-MOPS, pH 7.4 (and Pi-Tris as indicated in the Figure legends), supplemented with 5 mM Glutamate/2.5 mM Malate, 0.5 µM Calcium Green-5N. Further additions were as indicated in Figure legends.

2.2.4 Measurement of matrix swelling

Another useful parameter for studying PTP properties is the evaluation of matrix swelling. This can be achieved by measuring optical density changes of the mitochondrial suspension in response to various stimuli (**Figure 22**). Indeed, intact mitochondria scatter light at 540 nm and an increase in matrix volume (due to pore opening) leads to a decrease of light scattering. Changes in optical density were monitored with the Infinite®200 PRO (TECAN, Life Sciences) plate reader at 540 nm. Yeast mitochondria (0.5 mg/ml) were suspended in 250 mM Sucrose, 10 mM Tris-MOPS, 2 mM Pi, 1 mM NADH, 0.5 mg/ml bovine serum albumin, 5 µM ETH129, 10 µM EGTA, at pH 7.4. PTP inducers were added as indicated in Figure legends.

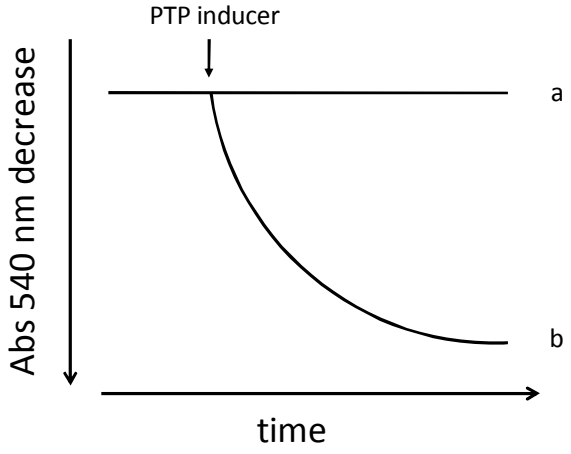

Figure 22. Schematic representation of Abs 540 nm changes as indicator of mitochondrial swelling.
Addition of PTP inducers (such as Ca^{2+} alone or together with oxidants) to isolated mitochondria leads to changes in mitochondrial volume (swelling), marked with a decrease in Abs 540 nm(trace b); trace a) control trace without any additions.

2.2.5 Measurement of ATP hydrolysis

The enzymatic function of F-ATP synthase can be assessed by evaluating either the rate of synthesis or of hydrolysis of ATP. Here, the hydrolysis capacity has been measured by using an ATP-regenerating system in which a constant ATP level is provided to the enzyme. Alamethacin-treated yeast mitochondria (10 µg/ml) were suspended in Harris buffer (50 mM Tris-HCl, 50 mM KCl, 30 mM sucrose, 2 mM $MgCl_2$, 2 mM EGTA), supplemented with 4 U/ml pyruvate kinase (PK), 3 U/ml lactate dehydrogenase (LDH), 4 mM phosphoenolpyruvate (PEP), 0.2 mM NADH and 2 mM ATP. The reaction sequence at 37°C is as following (**Figure 23**): F-ATP synthase converts ATP in ADP + Pi, substrates of PK that transfer Pi from PEP to ADP, yielding one molecule of ATP and pyruvate. To prevent reaction saturation, pyruvate is rapidly metabolized by lactate dehydrogenase that converts it into lactate at the expense of NADH. Thus, the hydrolysis will be directly proportional to NADH reduction, measured at 340 nm by Infinite®200 PRO (TECAN, Life Sciences) plate reader.

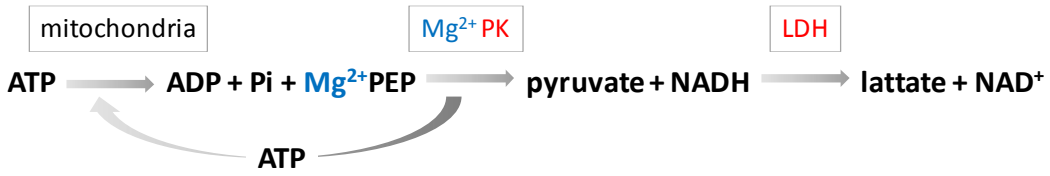

Figure 23. ATP-regenerative system.

The hydrolysis rate was quantified as nmol of ATP hydrolyzed per mg of protein per minute, according to the following equation: ATPase rate [nmol ATP x min^{-1}]= -dA340/dt [OD/min] x K_{path}^{-1} x $moles^{-1}$ ATPase; in which K_{path} is the molar absorption coefficient for NADH for a given optical pathlength.

2.3 Electrophysiology

Planar lipid bilayers, also called artificial lipid bilayers, allow the study of ion-conducting channels in a well-defined environment (**Figure 24**). These bilayers can be used for many different studies, such as the characterization of membrane-active peptides, the reconstitution of ion channels or investigations on how changes in lipid bilayer properties alter the function of bilayer-spanning channels.

Planar lipid bilayer experiments were performed as follows. Bilayers of 150-200 pF capacitance were prepared using purified soybean asolectin. The standard experimental medium was 150 mM KCl, 10 mM Hepes, pH 7.5. All reported voltages refer to the *cis* chamber, zero being assigned to the *trans* (grounded) side. Currents are considered as positive when carried by cations flowing from the *cis* to the *trans* compartment. Freshly prepared F-ATP synthase dimers were added to the *cis* side.

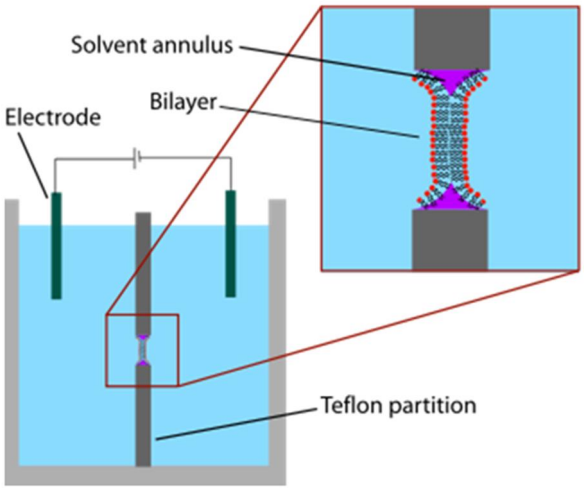

Figure 24. Planar lipid bilayer experiment setup.
The chamber is divided in two sides (called *cis* and *trans*) by a sheet of plastic with a small hole in the center. This hole can be pre-coated with a lipid film, allowing a more efficient creation of the bilayer during the experiment. The electrical features of the channel in subject can be measured by two electrodes added in each side of the chamber that record ions crossing the membrane. Before each experiment, the evaluation of membrane electrical properties (without any proteins) is mandatory.

2.4 Blue Native PAGE and cross-linking

Yeast mitochondria were suspended at 10 mg/ml in 150 mM K-acetate, 30 mM HEPES, 10% glycerol, 1 mM phenylmethylsulfonyl fluoride and solubilized with 1.5% (w/v) digitonin. After centrifugation at 100,000 x *g* with a Beckman TL-100 rotor for 25 min at 4°C, supernatants were collected, supplemented with 50 mg/ml Coomassie Blue and quickly loaded onto a 3-12% polyacrilamide gradient BNE gel (Invitrogen). Electrophoresis was carried out at 150 V for 20 min and

at 250 V for 2h, followed by gel staining with 0.25 mg/ml Coomassie Blue, 10% acetic acid or used for in-gel activity staining to detect bands corresponding to ATP synthase. Activity was monitored in 270 mM glycine, 35 mM Tris pH 7.4, 15 mM $MgSO_4$, 8 mM ATP-Tris, and 2 mg/ml $Pb(NO_3)_2$. Bands corresponding to monomeric and dimeric forms of ATP synthase were cut from the gels and protein complexes were eluted overnight by incubation at 4°C in 25 mM Tricine, 15 mM $MgSO_4$, 8 mM ATP, 7.5 mM Bis-Tris, 1% (w/v) n-heptyl β-D-thioglucopyranoside, pH 7.0. Samples were then centrifuged at 20,000 x *g* for 10 min at 4°C and supernatants were used for bilayer experiments. For cross-linking experiments, mitochondria were incubated 20 min at room temperature at 1 mg/ml in 250 mM sucrose, 2 mM Pi and 2 mM $CuCl_2$. Five millimolar N-ethylmaleimide and 5 mM EDTA were then added to block the cross-linking reaction, the incubations transferred on ice for 10 min followed by centrifugation and preparation for BN-PAGE as described above.

2.5 SDS-PAGE

2.5.1 Sample preparation

Yeast mitochondria: Bands of F-ATP synthase dimers were cut from the BNE gel, directly loaded into 12% SDS gel and incubated for 20 min at RT with Laemmli buffer 1X, before the running. SDS gel was used either for Western Blot analysis and for silver staining (Silver Stain Plus kit, BioRad).

Mouse liver mitochondria: Isolated mitochondria (1 mg/ml)were suspended in 250 mM Sucrose, 10 mM Tris-MOPS, 10 µM EGTA, pH 7.4 and treated 10 min at room temperature as indicated in the Figure legends. Mitochondria were then pellet at8,000 x *g* for 10 min and then suspended in an appropriate volume of double strength Laemmli buffer, containing 4% (w/v) SDS, 20% glycerol, 120 mM Tris-Cl (pH 6.8) and 0.02% (w/v) bromophenol blue. Samples were boiled 5 min at 99°C and then loaded in a 4-12% NuPAGE Bis-Tris gel (ThermoFischer Scientific) and processed for Western Blot analysis.

2.5.2 Immunoprecipitation (IP) of complex V

The IP of F-ATP synthase was performed using the ATP synthase Immunocapture kit (ab109715), a cocktail of monoclonal antibodies, recognizing epitopes of the F-ATP synthase, that are cross-linked to protein G-agarose beads. Briefly, 0.5 mg MLM, treated as indicated in Figure legends,

were pelleted and suspended in 50 µl Schägger buffer containing 1 g/g digitonin. After centrifugation at 100,000 x *g* with a Beckman TL-100 rotor for 25 min at 4°C, supernatants were collected and 10 µl of the Immunocapture kit was added. Samples were incubated overnight at 4°C in agitation. The next day, samples were centrifuged 5 min at 500 x *g* and surnatant was collected (proteins not bound to F-ATP synthase antibodies). Beads were incubated with 1X PBS supplemented with 0.01% DDM (n-Dodecyl β-D-maltoside) and centrifuged 5 min at 500 x *g* (twice). Then, the elution of bound proteins was carried out with a 15 min shacking incubation with 1X Laemmli buffer without β-Mercaptoethanol (to maintain crosslinks). Samples were then centrifuged 5 min at 500 x *g* and supernatants were collected. This operation was repeated three times. Finally, supernatants were loaded in 4-12% NuPAGE Bis-Tris gel (ThermoFischer Scientific) and processed for Western Blot analysis.

2.5.3 Western Blotting

Separated proteins were blotted electrophoretically to a nitrocellulose membrane in a buffer containing 0.5 M glycine, 0.4 M Tris and 20% methanol at 4°C using a Mini Trans-Blot system (Bio-Rad). The membranes were then saturated for 1h in PBS, 0.02% Tween, containing 3% nonfat dry milk, to avoid non-specific protein binding. After the saturation, membranes were incubated with specific dilutions of primary antibodies overnight at 4°C, as indicated in the table below (**Table VIII**). The next day, membranes were washed three times with PBS-0.02% Tween for 7 min each and then incubated for 1h 30 min at RT with either secondary peroxidase-conjugated antibodies, diluted in PBS-0.02% Tween containing 3% nonfat dry milk or IRDye® secondary antibodies conjugated with an infrared fluorescent dye (Li-COR Biosciences) , diluted in PBS-0.02% Tween. Other three PBS-0.02% Tween washes were performed and the antibody binding was then revealed either by ECL (Enhanced ChemiLuminescence; Millipore) kit or by Odyssey Infrared imaging system (Li-COR Biosciences).

Table VIII. List of antibodies.

Antibdoy	Dilution	Source	Company
anti- γ subunit	**1:10000**	**Rabbit polyclonal**	**Marie-France Giraud, Bordeaux, France**
anti- Tom20	**1:2000**	**Rabbit polyclonal**	**NikolausPfanner, Freiburg, Germany**
anti- Tim54	**1:2000**	**Rabbit polyclonal**	**NikolausPfanner, Freiburg, Germany**
anti- β subunit	**1:5000**	**Mouse monoclonal**	**ab43176**
anti- OSCP	**1:1000**	**Rabbit polyclonal**	**sc-74786**

3. Results

3.1 Properties of the Ca^{2+}-dependent permeability transition of yeast mitochondria

In order to investigate the properties of the yPTP, the Ca^{2+} ionophore ETH129 was added to energized mitochondria to allow Ca^{2+} uptake and the propensity of the yPTP to open was monitored as the Ca^{2+} retention capacity (CRC), i.e. the maximal Ca^{2+} load retained by mitochondria before onset of the PT. In keeping with previous observations[214] (i) energized yeast mitochondria were able to accumulate Ca^{2+} provided as a train of pulses (**Figure 26A**) until onset of the PT, which causes depolarization followed by Ca^{2+} release; and (ii) increasing concentrations of Pi increased the matrix Ca^{2+}load necessary to open the yPTP (**Figure 26A-B**), possibly following formation of matrix Pi-Ca^{2+} complexes. Furthermore, the effect of ADP/Mg^{2+} has been investigated and, like in mammalian mitochondria, increasing concentration of the adenine nucleotide increased the CRC, an effect consistent with yPTP inhibition (**Figure 26C**). On the other hand, the CRC was not affected by decavanadate (results not shown), which inhibits the ATP-induced, VDAC-dependent yeast permeability pathway[210].

The mammalian PTP is modulated by 2 classes of redox-sensitive thiols whose oxidation increases the pore sensitivity to Ca^{2+}, i.e. (i) matrix thiols that react with phenylarsine oxide (PhAsO)and can be oxidized by diamide[228]; and (ii) external thiols that can be oxidized by copper-*o*-phenanthroline ($Cu(OP)_2$)[136], as shown in the **Figure 25**.

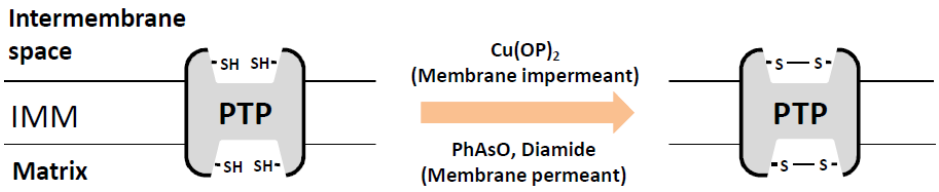

Figure 25. Schematic representation of PTP redox sensitive thiols and the reactivity with indicated oxidants.

The threshold Ca^{2+} load required for yPTP opening was moderately affected by PhAsO concentration up to 50 µM (**Figure 26D**) while it was very sensitive to diamide (**Figure 26E**) and to $Cu(OP)_2$ (**Figure 26F**). These experiments indicated that the yeast PTP is affected by the redox state of thiol groups as also suggested by a previous study.

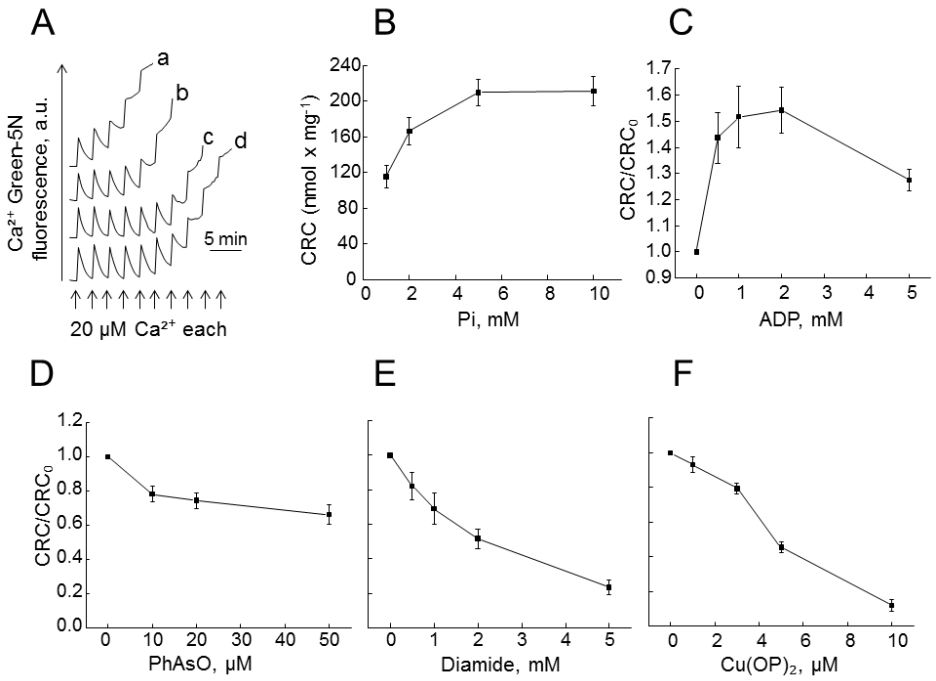

Figure 26. Properties of the permeability transition of yeast mitochondria. The incubation medium contained 250 mM Sucrose, 10 mM Tris-MOPS, 1 mM NADH, 10 µM EGTA-Tris, 5 µM ETH129, 1 µM Calcium Green-5N, final pH 7.4,0.5 mg/ml bovine serum albumin and 0.1 mg of mitochondria in a final volume of 0.2 ml. (A) The medium was supplemented with 1 mM (trace a), 2 mM (trace b), 5 mM (trace c) or 10 mM Pi (trace d), and where indicated Ca^{2+} was added; traces shown are representative of 13 independent experiments.(B) Experimental conditions as in panel A with the indicated Pi concentrations; values on the ordinate refer to the amount of Ca^{2+} accumulated prior to the precipitous release that follows the PT (n = 13±SE). (C) The experimental conditions were as in panel A with 2 mM Pi, and the medium supplemented with 2 mM $MgCl_2$ and the stated concentrations of ADP. (D-F)The experimental conditions were as in panel A with 2 mM Pi, and the medium supplemented with the stated concentrations of PhAsO(D),diamide(E) or $Cu(OP)_2$ (F). For panels D-F n (± SE) was 3, 8 and 6, respectively.

Mammalian PTP is strongly modulated by matrix pH and this is mediated by reversible protonation of a critical His residue[132]. Experiments performed with de-energized mitochondria showed a bell-shape dependence on matrix pH with an optimum for PTP opening at pH 7.4 and a marked desensitization at both basic and acidic pH values. However, in respiring-mitochondria an external acidic pH may also affect the pore indirectly through the uptake of Pi, leading to PTP induction rather than inhibition, given that Pi is one of the most effective inducers in mammalian mitochondria. In yeast, the effect of pH on PTP has never been assessed. Here, the impact of external pH was evaluated by performing a CRC assay with energized-mitochondria incubated in a range of pH between 6 and 8 (**Figure 27A**). Intriguingly, the mitochondrial Ca^{2+} load was strongly modulated by external pH, in the sense that pH below 7.4 (7 - 6.7 - 6) allowed a larger cations load before yPTP opening (**Figure 27B**). To further investigate whether this was due to a direct effect of the pH on the pore or to an alteration of the ΔΨ, the latter was measured with $Rhodamine_{123}$. No changes in ΔΨ were found with different buffers (**Figure 27C**). These data suggested that, also in yeast, the pH plays a role in pore regulation. This

could be due to the protonation of a critical His, but we cannot exclude that the increased uptake of Pi via PiC at acidic pH[133] might be the cause of the observed inhibition.

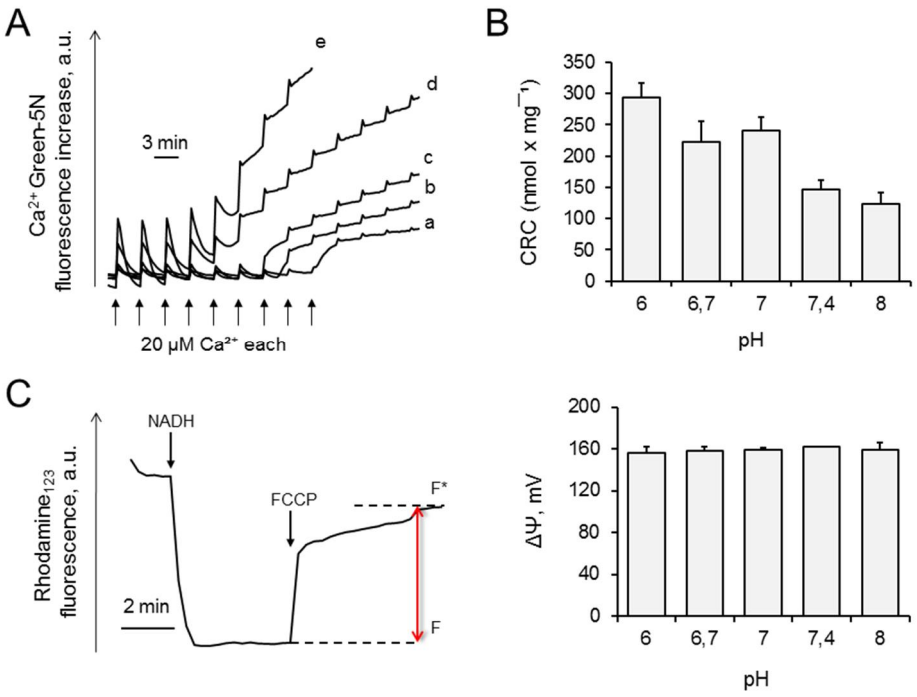

Figure 27. Effet of external pH on yPTP. (A) The incubation medium contained 250 mM Sucrose, 10 mM Tris-MOPS, 1 mM NADH, 2 mM Pi, 10 µM EGTA-Tris, 5 µM ETH129, 1 µM Calcium Green-5N, 0.5 mg/ml bovine serum albumin and 0.1 mg of mitochondria in a final volume of 0.2 ml. CRC assay was performed with respiring-mitochondria incubated in buffers at following pH: 6 (trace a), 6.7 (trace b), 7 (trace c), 7.4 (trace d), 8 (trace e); where indicated Ca^{2+} was added; traces shown are representative of 5 independent experiments. **(B)** Experimental conditions were as in panel A with buffers at the indicated pH; values on the ordinate refer to nmol of Ca^{2+} accumulated per mg of mitochondria, prior to its release following PTP opening (n=5±SE). **(C)** The incubation medium contained 250 mM Sucrose, 10 mM Tris-MOPS, 2 mM Pi, 10 µM EGTA-Tris, 0.15 µM $Rhodamine_{123}$ and 0.1 mg of mitochondria in a final volume of 0.2 ml. The final pH was as indicated in the figure. *Left panel*: representative trace. ΔΨ was measured as described in Materials and Methods. *Right panel*: quantification of ΔΨ (mV) obtained with buffers at the indicated pH (n=3±SE).

CsA desensitizes the mammalian pore to Ca^{2+} through matrix CyP D, a peptidyl-prolyl *cis-trans* isomerase that behaves as a PTP inducer. Through studies of CyP D-null mitochondria it became clear that CyP D is a modulator but not an obligatory constituent of the PTP[165]; and that a PT can occur in the absence of CyP D, or in the presence of CsA, albeit at higher matrix Ca^{2+} loads. Yeast mitochondria possess a matrix CyP (Cpr3) which facilitates folding of imported proteins in the matrix and is sensitive to CsA[229]; yet the yPTP was not affected by CsA, as also confirmed in the CRC assay (**Figure 28A**, compare traces a and b). These findings suggested that either Cpr3 does not interact with the pore or that CsA does not interfere with Cpr3 binding. To resolve this issue, the CRC of *ΔCPR3* mutants has been tested, which displayed a lower rate and slightly lower extent of Ca^{2+} accumulation (**Figure 28A**, trace c) indicating that Cpr3 does not sensitize the yPTP to Ca^{2+}, at variance from the

effects of CyP D in mammalian mitochondria. The small decrease of CRC in the mutants (**Figure 28B**) may be due to slower protein import and defective respiratory chain assembly and/or function[230]. It was recently established that rotenone is a good inhibitor of the PTP in mammalian mitochondria lacking CyP D, possibly because of decreased production of ROS through inhibition of reverse electron flow[215]. Rotenone did not affect the yPTP (**Figure 28A**, trace d), in keeping with the lack of a rotenone-sensitive, energy-conserving complex I and with the lack of "off-site" effects.

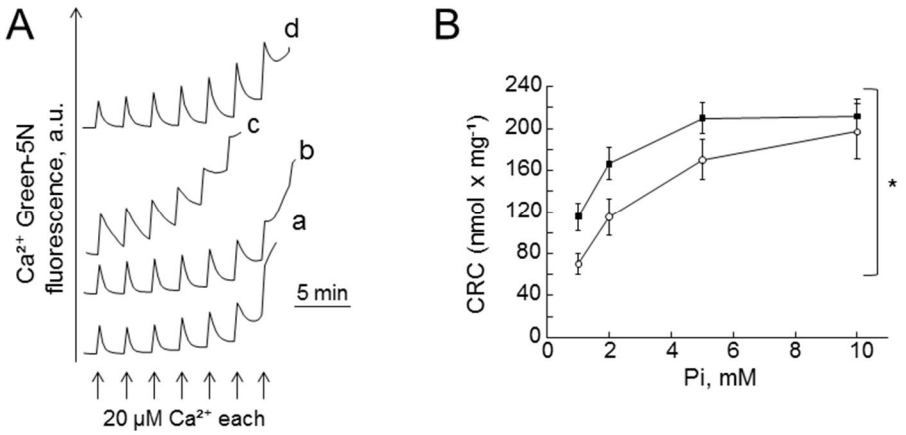

Figure 28. Figure 28. *CPR3* deletion does not affect the yeast permeability transition. (A) The experimental conditions were as in Figure 24 with 2 mM Pi; 0.8 μM CsA was added in trace b only and 2 μM rotenone in trace d only; where indicated Ca^{2+} was added to wild-type (traces a, b, d) or *ΔCPR3* (trace c) mitochondria (traces are representative of 3 independent experiments). **(B)** The experimental conditions were as in Fig 26 with Pi as indicated (n=4 ± SE). Closed symbols, wild-type mitochondria; open symbols, *ΔCPR3* mitochondria. Two-Way ANOVA test was performed, *p<0.05.

3.2 Purified F-ATP synthase dimers possess channel activity

To test whether yeast F-ATP synthase dimers can form channels similar to those found in mammals, mitochondrial proteins was separated by blue native (BN)-PAGE, identified dimers by in-gel activity staining, and eluted themfor incorporation into a planar asolectin membrane (an example of the dimer preparation can be seen in **Figure 29A**). Addition of 1-10 pmol of the dimers to the bilayers in symmetrical 150 mM KCl did not elicit current activity unless Ca^{2+}, PhAsO and $Cu(OP)_2$ were also added (**Figure 29A**). A clear activity was observed in 12 out of 14 reconstitutions, with channel unit conductance usually ranging between 250 and 300-pS (multiples of this unit conductance were often observed, in one case 1000-pS was reached). This conductance is compatible with the values exhibited by a channel observed in mitoplasts from a porin-less yeast strain, which was insensitive to CsA, ADP or protons and in which the combination of ADP and Mg^{2+} was not tested. The activity studied here was characterized by rapid oscillations between closed and open states (flickering), which is typical of the mammalian MMC-PTP, and by variable kinetics[44]. A

typical flickering behavior is illustrated in the bottom part of **Figure 29A**. As is the case for the mammalian F-ATP synthase and for the MMC-PTP measured in mitoplasts, addition of Mg^{2+}-ADP induced a clear-cut inhibition of the channel in 5 out of 6 experiments (total inhibition was observed in 2 cases and partial inhibition in 3 cases); the representative experiment of **Figure 29B** shows activity recorded before and immediately after addition of Mg^{2+}-ADP in one case of full inhibition, which is illustrated in the corresponding amplitude histograms (**Figure 29B**). Taken together, these data provide evidence that under conditions of oxidative stress yeast F-ATP synthase can form Ca^{2+}-activated channels with features resembling the MMC-PTP (although with lower conductance).

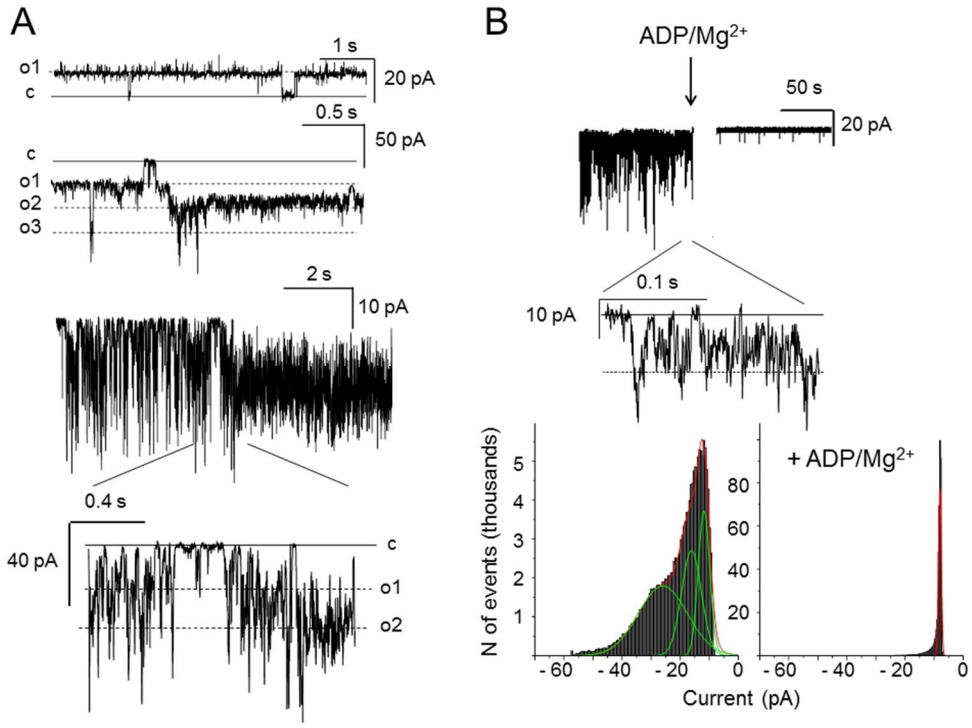

Figure 29. F-ATP synthase dimers reconstituted in planar lipid bilayers display Ca^{2+}-induced currents. Dimers were excised (see Figure 30D, wild-type) and eluted for planar bilayer experiments. (A) *Upper part*: Representative current traces recorded at +80 and -100 mV (*cis*) (upper and lower traces, conductance (g) = 125 and 250 -pS) upon incorporation of purified dimeric F-ATP synthase following addition of 3 mM Ca^{2+} (added to the *trans* side) plus 0.1 mM PhAsO and 20 µM $Cu(OP)_2$ (added to both sides). *Lower part*: typical, most often observed channel kinetics (see also expanded portion of the recording obtained at -60 mV *(cis)*; g= 250 pS) (B)*Top:* Effect of 2 mM ADP plus 1.6 mM Mg^{2+} added to the *trans* side on channel activity (-60 mV, g = 250 -pS); current trace before and immediately after addition of the modulators is shown; *bottom*, amplitude histograms obtained from the same experiment before (left panel) and after (right panel) addition of ADP/Mg^{2+}. Gaussian fitting (green lines) was obtained using the Origin 6.1 Program Set.

Notably, the dimeric but not the monomeric form could generate a pore in lipid bilayers, indicating that the interface between the two monomers would be the key site. However, although dimers and monomers are functionally distinct in the native membrane, it is not known whether this difference is maintained after incorporation into an artificial membrane. Indeed, dimers could either dissociate into monomers or rather form higher-order structures (tetramers and oligomers), due to the

generated membrane curvature[71]. We tried to solve this issue by taking advantage of the powerful yeast genetics.

3.3 Dimerization of F-ATP synthase is required for PTP formation

Dimers of F-ATP synthase are the "building blocks" of long rows of oligomers located deep into the cristae, which contribute to formation of membrane curvature and to maintenance of proper cristae shape and mitochondrial morphology[71,74,231]. Mammalian F-ATP synthase dimers appear also to be the units from which the PTP forms in a process that is highly favored by Ca^{2+} and oxidative stress, events that are required for channel formation[44]. To test the hypothesis that yPTP formation requires the presence of F-ATP synthase dimers, mutants lacking subunits involved in dimerization/oligomerization of the enzyme, i.e. subunit e (*TIM11*) and subunit g (*ATP20*) were analyzed. Strains lacking these subunits display balloon-shaped cristae with ATP synthase monomers distributed randomly in the membrane[71,232]. The *ΔTIM11*, *ΔATP20* and *ΔTIM11ΔATP20* mutants lacked dimers when analyzed by BN-PAGE while the monomeric F-ATP synthase was assembled and active (**Figure 30A**), consistent with their ability to grow on non-fermentable carbon sources; and developed a normal membrane potential upon energization with NADH (results not shown). CRC assays with ETH129 demonstrated that mitochondria from *ΔTIM11*, *ΔATP20* and *ΔTIM11ΔATP20* strains take up a larger Ca^{2+}load than wild-type strains (**Figure 30B**), with a doubling of the CRC (**Figure 30C**). Dimers may transiently form also in *ΔTIM11* and *ΔATP20* strains, a finding that could explain why Ca^{2+} release is eventually observed also in the "dimerization-less" mutants[76]. Consistent with this possibility, dimers in BN-PAGE were detected after treatment with $CuCl_2$ (**Figure 30D**), which promotes formation of disulfide bridges between adjacent Cys residues of the monomers[79]. Not all of the monomers dimerized after $CuCl_2$ treatment (**Figure 30D**) suggesting that Cys oxidation stabilizes pre-existing dimers that are otherwise dissociated by detergent treatment, but does not *induce* cross-linking of monomers.

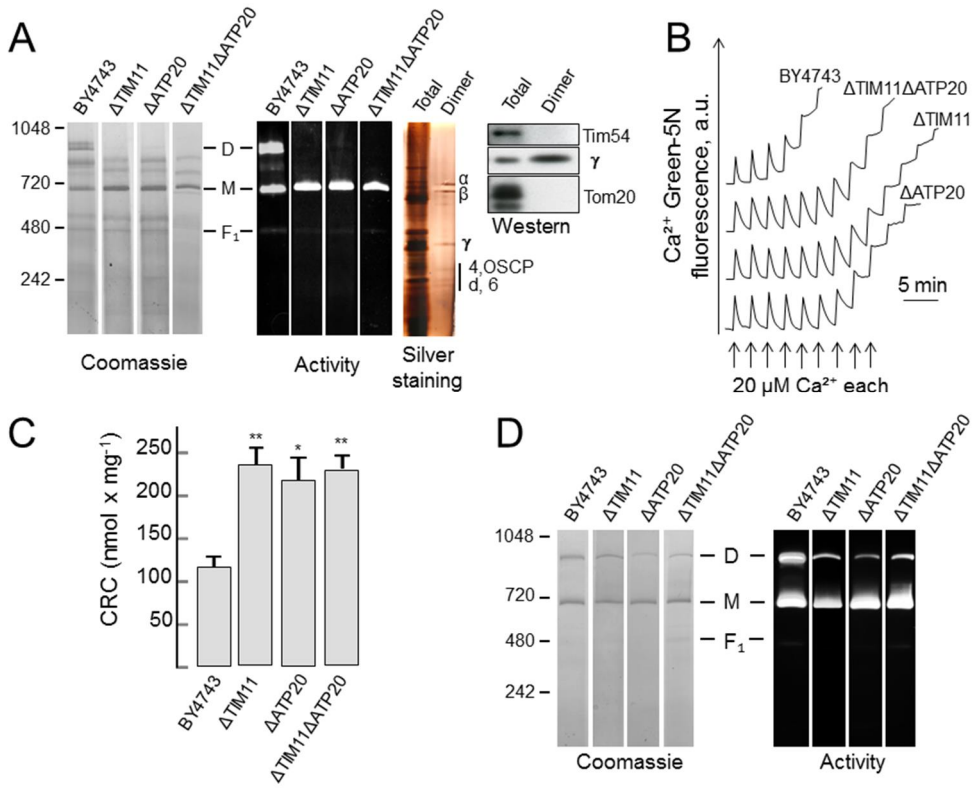

Figure 30. *ΔTIM11*, *ΔATP20* and *ΔTIM11ΔATP20* mutants lacking subunits involved in dimerization of F-ATP synthase are resistant to PTP opening. (A) Mitochondrial proteins were separated with BN-PAGE and stained with Coomassie blue (left lanes) or for in-gel activity (right lanes) to identify bands of F-ATP synthase dimers and monomers (note also a faint band corresponding to F_1). (B) The experimental conditions were as in Figure 26 with 1mM Pi; where indicated Ca^{2+} was added to wild type, *ΔTIM11ΔATP20*, *ΔTIM11*or *ΔATP20*mutants (traces are representative of 13, 6, 7 and 6independent experiments for the corresponding genotypes). (C) Experimental conditions as in (A) with 1 mM Pi. One-Way ANOVA test was performed to analyze CRC differences between BY4743 and mutants, *p<0.01, **p<0.001. (D) BN-PAGE (left lanes) and activity staining (right lanes) of mitochondria with the indicated genotypes after treatment with 2 mM $CuCl_2$.

3.4 Investigation of the putative PTP-forming subunits

According to these observations, subunits e and g appear to play a key role not only in dimer formation but also in PTP stabilization. However, whether these two small subunits constitute core components of the channel and contribute to the observed size of the PTP is an open question. To address this point, the PTP-dependent mitochondrial swelling in sucrose-based buffer in *ΔTIM11ΔATP20* mutants was tested. Swelling allows to monitor the onset of PTP opening and the presence of significant variations in its radius which -if small enough- can slow down or even prevent the diffusion of sucrose molecules, resulting in complete prevention of swelling. On the other hand, the swelling response also depends on mitochondrial ultrastructure and propensity to unfold, as shown by the marked tissue-specific differences observed in mammals where PTP-dependent swelling is marked in liver and much smaller in heart and muscle mitochondria.

We found that maximal swelling obtained upon treatment with Alamethacin, a pore-forming compound, was decreased in *ΔTIM11ΔATP20* mutants compared to control strain (**Figure 31A**). This observation matches the finding that absence of the e/g subunit(s) dramatically alters mitochondrial morphology, which may reduce the rate of PTP-dependent swelling, making in turn assessment of PT onset more difficult[232]. When Ca^{2+} was used to induce PTP opening, the consequent matrix swelling was the same irrespective of genotype (**Figure 31B**) suggesting that, in absence of subunits e and g, the pore size was large enough to let sucrose molecules through. We tried to further analyze pore size by adding PEG molecules of different molecular weights to swollen mitochondria and evaluating the ensuing contraction rate. Unfortunately, this kind of experiments gave inconsistent results with yeast mitochondria for the very reason that swelling is of limited extent and therefore PEG-induced contraction was almost undetectable.

We also performed lipid bilayer experiments with F-ATP synthase dimers obtained upon $CuCl_2$ treatment of mitochondria lacking the e and g subunits. Intriguingly, dimers displayed a channel activity in response to Ca^{2+}, PhAsO and $Cu(OP)_2$. Although higher conductances have also been observed (not shown), the typical conductance was about 30 -pS, which is markedly smaller than the ≈ 300-pS found in wild-type dimers (**Figure 31C**). As expected, channel activity was characterized by a flickering behavior, oscillating rapidly between the closed and open states, suggesting that the treatment with $CuCl_2$ did not alter other dynamic features of the PTP. These data provide evidence that subunits e and g may be involved in PTP formation not only by stabilizing the F-ATP synthase dimer ultrastructure, but also by representing core components of the channel. Further electrophysiological tests need to be done to clarify in detail the contribution of single subunits and even the involvement of specific residues in channel formation.

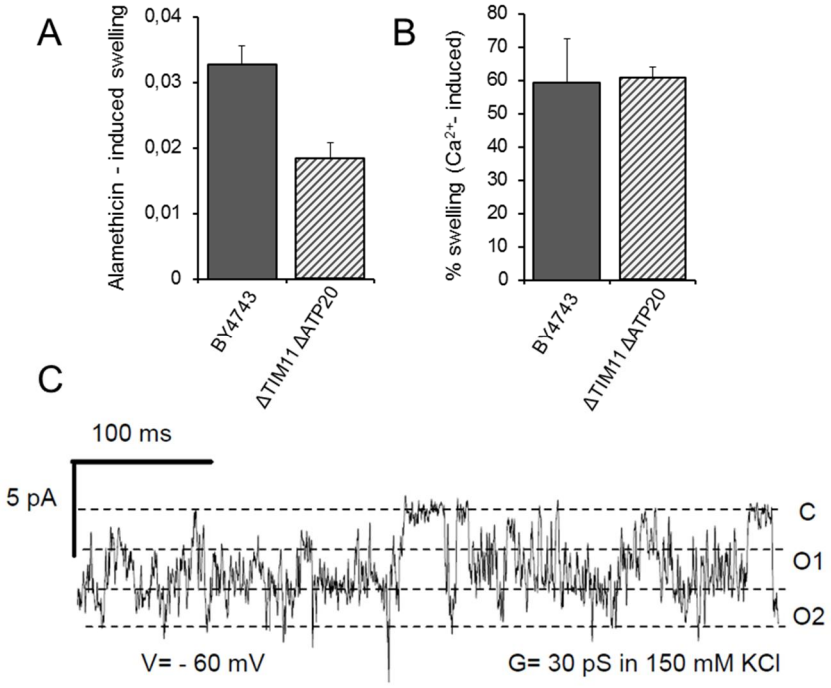

Figure 31. The PTP lacking e and g subunits shows alteration in channel conductance. (A)The incubation medium is the same as in Figure 26. Mitochondrial swelling of BY4743 and *ΔTIM11ΔATP20* mutants was evaluated by measuring Abs 540 nm. Mitochondria were treated with 2 µM Alamethacin to assess the maximal swelling. Bars graph reported Abs values obtained upon Alamethacin treatment and normalized to the initial Abs values (n=3±SE) (B) Experimental conditions were the same as in panel A and matrix swelling was evaluated in response to added Ca^{2+} (150 µM). Bars graph showed in ordinate the % of Ca^{2+} induced-swelling normalized to the maximal swelling (n=3±SE). (C) F-ATP synthase dimers obtained upon $CuCl_2$ treatment in *ΔTIM11ΔATP20* mutants (see Figure 30D) were excised and eluted for planar lipid bilayer experiments. Representative current trace recorded at -60 mV (*cis*) with a measured conductance of 30 -pS upon incorporation of purified dimers following additions of 3 mM Ca^{2+} (added to the *trans* side) plus 0.1 mM PhAsO and 10 µM $Cu(OP)_2$ (added to both sides).

A second interesting point is that occurrence of channel openings, in absence of e and g subunits, suggests that other subunits may contribute to generation of the full-conductance channel. In this regard, *in silico* analysis performed by Tosatto and Coworkers in our Department points to subunit b, a component of the lateral stalk that keeps contacts with the rotor and is connected with the catalytic domain via OSCP. Subunit b has two transmembrane domains (composed of α-helices) separated by a short loop, which is exposed to the IMS. Interestingly, the first α-helix of the *B. taurus* specie appears to have a particular orientation within the membrane (also called *reentrant α-helix*), detected with the OCTOPUS system, commonly used for the prediction of membrane protein topology. A reentrant helix was recently defined as a sequence that starts and ends on the same side of the membrane, penetrating the lipid bilayer to a depth of between 3 and -25 Å (with an average of about 10 Å)[233]. Intriguingly, this feature was detected in the structure of the Ryanodine receptor (an intracellular Ca^{2+} channel), exactly where channel formation takes place, indicating that it might be strictly required[234]. To address whether this is also essential for PTP formation, a yeast mutant for the

first α-helix of subunit b (*ATP4Δ1TM*) was generated in a *ΔTIM11ΔATP20* genetic background. Our initial experiments show that stimulation of respiration with ADP was decreased in the *ATP4Δ1TM* mutant compared to the control (**Figure 32A**), suggesting that the synthetic activity of the enzyme might be impaired, in keeping with the fact that subunit b, as well as the entire lateral stalk, plays a key role in enzyme stability and function. This is suggested by the ADP/NADH ratios, which were 1.6 for the control and 1.19 for the mutant. On the other hand, the sensitivity of the pore to Ca^{2+} was apparently not affected by the deletion (**Figure 32B**). Whether depletion of *ATP4Δ1TM* has an impact in channel conductance will require direct measurements in lipid bilayer experiments with reconstituted dimers.

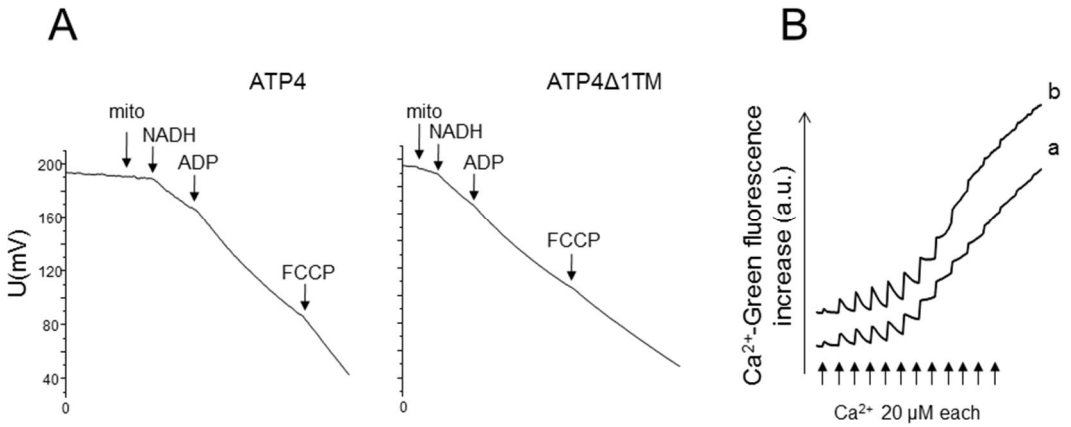

Figure 32. Characterization of *ATP4Δ1TM* mutant in *ΔTIM11ΔATP20* genetic background. (A) The medium contained 250 mM Sucrose,10 mM Tris-MOPS, 10 µM EGTA-Tris, final pH 7.4, 0.5 mg/ml bovine serum albumin and 1 mg of mitochondria in a final volume of 2 ml. Oxygen consumption was measured with a Clark electrode in control and mutant mitochondria (n=2). Sequential additions were made as following: 1 mg mitochondria, 1 mM NADH, 0.2 mM ADP and 2 µM FCCP. ADP/NADH ratios were calculated from the slopes of traces. (B) Experimental conditions were the same as Figure 26. Representative traces of a CRC experiment with Ca^{2+} pulses of 20 µM (n=2).

3.5 Identification of the Cys residue responsible for dimers stabilization by copper

Mutants lacking e and g subunits were able to form dimers in presence of $CuCl_2$, which mediates formation of disulfide bridges between free thiols of close Cys residues. The next questions were whether the reactive Cys residue(s) could be involved (i) in the stabilization of the channel (ii) and/or in PTP modulation by oxidative stress. Identification of this residue or residues thus appeared important to shed light on structural mechanims at the basis of channel opening.

The rationale to identify the relevant residues was to perform site-directed mutagenesis of all Cys residues of F-ATP synthase in the *ΔTIM11ΔATP20* genetic background (which does not form dimers) followed by BN-PAGE analysis after treatment of mitochondria with $CuCl_2$. Only mutants lacking the relevant Cys residues should not form dimers. The approach appeared feasible, as inspection of yeast F-ATP synthase revealed that only eight Cys residues are present in the enzyme complex, six in nuclear DNA-encoded subunits (α, γ, δ, OSCP, e and g) and 2 in mitochondrial DNA-encoded subunits (a and c) (**Table IX**).

subunit	nr. of cysteines
OSCP (ATP5)	1(C_{117})
α (ATP1)	1(C_{238})
β (ATP2)	1 (C_{32}TP)
γ (ATP3)	2 (C_{16}TP, C_{117})
δ (ATP16)	1(C_{106})
ε (ATP15)	none
a (ATP6)	1 (C_{33})
b (ATP4)	1(C_{26}TP)
c (ATP9)	1(C_{65})
d (ATP7)	none
e (TIM11)	1(C_{28})
F (ATP17)	none
g (ATP20)	1(C_{75})
A6L (ATP8)	none
h (ATP14)	1(C_{21}TP)
k (ATP19)	none
j (ATP18)	none

Table IX. Identification of Cys in yeast F-ATP synthase subunits.

The names of F-ATP synthase subunits were indicated with two nomenclature systems. Number of Cys residues in each subunit and the sequence position were marked in green and black colors, respectively. Cys residues labeled in light blue indicated those present in the transit peptide.

The redout of the screening is as shown in **Figure 33.** Here, for example *ATP1 C203S* and *ATP5 C100S* mutants (in *ΔTIM11ΔATP20* genetic background) were analyzed through the BN-PAGE and clearly it appeared that they form active dimers following $CuCl_2$ treatment (visible either from Coomassie and in-gel activity stainings). This meant that the target Cys was not that in *ATP1* (α subunit) or *ATP5* (OSCP).

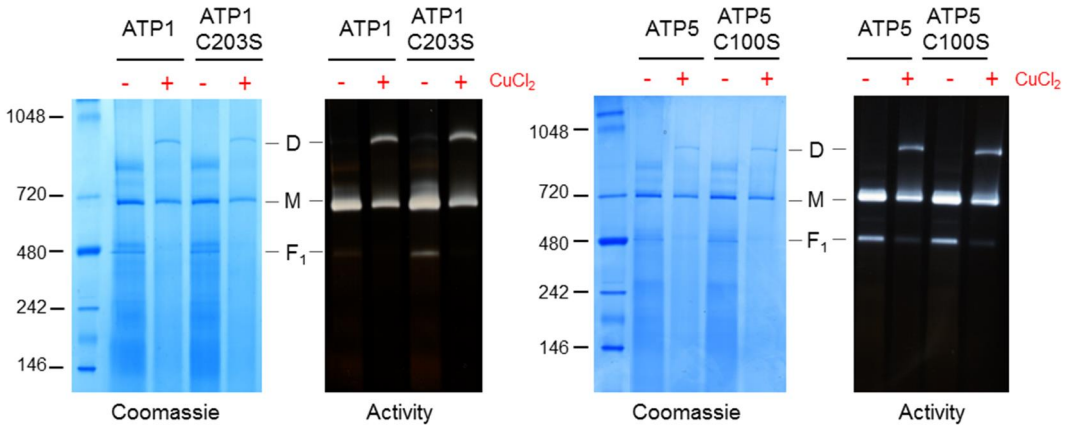

Figure 33. BN-PAGE screening of F-ATP synthase Cys mutants. Mitochondrial proteins from *ATP1/ATP1 C203S* (*left panel*) and *ATP5/ATP5 C100S* (*right panel*) were separated with BN-PAGE and stained with Coomassie blue or for in-gel activity, as indicated, to identify bands of F-ATP synthase dimers and monomers (-/+ treatment with 2 mM $CuCl_2$).

Mutant carrying the *ATP6 C23S* mutation in a *ΔTIM11* genetic background was kindly generated by the laboratory of Dr. Roza Kucharczyk (University of Warsaw). Previous reports showed that two subunits a created an homodimeric structure upon cross-linking, and hypothesized that this might be due to formation of a disulfide bridge between two Cys23 in close proximity at the interface between monomers[79]. In keeping with this proposal, we found that $CuCl_2$ treatment did not lead to dimerization in *ATP6 C23S* mutant, indicating that Cys23 was actually the target of this oxidation (**Figure 34A**). The mutants were significantly desensitized to Ca^{2+}, as they were able to take up a larger Ca^{2+} load before pore opening (**Figure 34B**). It should be recalled, however, that the mutation was inserted in a strain lacking the e subunit, and therefore that the specific contribution of Cys23 to PTP modulation requires further investigation. Of note, yeast Cys23 is not to conserved among species, i.e. *Drosophila* subunit a contains two close Cys residues at the C-terminus (Cys112-Cys144), whereas the human protein does not present Cys residues at all. Anyway, in higher organisms other small subunits could have emerged to hold this function; for instance, human A6L, a small subunit deeply in contact with subunit a and f[46], shows a Cys residue in position 59 that might participate in this kind of interaction.

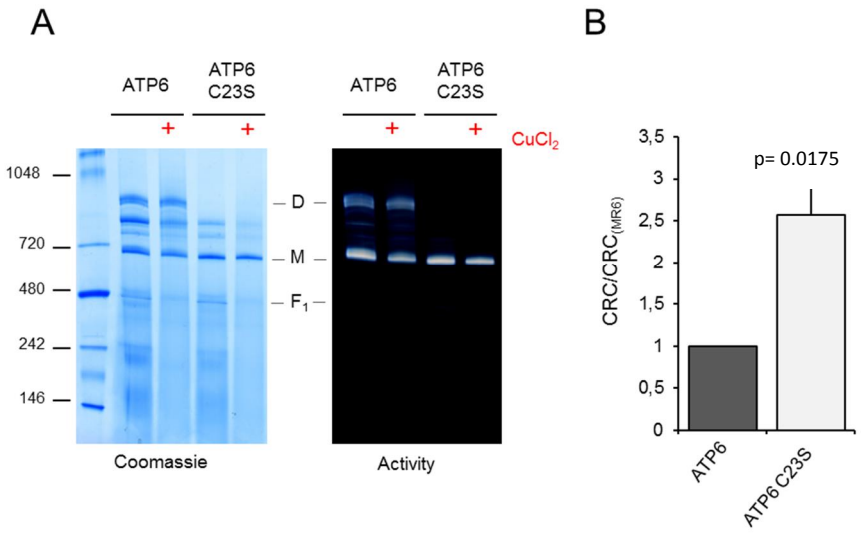

Figure 34. Cys23 of subunit a is the target of $CuCl_2$ treatment. (A) Mitochondrial proteins from *ATP6* (MR6 control) and *ATP6 C23S* (*ΔTIM11*) were separated with BN-PAGE and stained with Coomassie blue or for in-gel activity, as indicated, to identify bands of F-ATP synthase dimers and monomers (-/+ treatment with 2 mM $CuCl_2$). (B) Experimental conditions were as in Figure 26. Quantification of CRC experiments with *ATP6* and *ATP6 C23S* mitochondria were reported in bars graph (n=4±SE). The amount of Ca^{2+} accumulated prior to PTP opening was normalized to that of *ATP6* (MR6 control). A T-test was performed: p=0.0175.

3.6 OSCP Cys residue as target of diamide

The analysis of F-ATP synthase Cys mutants is extremely relevant because in principle it allows to identify redox-sensitive sites of the enzyme that participate in PTP regulation. From the initial screening, *ATP5 C100S* mutants were investigated more in detail for many reasons: (i) *ATP5* encodes for OSCP subunit, a fundamental component of the lateral stalk directly contacting the catalytic core, having a key role in the control of enzyme activity; (ii) in mammals, OSCP is the binding site for CyP D and for Bz-423 (an immunomodulatory benzodiazepine), two major inducers of the PTP; (iii) in mammals down-regulation of OSCP increased the sensitivity of the pore to Ca^{2+} [44]. All together, these observations point to a key role of this subunit in enzyme/PTP modulation. To test whether the *C100S* mutation affected the activity of F-ATP synthase, the ATP-hydrolysis capacity was evaluated by using an ATP-regenerating system that provides a constant ATP level to the enzyme. ATP hydrolysis was decreased in the mutant compared to that of control (2.71 versus 4.05 nmol ATP x min^{-1} x mg $protein^{-1}$, respectively), while sensitivity to oligomycin (inhibitor of the enzyme) was unaffected (**Table X**). This set of data suggested that Cys100 might be involved in regulation of the catalysis, possibly through oxidation-reduction events.

	nmol ATP/min*mg	Oligomycin sensitivity (%)
ATP5	4.05 ± 0.62	51.69 ± 10.33
ATP5 C100S	2.71 ± 0.25	52.33 ± 2.90

Table X. ATP hydrolysis capacity of ATP5 C100S mutant. ATP hydrolysis was quantified as nmol of ATP molecules hydrolyzed by 1 mg of mitochondria in 1 min. The sensitivity to oligomycin was given as percentage of ATP hydrolysis activity inhibited by 6.5 µM of the compound (n=3±SE).

To test the impact of the *C100S* mutation on PTP modulation by oxidants, CRC experiments were performed in presence of PhAsO, $Cu(OP)_2$ and diamide, all thiol-reactive reagents. The sensitivity of the pore to increasing concentration of PhAsO and $Cu(OP)_2$ did not change, indicating that these two compounds probably act on another site (**Figure 35A-B**). Conversely, the *ATP5 C100S* (*open symbols*) mutant showed a remarkably decreased sensitivity to low concentrations of diamide (*closed symbols*) (**Figure 35C**).

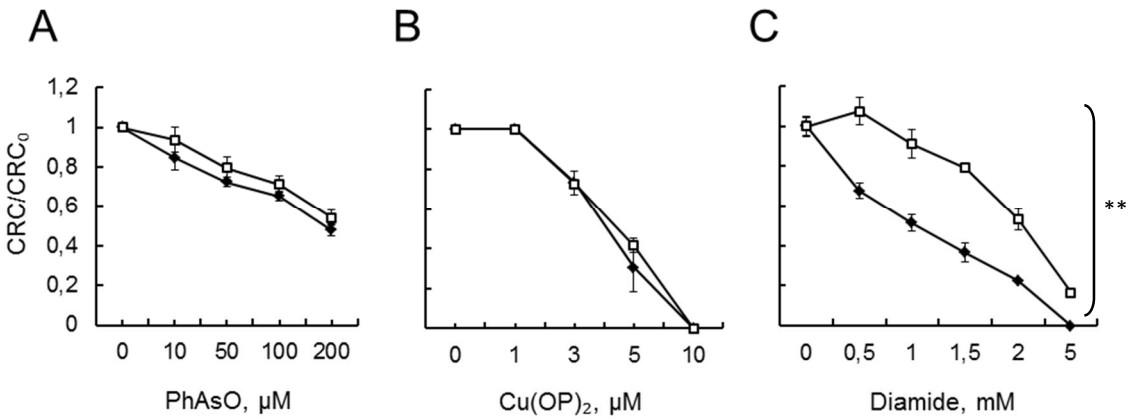

Figure 35. Sensitivity to oxidants of the PTP in *ATP5 C100S* mutant. Experimental conditions were as in Figure 26. Mitochondria were incubated with increasing µM concentration of PhAsO (A), $Cu(OP)_2$ (B) and diamide (C). The Ca^{2+} amount required for PTP opening in presence of different concentration of oxidants was normalized to that in control condition (no additions). The CRC/CRC_0 ratio was calculated for *ATP5 C100S* (open symbols) and for the control strain (close symbols) (n=4±SE). Two-Way ANOVA test was performed: **p<0.001.

This was the first indication that OSCP Cys could be one of the residues targeted by oxidation, thus being a critical site for the redox-mediated regulation of the PTP, at least in yeast. The murine OSCP subunit contains a single Cys residue located in position 141, which is presumed to be part of the binding site of CyP D[44,48]. It appears thus conceivable that the interaction with CyP D could mask the putative diamide-sensitive Cys141 in OSCP. To test this hypothesis mouse liver mitochondria (MLM) were incubated either with low (*closed symbols*) or high (*open symbols*) [Pi], the latter being a

condition that favors the binding of CyP D to OSCP[44], and analyzed for their CRC in the presence of increasing concentration of diamide. Clearly, the sensitivity of the pore to diamide decreased at high [Pi], in keeping with the idea that CyP D could protect Cys141 from oxidiation (**Figure 36A**). This effect was not observed if Pi was replaced with vanadate, which as Pi support Ca^{2+} uptake and acts as a PTP inducer, but at variance from Pi, does not inhibit the pore in the presence of CsA or in CyP D-null mitochondria. This finding suggests that the unique effect of Pi may be mediated by promoting CyP D binding to OSCP. Indeed, the sensitivity of the pore to diamide does not change with vanadate (**Figure 36C** compare *open* and *closed red symbols*). As for yPTP, the difference was observed with diamide but not PhAsO (**Figure 36B**). Strong evidence supporting the hypothesis that CyP D could be a protective factor, was obtained from similar experiments carried out in *Ppif*$^{-/-}$ MLM, where lack of CyP D should expose Cys141 and thus allow its oxidation. Indeed, CRC analysis in the presence of low (*closed symbols*) and high (*open symbols*) [Pi] did not reveal major differences in diamide sensitivity (**Figure 36D**). Like in yeast, the effect was specific for diamide as the inducing affect of PhAsO was instead unaffected (**Figure 36E**).

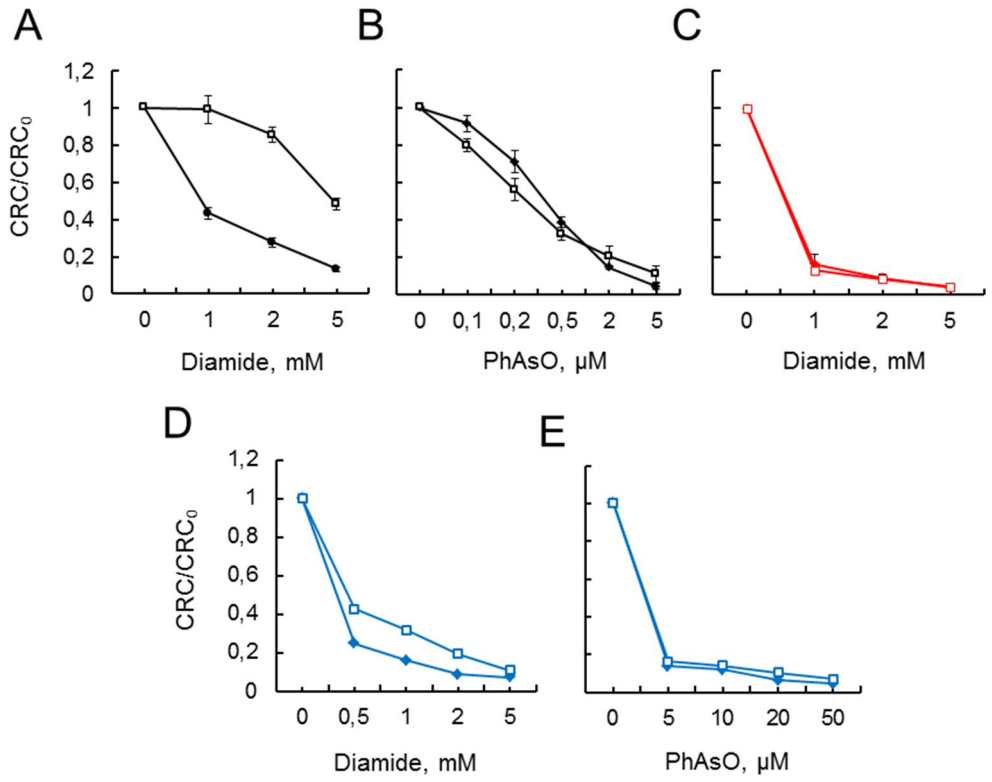

Figure 36. Sensitivity of the mPTP to diamide: "protective" role of CyP D. The incubation medium contained 250 mM Sucrose, 10 mM Tris-MOPS, 5 mM Glutammate/2.5 mM Malate, 10 µM EGTA-Tris, 1 µM Calcium Green-5N, final pH 7.4, and 0.2 mg of mitochondria in a final volume of 0.2 ml. Wild-type MLM were treated with 0.5 mM Pi (*close symbols*) or 5 mM Pi (*open symbols*) and analyzed by CRC experiments in presence of increasing concentration of diamide (n=11±SE) (A) and PhAsO (n=3±SE) (B). (C) MLM were treated with 0.5 mM vanadate (*red close symbols*) or 5 mM vanadate (*red close symbols*) and tested in CRC experiments at increasing concentrations of diamide (n=3±SE). Similar CRC assays were performed for *Pfif*$^{-/-}$ mitochondria in presence of 0.5 mM Pi (*blue close symbols*) and 5 mM Pi (*blue open symbols*) at increasing concentration of diamide (D) and PhAsO(E)(n=2, in both cases).

Analysis was extended to the HEK293T human cell line. Here, CRC assays were carried out with digitonin-permeabilized cells incubated at low (*closed symbols*) and high (*open symbols*) [Pi] in presence of increasing concentration of diamide. As shown in **Figure 37A**, the sensitivity to diamide slightly decreased at high [Pi]. At variance from MLM, diamide-mediated PTP opening in HEK293T cells appeared to be marginally protected from the CyP D binding to OSCP.

We suspect that some CyP D might be already bound at low [Pi], masking the OSCP Cys, so that no major differences can be appreciated by increasing [Pi]. To overcome this problem and prevent CyP D binding to OSCP, the previous experiment was performed by adding CsA to permeabilized cells, a condition under which CsA protected cells from PhAsO (**Figure 37C**), but not diamide (**Figure 37B**).

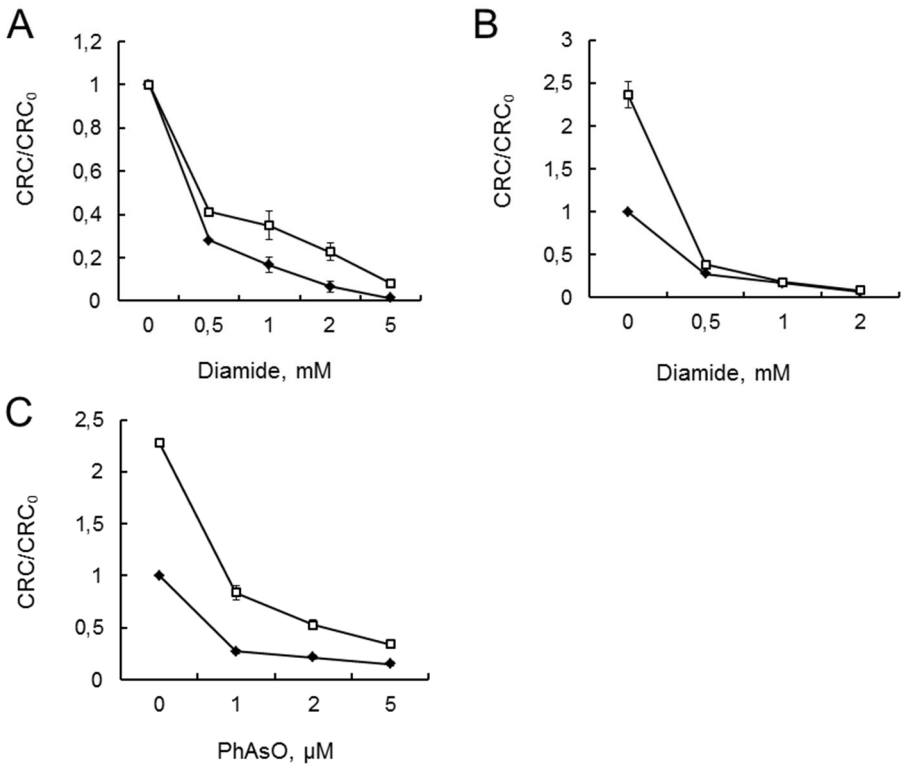

Figure 37. Sensitivity of the mPTP to diamide in HEK293T cells. CRC experiments with permeabilized cells. The medium contained 250 mM Sucrose, 10 mM MOPS-Tris, pH 7.4 buffer, supplemented with 5 mM Glutamate/2.5 mM Malate, 0.5 µM Calcium Green-5N fluorescence probe. A final concentration of 5 x 10^6 cells/ml was used. **A)** HEK293T cells incubated at 0.5 mM (*close symbols*) or 5 mM (*open symbols*) Pi in presence of increasing concentration of diamide. CRC/CRC_0 ratio was quantified in both conditions (n=5±SE). **B-C)** Experimental conditions were as in panel A, with the addition of 0.5 mM Pi. Cells were treated with (*open symbols*) or w/o (*close symbols*) 2 µM CsA and CRC was evaluated in presence of increasing concentration of diamide **(B)** (n=4±SE) or PhAsO**(C)** (n=3±SE).

In conclusion, all these data on yeast, mouse and HEK293T cells strongly suggested a novel function of OSCP in sensing a specific oxidative condition and thus modulating PTP opening.

Given that diamide can promote formation of disulfide bridges between vicinal thiols, our working hypothesis was that this may occur between OSCP Cys and an unknown partner protein. To address this point, Western Blot experiments were carried out with MLM treated with diamide in presence of low [Pi], in order to investigate possible changes in OSCP protein level as well as the appearance of higher molecular weight OSCP complexes. As shown in **Figure 38A**, treatment with diamide markedly decreased the level of OSCP at 23 kDa. Thus, the oxidation of OSCP Cys 141 decreased the fraction of OSCP subunit that can be detected at 23 kDa, and the effect was reverted by the thiol-reducing agent, DTT (**Figure 38A**). This effect appeared to be selective for diamide, since it could not be obtained with PhAsO. We performed IP of complex V, following treatment with CsA (to force unbinding of CyP D and allow exposure of OSCP Cys to oxidant), and with diamide (**Figure 38B**). Again, OSCP protein level at 23 kDa was decreased by diamide and restored by DTT, and these changes were stronger in presence of CsA. Further studies are required to consolidate or disprove our working hypothesis and to identify the putative interactor that may bind to OSCP upon oxidation with diamide.

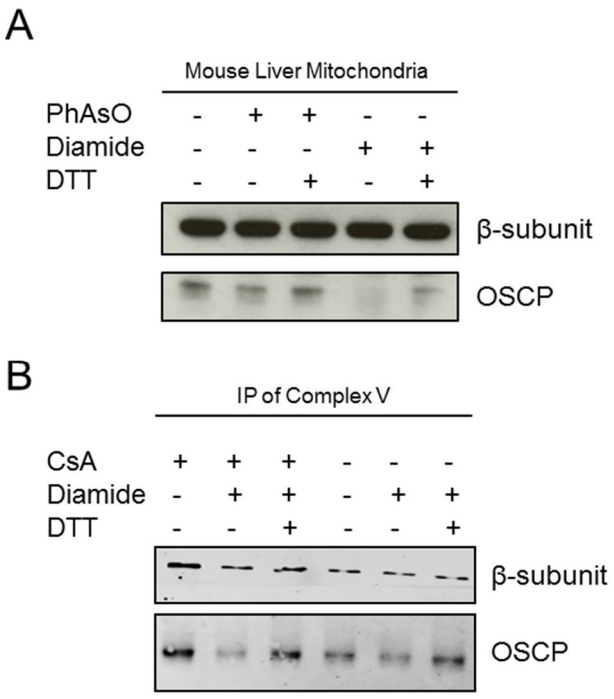

Figure 38. OSCP protein level is affected by diamidetreatment. MLM were incubated in CRC buffer (as in Figure 36) in presence of 0.5 mM Pi and treated, as indicated, with: 5 µM PhAsO, 1 mM diamide, 2 mM DTT, and 2 µM CsA. (A) MLM were subjected directly to Western blot analysis (A) or to the IP of Complex V (B). (A-B) The antibodies used were: mouse monoclonal anti-β subunit (52 kDa) and rabbit polyclonal anti-OSCP (23 kDa).

Taken together, these data indicate that CyP D might have a “protective” role when specific thiol oxidants are used as PTP-inducing stimulus. This would be consistent with hitherto unexplained and intriguing findings of Lin and Lechleiter, who reported that overexpression of CyP D in HEK293 and C6 glioma cells prolongs the time before the PTP-dependent collapse of ΔΨ after treatment with TBH[235].

4. Conclusions

Conclusions

In this study we characterized the Ca^{2+} dependent-Permeability Transition Pore in *S. cerevisiae*. We demonstrated that its opening (i) is sensitive to thiol-reagents, (ii) is unaffected by rotenone and CsA and (iii) is inhibited by ADP/Mg^{2+}, Pi and acidic pH. For the first time we demonstrated that the genetic ablation of *CPR3*, the yeast homologue of CyP D, does not affect the sensitivity of the yPTP to Ca^{2+}, a finding that explains why the yPTP is insensitive to CsA in spite of the presence of a mitochondrial CyP, which appears not to interact with the pore.

We showed that purified yeast F-ATP synthase dimers form the PTP in response to Ca^{2+}, demonstrating that channel formation is a conserved feature of the enzyme that had only been described in mitochondria from *B. taurus* and then, consistently *D. melanogaster*. This finding thus represents a turning point in the field that also provided an excellent model to unravel many open questions about structure and regulation of the PTP.

We demonstrated that "dimerization" subunits of the F-ATP synthase play a role in yPTP formation, probably making the dimeric form of the enzyme more stable. Whether or not these subunits directly contribute to the full conductance channel still needs to be investigated.

Our investigation of Cys mutants revealed that OSCP confers sensitivity of the PTP to the thiol oxidant diamide, both in yeast and mammals. These results strongly suggest that this subunit, located on the top of the lateral stalk of F-ATP synthase in contact with the catalytic core and with the membrane-bound domain, could be a major regulatory site of the pore.

Finally, it is now not surprising that in yeast the lack of a correct assembly of the F-ATP synthase is correlated to a resistance to cell death induced by ROS and increase cytosolic [Ca^{2+}]. Indeed, this finding should acquire a new meaning in the light of our demonstration that dimers form the PTP when subjected to oxidative stress in the presence of Ca^{2+}. We suspect that the yPTP could be a final common pathway in a variety of forms of yeast programmed cell death.

The general implication of my work is that the yPTP may participate in Ca^{2+} homeostasis and represents a final common pathway in a variety of forms of yeast programmed cell death.

5. Bibliography

Bibliography

1. Lane, N. & Martin, W. The energetics of genome complexity. *Nature* **467,** 929–34 (2010).

2. McBride, H. M., Neuspiel, M. & Wasiak, S. Mitochondria: more than just a powerhouse. *Curr. Biol.* **16,** R551–60 (2006).

3. Youle, R. J. & van der Bliek, A. M. Mitochondrial fission, fusion, and stress. *Science* **337,** 1062–5 (2012).

4. Pernas, L. & Scorrano, L. Mito-Morphosis: Mitochondrial Fusion, Fission, and Cristae Remodeling as Key Mediators of Cellular Function. *Annu. Rev. Physiol.* **78,** 11.1-11.27 (2016).

5. Mannella, C. a *et al.* Topology of the mitochondrial inner membrane: dynamics and bioenergetic implications. *IUBMB Life* **52,** 93–100 (2001).

6. Anderson, S. *et al.* Sequence and organization of the human mitochondrial genome. *Nature* **290,** 457–65 (1981).

7. Friedman, J. R. and Nunnari J. Mitochondrial form and function. *Nature* **505**, 335-343 (2014).

8. Itagaki, K. & Hauser, C. J. Responses to Injury. *Nature* **464,** 104–107 (2010).

9. Frey, T. G., Renken, C. W. & Perkins, G. a. Insight into mitochondrial structure and function from electron tomography. *Biochim. Biophys. Acta - Bioenerg.* **1555,** 196–203 (2002).

10. Vogel, F., Bornhovd, C., Neupert, W. & Reichert, A. S. Dynamic subcompartmentalization of the mitochondrial inner membrane. *J. Cell Biol.* **175,** 237–247 (2006).

11. Brdiczka, D. G., Zorov, D. B. & Sheu, S.-S. Mitochondrial contact sites: Their role in energy metabolism and apoptosis. *Biochim. Biophys. Acta - Mol. Basis Dis.* **1762,** 148–163 (2006).

12. Zick, M., Rabl, R. & Reichert, A. S. Cristae formation—linking ultrastructure and function of mitochondria. *Biochim. Biophys. Acta - Mol. Cell Res.* **1793,** 5–19 (2009).

13. Hackenbrock, C. R. Ultrastructural bases for metabolically linked mechanical activity in mitochondria. I. Reversible ultrastructural changes with change in metabolic steady state in isolated liver mitochondria. *J. Cell Biol.* **30,** 269–297 (1966).

14. Mannella, C. A. Structure and dynamics of the mitochondrial inner membrane cristae. *Biochim. Biophys. Acta.* **1763,** 542–8 (2006).

15. Chan, D. C. Fusion and Fission: Interlinked Processes Critical for Mitochondrial Health. *Annu. Rev. Genet.* **46,** 265–287 (2012).

16. Malka, F. *et al.* Separate fusion of outer and inner mitochondrial membranes. *EMBO Rep.* **6,** 853–859 (2005).

17. van der Bliek, A. M., Shen, Q. & Kawajiri, S. Mechanisms of mitochondrial fission and fusion. *Cold Spring Harb Perspect Biol* **5,** 1–16 (2013).

18. Koopman, W. J. H., Distelmaier, F., Smeitink, J. a M. & Willems, P. H. G. M. OXPHOS mutations and neurodegeneration. *EMBO J.* **32,** 9–29 (2013).

19. de Vries, S. & Marres, C. A. The mitochondrial respiratory chain of yeast. Structure and biosynthesis and the role in cellular metabolism. *Biochim. Biophys. Acta* **895,** 205–39 (1987).

20. Mitchell, P. Coupling of phosphorylation to electron and hydrogen transfer by a chemi-osmotic type of mechanism. *Nature* **191,** 144–8 (1961).

21. Granata, S. *et al.* Mitochondrial dysregulation and oxidative stress in patients with chronic kidney disease. *BMC Genomics* **10,** 388 (2009).

22. Sazanov, L. A. The mechanism of coupling between electron transfer and proton translocation in respiratory complex I. *J. Bioenerg. Biomembr.* **46,** 247–53 (2014).

23. Smeitink, J., van den Heuvel, L. & DiMauro, S. The genetics and pathology of oxidative phosphorylation. *Nat. Rev. Genet.* **2,** 342–52 (2001).

24. Overkamp, K. M. *et al.* In vivo analysis of the mechanisms for oxidation of cytosolic NADH by *Saccharomyces cerevisiae* mitochondria. *J. Bacteriol.* **182,** 2823–30 (2000).

25. de Vries, S. & Grivell, L. A. Purification and characterization of a rotenone-insensitive NADH:Q6 oxidoreductase from mitochondria of *Saccharomyces cerevisiae*. *Eur. J. Biochem.* **176,** 377–84 (1988).

26. Iwata, M. *et al.* The structure of the yeast NADH dehydrogenase (Ndi1) reveals overlapping binding sites for water- and lipid-soluble substrates. *Proc. Natl. Acad. Sci. U. S. A.* **109,** 15247–52 (2012).

27. Lasserre, J.-P. *et al.* Yeast as a system for modeling mitochondrial disease mechanisms and discovering therapies. *Dis. Model. Mech.* **8,** 509–26 (2015).

28. Hoekstra, A. S. & Bayley, J. P. The role of complex II in disease. *Biochim. Biophys. Acta - Bioenerg.* **1827,** 543–551 (2013).

29. Selak, M. A. *et al.* Succinate links TCA cycle dysfunction to oncogenesis by inhibiting HIF-α prolyl hydroxylase. *Cancer Cell* **7,** 77–85 (2005).

30. Xia, D. *et al.* Structural analysis of cytochrome *bc*1 complexes: implications to the mechanism of function. *Biochim. Biophys. Acta* **1827,** 1278–94 (2013).

31. Acin-Perez, R. & Enriquez, J. A. The function of the respiratory supercomplexes: the plasticity model. *Biochim. Biophys. Acta - Bioenerg.* **1837,** 444–450 (2014).

32. Wittig, I. & Schägger, H. Supramolecular organization of ATP synthase and respiratory chain in mitochondrial membranes. *Biochim. Biophys. Acta* **1787,** 672–80 (2009).

33. Wittig, I., Carrozzo, R., Santorelli, F. M. & Schägger, H. Supercomplexes and subcomplexes of mitochondrial oxidative phosphorylation. *Biochim. Biophys. Acta - Bioenerg.* **1757,** 1066–1072 (2006).

34. McKenzie, M., Lazarou, M., Thorburn, D. R. & Ryan, M. T. Mitochondrial respiratory chain supercomplexes are destabilized in Barth Syndrome patients. *J. Mol. Biol.* **361,** 462–9 (2006).

35. Schägger, H. & Pfeiffer, K. Supercomplexes in the respiratory chains of yeast and mammalian mitochondria. *EMBO J.* **19,** 1777–1783 (2000).

36. Grandier-Vazeille, X. *et al.* Yeast mitochondrial dehydrogenases are associated in a

supramolecular complex. *Biochemistry* **40,** 9758–69 (2001).

37. Maranzana, E., Barbero, G., Falasca, A. I., Lenaz, G. & Genova, M. L. Mitochondrial respiratory supercomplex association limits production of reactive oxygen species from complex I. *Antioxid. Redox Signal.* **19,** 1469–80 (2013).

38. Genova, M. L. & Lenaz, G. The Interplay Between Respiratory Supercomplexes and ROS in Aging. *Antioxid. Redox Signal.* **23,** 208–38 (2015).

39. Murphy, M. P. How mitochondria produce reactive oxygen species. *Biochem. J.* **417,** 1–13 (2009).

40. Quinlan, C. L. *et al.* Mitochondrial complex II can generate reactive oxygen species at high rates in both the forward and reverse reactions. *J. Biol. Chem.* **287,** 27255–64 (2012).

41. Mailloux, R. J., Jin, X. & Willmore, W. G. Redox Biology Redox regulation of mitochondrial function with emphasis on cysteine oxidation reactions. *Redox Biol.* **2,** 123–139 (2014).

42. Wang, S.-B., Murray, C. I., Chung, H. S. & Van Eyk, J. E. Redox regulation of mitochondrial ATP synthase. *Trends Cardiovasc. Med.* **23,** 14–8 (2013).

43. Walker, J. E. The ATP synthase : the understood , the uncertain and the unknown. *Biochem. Soc. Trans.* **41**, 1–16 (2013).

44. Giorgio, V. *et al.* Dimers of mitochondrial ATP synthase form the permeability transition pore. *Proc. Natl. Acad. Sci. U. S. A.* **110,** 5887–92 (2013).

45. Wittig, I. & Schägger, H. Structural organization of mitochondrial ATP synthase. *Biochim. Biophys. Acta* **1777,** 592–8 (2008).

46. Baker, L. A., Watt, I. N., Runswick, M. J., Walker, J. E. & Rubinstein, J. L. Arrangement of subunits in intact mammalian mitochondrial ATP synthase determined by cryo-EM. *Proc. Natl. Acad. Sci. U. S. A.* **109,** 11675–80 (2012).

47. Rees, D. M., Leslie, A. G. W. & Walker, J. E. The structure of the membrane extrinsic region of bovine ATP synthase. *Proc. Natl. Acad. Sci. U. S. A.* **106,** 21597–601 (2009).

48. Antoniel, M. *et al.* The oligomycin-sensitivity conferring protein of mitochondrial ATP synthase: emerging new roles in mitochondrial pathophysiology. *Int. J. Mol. Sci.* **15,** 7513–36 (2014).

49. Carbajo, R. J. *et al.* Structure of the F1-binding domain of the stator of bovine F_1F_o-ATPase and how it binds an alpha-subunit. *J. Mol. Biol.* **351,** 824–38 (2005).

50. Arechaga, I., Butler, P. J. G. & Walker, J. E. Self-assembly of ATP synthase subunit *c* rings. *FEBS Lett.* **515,** 189–193 (2002).

51. Watt, I. N., Montgomery, M. G., Runswick, M. J., Leslie, A. G. W. & Walker, J. E. Bioenergetic cost of making an adenosine triphosphate molecule in animal mitochondria. *Proc. Natl. Acad. Sci. U. S. A.* **107,** 16823–7 (2010).

52. Allegretti, M. *et al.* Horizontal membrane-intrinsic α-helices in the stator a-subunit of an F-type ATP synthase. *Nature* **521,** 237–240 (2015).

53. Meyer, B., Wittig, I., Trifilieff, E., Karas, M. & Schägger, H. Identification of two proteins

associated with mammalian ATP synthase. *Mol. Cell. Proteomics* **6,** 1690–1699 (2007).

54. Arnold, I., Bauer, M. F., Brunner, M., Neupert, W. & Stuart, R. A. Yeast mitochondrial F_1F_o-ATPase: the novel subunit e is identical to Tim11. *FEBS Lett.* **411,** 195–200 (1997).

55. Arselin, G. *et al.* The GxxxG motif of the transmembrane domain of subunit e is involved in the dimerization/oligomerization of the yeast ATP synthase complex in the mitochondrial membrane. *Eur. J. Biochem.* **270,** 1875–1884 (2003).

56. Bustos, D. M. & Velours, J. The modification of the conserved GXXXG motif of the membrane-spanning segment of subunit g destabilizes the supramolecular species of yeast ATP synthase. *J. Biol. Chem.* **280,** 29004–10 (2005).

57. Saddar, S. The Yeast F_1F_o-ATP Synthase: analysis of the molecular organization of subunit g and the importance of a conserved GXXXG motif. *J. Biol. Chem.* **280,** 24435–24442 (2005).

58. Falson, P., Goffeau, A., Boutry, M. & Jault, J. M. Structural insight into the cooperativity between catalytic and noncatalytic sites of F_1-ATPase. *Biochim. Biophys. Acta - Bioenerg.* **1658,** 133–140 (2004).

59. Kabaleeswaran, V., Puri, N., Walker, J. E., Leslie, A. G. W. & Mueller, D. M. Novel features of the rotary catalytic mechanism revealed in the structure of yeast F1 ATPase. *EMBO J.* **25,** 5433–42 (2006).

60. Bason, J. V, Montgomery, M. G., Leslie, A. G. W. & Walker, J. E. How release of phosphate from mammalian F_1-ATPase generates a rotary substep. *Proc. Natl. Acad. Sci.* **112,** 6009-6014 (2015).

61. Rees, D. M., Montgomery, M. G., Leslie, A. G. W. & Walker, J. E. Structural evidence of a new catalytic intermediate in the pathway of ATP hydrolysis by F_1-ATPase from bovine heart mitochondria. *Proc. Natl. Acad. Sci. U. S. A.* **109,** 11139–43 (2012).

62. Pullman, M. E. & Monroy, G. C. a Naturally Occurring Inhibitor of Mitochondrial Adenosine Triphosphatase. *J. Biol. Chem.* **238,** 3762–9 (1963).

63. Norling, B., Tourikas, C., Hamasur, B. & Glaser, E. Evidence for an endogenous ATPase inhibitor protein in plant mitochondria. Purification and characterization. *Eur. J. Biochem.* **188,** 247–52 (1990).

64. Matsubara, H., Hase, T., Hashimoto, T. and Tagawa K. Amino acid sequence of an intrinsic inhibitor of mitochondrial ATPase from yeast. **90,** 1159–1165 (1981).

65. Cabezón, E., Montgomery, M. G., Leslie, A. G. W. & Walker, J. E. The structure of bovine F_1-ATPase in complex with its regulatory protein IF1. *Nat. Struct. Biol.* **10,** 744–50 (2003).

66. Cabezon, E., Butler, P. J., Runswick, M. J. & Walker, J. E. Modulation of the oligomerization state of the bovine F_1-ATPase inhibitor protein, IF1, by pH. *J. Biol. Chem.* **275,** 25460–4 (2000).

67. Sánchez-Aragó, M. *et al.* Expression, regulation and clinical relevance of the ATPase inhibitory factor 1 in human cancers. *Oncogenesis* **2,** e46 (2013).

68. Sánchez-Cenizo, L. *et al.* Up-regulation of the ATPase Inhibitory Factor 1 (IF1) of the mitochondrial H^+-ATP synthase in human tumors mediates the metabolic shift of cancer cells to a warburg phenotype. *J. Biol. Chem.* **285,** 25308–25313 (2010).

69. Cabezon, E., Butler, P. J. G., Runswick, M. J., Carbajo, R. J. & Walker, J. E. Homologous and heterologous inhibitory effects of ATPase inhibitor proteins on F-ATPases. *J. Biol. Chem.* **277,** 41334–41 (2002).

70. Allen, R. D. Membrane tubulation and proton pumps. *Protoplasma* **189,** 1–8 (1995).

71. Davies, K. M., Anselmi, C., Wittig, I., Faraldo-Gomez, J. D. & Kuhlbrandt, W. Structure of the yeast F_1F_o-ATP synthase dimer and its role in shaping the mitochondrial cristae. *Proc. Natl. Acad. Sci.* **109,** 13602–13607 (2012).

72. Dudkina, N. V, Sunderhaus, S., Braun, H.-P. & Boekema, E. J. Characterization of dimeric ATP synthase and cristae membrane ultrastructure from Saccharomyces and Polytomella mitochondria. *FEBS Lett.* **580,** 3427–32 (2006).

73. Seelert, H. & Dencher, N. A. ATP synthase superassemblies in animals and plants: Two or more are better. *Biochim. Biophys. Acta - Bioenerg.* **1807,** 1185–1197 (2011).

74. Paumard, P. *et al.* The ATP synthase is involved in generating mitochondrial cristae morphology. *EMBO J.* **21,** 221–30 (2002).

75. Arnold, I., Pfeiffer, K., Neupert, W., Stuart, R. a & Schägger, H. Yeast mitochondrial F_1F_o-ATP synthase exists as a dimer: identification of three dimer-specific subunits. *EMBO J.* **17,** 7170–8 (1998).

76. Gavin, P. D., Prescott, M. & Devenish, R. J. F_1F_o-ATP synthase complex interactions in vivo can occur in the absence of the dimer specific subunit e. *J. Bioenerg. Biomembr.* **37,** 55–66 (2005).

77. Soubannier, V. *et al.* In the absence of the first membrane-spanning segment of subunit 4(b), the yeast ATP synthase is functional but does not dimerize or oligomerize. *J. Biol. Chem.* **277,** 10739–45 (2002).

78. Rubinstein, J. L., Dickson, V. K., Runswick, M. J. & Walker, J. E. ATP synthase from *Saccharomyces cerevisiae*: location of subunit h in the peripheral stalk region. *J. Mol. Biol.* **345,** 513–20 (2005).

79. Velours, J. *et al.* Evidence of the proximity of ATP synthase subunits 6 (a) in the inner mitochondrial membrane and in the supramolecular forms of *Saccharomyces cerevisiae* ATP synthase. *J. Biol. Chem.* **286,** 35477–35484 (2011).

80. Buzhynskyy, N., Sens, P., Prima, V., Sturgis, J. N. & Scheuring, S. Rows of ATP synthase dimers in native mitochondrial inner membranes. *Biophys. J.* **93,** 2870–6 (2007).

81. Davies, K. M. *et al.* Macromolecular organization of ATP synthase and complex I in whole mitochondria. *Proc. Natl. Acad. Sci. U. S. A.* **108,** 14121–6 (2011).

82. Floyd, R. & Wray, S. Calcium transporters and signalling in smooth muscles. *Cell Calcium* **42,** 467–76 (2007).

83. Balaban, R. S. The role of Ca^{2+} signaling in the coordination of mitochondrial ATP production with cardiac work. *Biochim. Biophys. Acta* **1787,** 1334–41 (2009).

84. DeLuca, H. F. & Engstrom, G. Calcium uptake by rat kidney mitochondria. *Proc. Natl. Acad. Sci. U. S. A.* **47**, 1744–1750 (1961).

85. Pizzo, P., Drago, I., Filadi, R. & Pozzan, T. Mitochondrial Ca^{2+} homeostasis: mechanism, role,

and tissue specificities. *Pflügers Arch. Eur. J. Physiol.* **464,** 3–17 (2012).

86. Rizzuto, R. & Pozzan, T. Microdomains of Intracellular Ca^{2+} : Molecular Determinants and Functional Consequences. *Physiol. Rev.* **86,** 369–408 (2006).

87. Rizzuto, R., Stefani, D. De, Raffaello, A. & Mammucari, C. Mitochondria as sensors and regulators of calcium signalling. *Nat. Publ. Gr.* **13,** 566–578 (2012).

88. De Stefani, D., Raffaello, A., Teardo, E., Szabò, I. & Rizzuto, R. A forty-kilodalton protein of the inner membrane is the mitochondrial calcium uniporter. *Nature* **476,** 336–40 (2011).

89. Baughman, J. M. *et al.* Integrative genomics identifies MCU as an essential component of the mitochondrial calcium uniporter. *Nature* **476,** 341–5 (2011).

90. Rizzuto, R. *et al.* Close contacts with the endoplasmic reticulum as determinants of mitochondrial Ca^{2+} responses. *Science* **280,** 1763–6 (1998).

91. Rossi, C. S., Vasington, F. D. & Carafoli, E. The effect of ruthenium red on the uptake and release of Ca^{2+} by mitochondria. *Biochem. Biophys. Res. Commun.* **50,** 846–52 (1973).

92. Kirichok, Y., Krapivinsky, G. & Clapham, D. E. The mitochondrial calcium uniporter is a highly selective ion channel. *Nature* **427,** 360–4 (2004).

93. Nicholls, D. G. Mitochondrial calcium function and dysfunction in the central nervous system. *Biochem. Biophys. Res. Commun.* **1787,** 1416–1424 (2010).

94. Bernardi, P. & Pietrobon, D. On the nature of Pi-induced, Mg^{2+}-prevented Ca^{2+} release in rat liver mitochondria. *FEBS Lett* **139,** 9–12 (1982).

95. Kristian, T., Pivovarova, N. B., Fiskum, G. & Andrews, S. B. Calcium-induced precipitate formation in brain mitochondria: composition, calcium capacity, and retention. *J. Neurochem.* **102,** 1346–56 (2007).

96. Rizzuto, R., Bernardi, P. & Pozzan, T. Mitochondria as all-round players of the calcium game. *J. Physiol.* **529 Pt 1,** 37–47 (2000).

97. Pfeiffer, D. R., Gunter, T. E., Eliseev, R., Broekemeier, K. M. & Gunter, K. K. Release of Ca^{2+} from mitochondria via the saturable mechanisms and the permeability transition. *IUBMB Life* **52,** 205–12 (2001).

98. Palty, R. *et al.* NCLX is an essential component of mitochondrial Na^{+}/Ca^{2+} exchange. *Proc. Natl. Acad. Sci.* **107,** 436–441 (2010).

99. Lu, X., Kwong, J., Molkentin, J. D. & Bers, D. M. Individual cardiac mitochondria undergo rare transient permeability transition pore openings. *Circ. Res.* (2015).

100. Drago, I., Pizzo, P. & Pozzan, T. After half a century mitochondrial calcium in- and efflux machineries reveal themselves. *EMBO J.* **30,** 4119–4125 (2011).

101. Koonin, E. V & Aravind, L. Origin and evolution of eukaryotic apoptosis: the bacterial connection. *Cell Death Differ.* **9,** 394–404 (2002).

102. Ellis, H. M. & Horvitz, H. R. Genetic control of programmed cell death in the nematode *C. elegans*. *Cell* **44,** 817–29 (1986).

103. Norbury, C. J. & Hickson, I. D. Cellular responses to DNA damage. *Annu. Rev. Pharmacol. Toxicol.* **41,** 367–401 (2001).

104. Taylor, R. C., Cullen, S. P. & Martin, S. J. Apoptosis: controlled demolition at the cellular level. *Nat. Rev. Mol. Cell Biol.* **9,** 231–41 (2008).

105. Favaloro, B., Allocati, N., Graziano, V., Di Ilio, C. & De Laurenzi, V. Role of apoptosis in disease. *Aging.* **4,** 330–49 (2012).

106. Kerr, J. F. R. History of the events leading to the formulation of the apoptosis concept. *Toxicology* **181-182,** 471–4 (2002).

107. Bakhshi, A. *et al.* Cloning the chromosomal breakpoint of t(14;18) human lymphomas: clustering around JH on chromosome 14 and near a transcriptional unit on 18. *Cell* **41,** 899–906 (1985).

108. Riedl, S. J. & Salvesen, G. S. The apoptosome: signalling platform of cell death. *Nat. Rev. Mol. Cell Biol.* **8,** 405–13 (2007).

109. Katz, C. *et al.* Molecular Basis of the Interaction between Proapoptotic Truncated BID (tBID) Protein and Mitochondrial Carrier Homologue 2 (MTCH2) Protein: Key players in mitochondrial death pathway. *J. Biol. Chem.* **287,** 15016–15023 (2012).

110. Ashkenazi, A. Directing cancer cells to self-destruct with pro-apoptotic receptor agonists. *Nat. Rev. Drug Discov.* **7,** 1001–12 (2008).

111. Sun, L. *et al.* Mixed Lineage Kinase Domain-like Protein Mediates Necrosis Signaling Downstream of RIP3 Kinase. *Cell* **148,** 213–227 (2012).

112. Vandenabeele, P., Galluzzi, L., Vanden Berghe, T. & Kroemer, G. Molecular mechanisms of necroptosis: an ordered cellular explosion. *Nat. Rev. Mol. Cell Biol.* **11,** 700–14 (2010).

113. Degterev, A. *et al.* Identification of RIP1 kinase as a specific cellular target of necrostatins. *Nat. Chem. Biol.* **4,** 313–21 (2008).

114. Vanden Berghe, T., Linkermann, A., Jouan-Lanhouet, S., Walczak, H. & Vandenabeele, P. Regulated necrosis: the expanding network of non-apoptotic cell death pathways. *Nat. Rev. Mol. Cell Biol.* **15,** 135–47 (2014).

115. Devalaraja-Narashimha, K., Diener, A. M. & Padanilam, B. J. Cyclophilin D gene ablation protects mice from ischemic renal injury. *Am. J. Physiol. Renal Physiol.* **297,** F749–59 (2009).

116. Nakagawa, T. *et al.* Cyclophilin D-dependent mitochondrial permeability transition regulates some necrotic but not apoptotic cell death. *Nature* **434,** 652–8 (2005).

117. Piot, C. *et al.* Effect of cyclosporine on reperfusion injury in acute myocardial infarction. *N. Engl. J. Med.* **359,** 473–81 (2008).

118. Hunter, F. E., Washington and Ford L. Inactivation of oxidative and phosphorylative systems in mitochondria by preincubation with phosphate and other anions. J. Biol. Chem. **216**, 357-369 (1955)

119. Chappell, J. B. & Crofts, A. R. Calcium ion Accumulation and volume changes of isolated liver mitochondria. calcium ion-induced swelling. *Biochem. J.* **95,** 378–86 (1965).

120. Azzone, G. F. & Azzi, A. Volume changes in liver mitochondria. *Proc. Natl. Acad. Sci. U. S. A.* **53,** 1084–1089 (1965).

121. Newmeyer, D. D. & Ferguson-Miller, S. Mitochondria: releasing power for life and unleashing the machineries of death. *Cell* **112,** 481–490 (2003).

122. Bernardi, P., Rasola, A., Forte, M. & Lippe, G. The Mitochondrial Permeability Transition Pore: Channel Formation by F-ATP Synthase, Integration in Signal Transduction, and Role in Pathophysiology. *Physiol. Rev.* **95,** 1111–55 (2015).

123. Gunter, T. E. & Pfeiffer, D. R. Mechanisms by which mitochondria transport calcium. *Am. J. Physiol.* **258,** C755–C786 (1990).

124. Haworth, R. A. & Hunter, D. R. The Ca^{2+}-induced membrane transition in mitochondria. II. Nature of the Ca^{2+} trigger site. *Arch. Biochem. Biophys.* **195,** 460–7 (1979).

125. Massari, S. & Azzone, G. F. The equivalent pore radius of intact and damaged mitochondria and the mechanism of active shrinkage. *Biochim. Biophys. Acta* **283,** 23–9 (1972).

126. Broekemeier, K. M., Dempsey, M. E. & Pfeiffer, D. R. Cyclosporin A is a potent inhibitor of the inner membrane permeability transition in liver mitochondria. *J. Biol. Chem.* **264,** 7826–7830 (1989).

127. Connern, C. P. & Halestrap, a P. Purification and N-terminal sequencing of peptidyl-prolyl cis-trans-isomerase from rat liver mitochondrial matrix reveals the existence of a distinct mitochondrial cyclophilin. *Biochem. J.* **284 (Pt 2,** 381–385 (1992).

128. Marchetti, P. *et al.* Mitochondrial permeability transition is a central coordinating event of apoptosis. *J. Exp. Med.* **184,** 1155–1160 (1996).

129. Bernardi, P. Mitochondrial transport of cations: channels, exchangers, and permeability transition. *Physiol. Rev.* **79,** 1127–1155 (1999).

130. Hüser, J., Rechenmacher, C. E. & Blatter, L. A. Imaging the permeability pore transition in single mitochondria. *Biophys. J.* **74,** 2129–37 (1998).

131. Bernardi, P. *et al.* Modulation of the mitochondrial permeability transition pore: Effect of protons and divalent cations. *J. Biol. Chem.* **267,** 2934–2939 (1992).

132. Nicolli, A., Petronilli, V. & Bernardi, P. Modulation of the mitochondrial cyclosporin A-sensitive permeability transition pore by matrix pH. Evidence that the pore open-closed probability is regulated by reversible histidine protonation. *Biochemistry* **32,** 4461–5 (1993).

133. Kristian, T., Bernardi, P. & Siesjö, B. K. Acidosis promotes the permeability transition in energized mitochondria: implications for reperfusion injury. *J. Neurotrauma* **18,** 1059–74 (2001).

134. Bernardi, P. Modulation of the Mitochondrial CyclosporinA-sensitive Permeability Transition Pore by the Proton Electrochemical Gradient. *Biochemistry* **267,** 8834–8839 (1992).

135. Johans, M. *et al.* Modification of Permeability Transition Pore Arginine(s) by Phenylglyoxal Derivatives in Isolated Mitochondria and. **280,** 12130–12136 (2005).

136. Costantini, P., Chernyak, B. V., Petronilli, V. & Bernardi, P. Modulation of the mitochondrial permeability transition pore by pyridine nucleotides and dithiol oxidation at two separate

sites. *J. Biol. Chem.* **271,** 6746–6751 (1996).

137. Zamzami, N. & Kroemer, G. The mitochondrion in apoptosis: how Pandora's box opens. *Nat. Rev. Mol. Cell Biol.* **2,** 67–71 (2001).

138. Papadopoulos, V. *et al.* Peripheral benzodiazepine receptor in cholesterol transport and steroidogenesis. *Steroids* **62,** 21–8 (1997).

139. Taketani, S., Kohno, H., Furukawa, T. & Tokunaga, R. Involvement of peripheral-type benzodiazepine receptors in the intracellular transport of heme and porphyrins. *J. Biochem.* **117,** 875–80 (1995).

140. Chelli, B. *et al.* Peripheral-type benzodiazepine receptor ligands: *Biochem. Pharmacol.* **61,** 695–705 (2001).

141. Sileikyte, J. *et al.* Regulation of the Mitochondrial Permeability Transition Pore by the Outer Membrane does not Involve the Peripheral Benzodiazepine Receptor (TSPO). *J. Biol. Chem.* **289,** 13769–13781 (2014).

142. Cleary, J., Johnson, K. M., Opipari, A. W. & Glick, G. D. Inhibition of the mitochondrial F1F0-ATPase by ligands of the peripheral benzodiazepine receptor. *Bioorg. Med. Chem. Lett.* **17,** 1667–1670 (2007).

143. Raghavan, A., Sheiko, T., Graham, B. H. & Craigen, W. J. Voltage-dependant anion channels: novel insights into isoform function through genetic models. *Biochim. Biophys. Acta* **1818,** 1477–85 (2012).

144. Szabó, I., De Pinto, V. & Zoratti, M. The mitochondrial permeability transition pore may comprise VDAC molecules. II. The electrophysiological properties of VDAC are compatible with those of the mitochondrial megachannel. *FEBS Lett.* **330,** 206–10 (1993).

145. Crompton, M., Barksby, E., Johnson, N. & Capano, M. Mitochondrial intermembrane junctional complexes and their involvement in cell death. *Biochimie* **84,** 143–52

146. Halestrap, A. P. & Richardson, A. P. The mitochondrial permeability transition: a current perspective on its identity and role in ischaemia/reperfusion injury. *J. Mol. Cell. Cardiol.* **78,** 129–41 (2015).

147. Krauskopf, A., Eriksson, O., Craigen, W. J., Forte, M. a & Bernardi, P. Properties of the permeability transition in VDAC1($^{-/-}$) mitochondria. *Biochim. Biophys. Acta* **1757,** 590–5 (2006).

148. Baines C.P., *et al*. Voltage-Dependent Anion Channels are dispensable for Mtochondrial-Dependent Cell death. *Nat. Cell. Biol.* **5,** 550–555 (2007).

149. Haworth, R. A. & Hunter, D. R. Control of the mitochondrial permeability transition pore by high-affinity ADP binding at the ADP/ATP translocase in permeabilized mitochondria. *J. Bioenerg. Biomembr.* **32,** 91–6 (2000).

150. Brustovetsky, N., Becker, A., Klingenberg, M. & Bamberg, E. Electrical currents associated with nucleotide transport by the reconstituted mitochondrial ADP/ATP carrier. *Proc. Natl. Acad. Sci. U. S. A.* **93,** 664–8 (1996).

151. Kokoszka, J. E. *et al.* The ADP/ATP translocator is not essential for the mitochondrial permeability transition pore. *Nature* **427,** 461–465 (2004).

152. Masgras, I., Rasola, A. & Bernardi, P. Induction of the permeability transition pore in cells depleted of mitochondrial DNA. *Biochim. Biophys. Acta* **1817,** 1860–6 (2012).

153. Chiara, F. *et al.* Hexokinase II detachment from mitochondria triggers apoptosis through the permeability transition pore independent of voltage-dependent anion channels. *PLoS One* **3,** e1852 (2008).

154. Herick, K., Krämer, R. & Lühring, H. Patch clamp investigation into the phosphate carrier from Saccharomyces cerevisiae mitochondria. *Biochim. Biophys. Acta* **1321,** 207–20 (1997).

155. Leung, A. W. C., Varanyuwatana, P. & Halestrap, A. P. The mitochondrial phosphate carrier interacts with cyclophilin D and may play a key role in the permeability transition. *J. Biol. Chem.* **283,** 26312–23 (2008).

156. Fontaine, E., Ichas, F. & Bernardi, P. A ubiquinone-binding site regulates the mitochondrial permeability transition pore. *J. Biol. Chem.* **273,** 25734–25740 (1998).

157. Kwong, J. Q. *et al.* Genetic deletion of the mitochondrial phosphate carrier desensitizes the mitochondrial permeability transition pore and causes cardiomyopathy. *Cell Death Differ.* **21,** 1209–17 (2014).

158. Giorgio, V. *et al.* Cyclophilin D in mitochondrial pathophysiology. *Biochim. Biophys. Acta* **1797,** 1113–8 (2010).

159. Liu, J. *et al.* Calcineurin is a common target of cyclophilin-cyclosporin A and FKBP-FK506 complexes. *Cell* **66,** 807–15 (1991).

160. Fournier, N., Ducet, G. & Crevat, A. Action of cyclosporine on mitochondrial calcium fluxes. *J. Bioenerg. Biomembr.* **19,** 297–303 (1987).

161. Nicolli, a *et al.* Interactions of cyclophilin with the mitochondrial inner membrane and regulation of the permeability transition pore, and cyclosporin A- sensitive channel. *J Biol Chem* **271,** 2185–2192 (1996).

162. Eliseev, R. a *et al.* Cyclophilin D interacts with Bcl2 and exerts an anti-apoptotic effect. *J. Biol. Chem.* **284,** 9692–9 (2009).

163. W.A., I., L.D., G. & J.A., T. Inhibition of the mitochondrial permeability transition by aldehydes. *Biochem. Biophys. Res. Commun.* **291,** 215–219 (2002).

164. Gomez, L. *et al.* Inhibition of mitochondrial permeability transition improves functional recovery and reduces mortality following acute myocardial infarction in mice. *Am. J. Physiol. Heart Circ. Physiol.* **293**, 1654–1661 (2007).

165. Basso, E. *et al.* Properties of the permeability transition pore in mitochondria devoid of Cyclophilin D. *J. Biol. Chem.* **280,** 18558–61 (2005).

166. Baines, C. P. *et al.* Loss of cyclophilin D reveals a critical role for mitochondrial permeability transition in cell death. *Nature* **434,** 658–62 (2005).

167. Basso, E., Petronilli, V., Forte, M. a & Bernardi, P. Phosphate is essential for inhibition of the mitochondrial permeability transition pore by cyclosporin A and by cyclophilin D ablation. *J. Biol. Chem.* **283,** 26307–11 (2008).

168. Giorgio, V. *et al.* Cyclophilin D modulates mitochondrial F_oF_1-ATP synthase by interacting with

the lateral stalk of the complex. *J. Biol. Chem.* **284,** 33982–8 (2009).

169. Petronilli, V., Szabò, I. & Zoratti, M. The inner mitochondrial membrane contains ion-conducting channels similar to those found in bacteria. *FEBS Lett.* **259,** 137–43 (1989).

170. Szabó, I. & Zoratti, M. The mitochondrial megachannel is the permeability transition pore. *J. Bioenerg. Biomembr.* **24,** 111–7 (1992).

171. Bernardi, P. The mitochondrial permeability transition pore : a mystery solved ? *Front. Physiol.* **4,** 1–12 (2013).

172. Alavian, K. N. *et al.* An uncoupling channel within the c-subunit ring of the F_1F_O ATP synthase is the mitochondrial permeability transition pore. *Proc. Natl. Acad. Sci.* **111,** 10580–10585 (2014).

173. Azzolin, L. *et al.* The mitochondrial permeability transition from yeast to mammals. **584,** 2504–2509 (2011).

174. Azzolin, L., Basso, E., Argenton, F. & Bernardi, P. Mitochondrial Ca^{2+} transport and permeability transition in zebrafish (*Danio rerio*). *Biochim. Biophys. Acta* **1797,** 1775–9 (2010).

175. von Stockum, S. *et al.* Properties of Ca^{2+} transport in mitochondria of Drosophila melanogaster. *J. Biol. Chem.* **286,** 41163–70 (2011).

176. von Stockum, S. *et al.* F-ATPase of *D. melanogaster* forms 53 -pS channels responsible for mitochondrial Ca^{2+}-induced Ca^{2+} Release. *J. Biol. Chem.* **290**, 4537-44 (2015).

177. Tong, A. H. *et al.* Systematic genetic analysis with ordered arrays of yeast deletion mutants. *Science* **294,** 2364–8 (2001).

178. Jones, G. M. *et al.* A systematic library for comprehensive overexpression screens in *Saccharomyces cerevisiae*. *Nat. Methods* **5,** 239–41 (2008).

179. Herskowitz, I. R. a & Of, T. Life cycle of the budding yeast *Saccharomyces cerevisiae*. *Microbiol Rev* **52,** 536–553 (1988).

180. Busti, S., Coccetti, P., Alberghina, L. & Vanoni, M. Glucose signaling-mediated coordination of cell growth and cell cycle in *Saccharomyces cerevisiae*. *Sensors* **10,** 6195–6240 (2010).

181. Wallace, D. C. Mitochondrial diseases in man and mouse. *Science* **283,** 1482–1488 (1999).

182. Baile, M. G. & Claypool, S. M. The power of yeast to model diseases of the powerhouse of the cell. *Front. Biosci. (Landmark Ed.* **18,** 241–78 (2013).

183. Houstek, J. *et al.* Mitochondrial diseases and genetic defects of ATP synthase. *Biochim. Biophys. Acta* **1757,** 1400–5 (2006).

184. Iida, H., Nakamura, H., Ono, T., Okumura, M. S. & Anraku, Y. MID1, a novel *Saccharomyces cerevisiae* gene encoding a plasma membrane protein, is required for Ca^{2+} influx and mating. *Mol. Cell. Biol.* **14,** 8259–8271 (1994).

185. Serrano, R., Ruiz, A., Bernal, D., Chambers, J. R. & Ariño, J. The transcriptional response to alkaline pH in *Saccharomyces cerevisiae*: evidence for calcium-mediated signalling. *Mol. Microbiol.* **46,** 1319–33 (2002).

186. Batiza, A. F., Schulz, T. & Masson, P. H. Yeast respond to hypotonic shock with a calcium pulse. *J. Biol. Chem.* **271,** 23357–23362 (1996).

187. Cui, J. *et al.* Simulating calcium influx and free calcium concentrations in yeast. *Cell Calcium* **45,** 123–132 (2009).

188. Fischer, M. *et al.* The *Saccharomyces cerevisiae* CCH1 gene is involved in calcium influx and mating. *FEBS Lett.* **419,** 259–62 (1997).

189. Cunningham, K. W. & Fink, G. R. Ca2+ transport in *Saccharomyces cerevisiae*. *J. Exp. Biol.* **196,** 157–166 (1994).

190. Miseta, a, Kellermayer, R., Aiello, D. P., Fu, L. & Bedwell, D. M. The vacuolar Ca^{2+}/H^{+} exchanger Vcx1p/Hum1p tightly controls cytosolic Ca^{2+} levels in *S. cerevisiae*. *FEBS Lett.* **451,** 132–6 (1999).

191. Tökés-Füzesi, M. *et al.* Hexose phosphorylation and the putative calcium channel component Mid1p are required for the hexose-induced transient elevation of cytosolic calcium response in Saccharomyces cerevisiae. *Mol. Microbiol.* **44,** 1299–1308 (2002).

192. D'hooge, P. *et al.* Ca^{2+} homeostasis in the budding yeast *Saccharomyces cerevisiae*: Impact of ER/Golgi Ca^{2+} storage. *Cell Calcium* **58,** 1–10 (2015).

193. De Stefani, D., Patron, M. & Rizzuto, R. Structure and function of the mitochondrial calcium uniporter complex. *Biochim. Biophys. Acta* **1853,** 2006–11 (2015).

194. Carafoli, E. & Lehninger, A. L. A survey of the interaction of calcium ions with mitochondria from different tissues and species. *Biochem. J.* **122,** 681–90 (1971).

195. Balcavage, W. X., Lloyd, J. L., Mattoon, J. R., Ohnishi, T. & Scarpa, A. Cation movements and respiratory response in yeast mitochondria treated with high Ca^{2+} concentrations. *Biochim. Biophys. Acta* **305,** 41–51 (1973).

196. Bradshaw, P. C., Jung, D. W. & Pfeiffer, D. R. Free fatty acids activate a vigorous Ca^{2+}:$2H^{+}$ antiport activity in yeast mitochondria. *J. Biol. Chem.* **276,** 40502–9 (2001).

197. Bazhenova, E. N., Deryabina, Y. I., Eriksson, O., Zvyagilskaya, R. a & Saris, N. E. Characterization of a high capacity calcium transport system in mitochondria of the yeast *Endomyces magnusii*. *J. Biol. Chem.* **273,** 4372–7 (1998).

198. Votyakova, T. V, Bazhenova, E. N. & Zvjagilskaya, R. A. Yeast mitochondrial calcium uptake: regulation by polyamines and magnesium ions. *J. Bioenerg. Biomembr.* **25,** 569–74 (1993).

199. Bazhenova, E. N., Saris, N. E. & Zvyagilskaya, R. a. Stimulation of the yeast mitochondrial calcium uniporter by hypotonicity and by ruthenium red. *Biochim. Biophys. Acta* **1371,** 96–100 (1998).

200. James, a G., Cook, R. M., West, S. M. & Lindsay, J. G. The pyruvate dehydrogenase complex of *Saccharomyces cerevisiae* is regulated by phosphorylation. *FEBS Lett.* **373,** 111–4 (1995).

201. Szabó, I. *et al.* The high-conductance channel of porin-less yeast mitochondria. *Biochim. Biophys. Acta* **1235,** 115–25 (1995).

202. Lohret, T. a & Kinnally, K. W. Multiple conductance channel activity of wild-type and voltage-dependent anion-selective channel (VDAC)-less yeast mitochondria. *Biophys. J.* **68,** 2299–309

(1995).

203. Lohret, T. A., Murphy, R. C., Drgoñ, T. & Kinnally, K. W. Activity of the mitochondrial multiple conductance channel is independent of the adenine nucleotide translocator. *J. Biol. Chem.* **271,** 4846–4849 (1996).

204. de Chateaubodeau, G., Guerin, M. & Guerin, B. Studies on anionic transport in yeast mitochondria and promitochondria. Swelling in ammonium phosphate, glutamate, succinate and fumarate solutions. *FEBS Lett.* **46,** 184–7 (1974).

205. Bradshaw, P. C. & Pfeiffer, D. R. Characterization of the respiration-induced yeast mitochondrial permeability transition pore. *Yeast* **30,** 471–83 (2013).

206. Jung, D. W., Bradshaw, P. C. & Pfeiffer, D. R. Properties of a cyclosporin-insensitive permeability transition pore in yeast mitochondria. *J. Biol. Chem.* **272,** 21104–21112 (1997).

207. Prieto, S., Bouillaud, F., Ricquier, D. & Rial, E. Activation by ATP of a proton-conducting pathway in yeast mitochondria. *Eur. J. Biochem.* **208,** 487–91 (1992).

208. Prieto, S., Bouillaud, F. & Rial, E. The mechanism for the ATP-induced uncoupling of respiration in mitochondria of the yeast Saccharomyces cerevisiae. *Biochem. J.* **307 (Pt 3,** 657–661 (1995).

209. Guérin, B., Bunoust, O., Rouqueys, V. & Rigoulet, M. ATP-induced unspecific channel in yeast mitochondria. *J. Biol. Chem.* **269,** 25406–25410 (1994).

210. Roucou, X., Manon, S. & Guérin, M. Conditions allowing different states of ATP- and GDP-induced permeability in mitochondria from different strains of *Saccharomyces cerevisiae*. *Biochim. Biophys. Acta* **1324,** 120–132 (1997).

211. Tropschug, M., Barthelmess, I. B. & Neupert, W. Sensitivity to cyclosporin A is mediated by cyclophilin in Neurospora crassa and Saccharomyces cerevisiae. *Nature* **342,** 953–5

212. Velours, J., Rigoulet, M. & Guerin, B. Protection of yeast mitochondrial structure by phosphate and other H^+ -donating anions. *FEBS Lett*. **81**, 18–22 (1977).

213. Manon, S., Roucou, X., Guérin, M., Rigoulet, M. & Guérin, B. Characterization of the yeast mitochondria unselective channel: a counterpart to the mammalian permeability transition pore? *J. Bioenerg. Biomembr.* **30,** 419–29 (1998).

214. Yamada, A. *et al.* Ca^{2+}-induced permeability transition can be observed even in yeast mitochondria under optimized experimental conditions. *Biochim. Biophys. Acta* **1787,** 1486–91 (2009).

215. Li, B. *et al.* Inhibition of complex I regulates the mitochondrial permeability transition through a phosphate-sensitive inhibitory site masked by cyclophilin D. *Biochim. Biophys. Acta* **1817,** 1628–34 (2012).

216. Côrte-Real, M. & Madeo, F. Yeast programed cell death and aging. *Front. Oncol.* **3,** 283 (2013).

217. Pereira, C. *et al.* Mitochondria-dependent apoptosis in yeast. *Biochim. Biophys. Acta* **1783,** 1286–302 (2008).

218. Guaragnella, N. *et al.* The role of mitochondria in yeast programmed cell death. *Front. Oncol.* **2,** 70 (2012).

219. Madeo, F. Oxygen Stress: A Regulator of Apoptosis in Yeast. *J. Cell Biol.* **145,** 757–767 (1999).

220. Ludovico, P. Cytochrome c Release and Mitochondria Involvement in Programmed Cell Death Induced by Acetic Acid in *Saccharomyces cerevisiae*. *Mol. Biol. Cell* **13,** 2598–2606 (2002).

221. Severin, F. F. & Hyman, A. A. Pheromone induces programmed cell death in *S. cerevisiae*. *Curr. Biol.* **12,** R233–5 (2002).

222. Pozniakovsky, A. I. *et al.* Role of mitochondria in the pheromone- and amiodarone-induced programmed death of yeast. *J. Cell Biol.* **168,** 257–269 (2005).

223. Kitagaki, H., Araki, Y., Funato, K. & Shimoi, H. Ethanol-induced death in yeast exhibits features of apoptosis mediated by mitochondrial fission pathway. *FEBS Lett.* **581,** 2935–42 (2007).

224. Huh, G.-H. *et al.* Salt causes ion disequilibrium-induced programmed cell death in yeast and plants. *Plant J.* **29,** 649–59 (2002).

225. Kajiwara, K. *et al.* Perturbation of sphingolipid metabolism induces endoplasmic reticulum stress-mediated mitochondrial apoptosis in budding yeast. *Mol. Microbiol.* **86,** 1246–61 (2012).

226. Büttner, S. *et al.* A yeast BH3-only protein mediates the mitochondrial pathway of apoptosis. *EMBO J.* **30,** 2779–92 (2011).

227. Gietz, R. D. & Schiestl, R. H. Large-scale high-efficiency yeast transformation using the LiAc/SS carrier DNA/PEG method. *Nat. Protoc.* **2,** 38–41 (2007).

228. Petronilli, V. *et al.* The voltage sensor of the mitochondrial permeability transition pore is tuned by the oxidation-reduction state of vicinal thiols. Increase of the gating potential by oxidants and its reversal by reducing agents. *J. Biol. Chem.* **269,** 16638–42 (1994).

229. Matouschek, A., Rospert, S., Schmid, K., Glick, B. S. & Schatz, G. Cyclophilin catalyzes protein folding in yeast mitochondria. *Proc. Natl. Acad. Sci. U. S. A.* **92,** 6319–23 (1995).

230. Rassow, J. *et al.* Cyclophilin 20 is involved in mitochondrial protein folding in cooperation with molecular chaperones Hsp70 and Hsp60. *Mol. Cell. Biol.* **15,** 2654–62 (1995).

231. Thomas, D. *et al.* Supramolecular organization of the yeast F_1F_o-ATP synthase. *Biol. Cell* **100,** 591–601 (2008).

232. Arselin, G. *et al.* The modulation in subunits e and g amounts of yeast ATP synthase modifies mitochondrial cristae morphology. *J. Biol. Chem.* **279,** 40392–40399 (2004).

233. Viklund, H., Granseth, E. & Elofsson, A. Structural classification and prediction of reentrant regions in alpha-helical transmembrane proteins: application to complete genomes. *J. Mol. Biol.* **361,** 591–603 (2006).

234. Zalk, R. *et al.* Structure of a mammalian ryanodine receptor. *Nature* **517,** 44–49 (2014).

235. Lin, D.-T. & Lechleiter, J. D. Mitochondrial targeted cyclophilin D protects cells from cell death by peptidyl prolyl isomerization. *J. Biol. Chem.* **277,** 31134–41 (2002).

236. Sun, S. & Heitman, J. Is sex necessary? *BMC Biol.* **9,** 56 (2011).

6. Appendix

REPORT

THE JOURNAL OF BIOLOGICAL CHEMISTRY VOL. 289, NO. 23, pp. 15980–15985, June 6, 2014

Channel Formation by Yeast F-ATP Synthase and the Role of Dimerization in the Mitochondrial Permeability Transition*◆

Received for publication, February 19, 2014, and in revised form, April 18, 2014
Published, JBC Papers in Press, May 1, 2014, DOI 10.1074/jbc.C114.559633

Michela Carraro[‡1,2], **Valentina Giorgio**[‡1], **Justina Šileikytė**[‡], **Geppo Sartori**[‡], **Michael Forte**[§], **Giovanna Lippe**[¶], **Mario Zoratti**[‡], **Ildikò Szabò**[‖], **and Paolo Bernardi**[‡3]

From the [‡]*Consiglio Nazionale delle Ricerche Neuroscience Institute and Department of Biomedical Sciences and the* [‖]*Department of Biology, University of Padova, I-35121 Padova, Italy the* [§]*Vollum Institute, Oregon Health and Sciences University, Portland, Oregon 97239-3098, and the* [¶]*Department of Food Science, University of Udine, 33100 Udine, Italy*

Background: Whether channel formation is a general feature of F-ATP synthase dimers across species is unknown.
Results: Yeast F-ATP synthase dimers form Ca^{2+}-dependent channels, and the e and g subunits facilitate pore formation *in situ* through dimerization.
Conclusion: F-ATP synthase dimers form the permeability transition pore of yeast.
Significance: Ca^{2+}-dependent channel formation is a conserved feature of F-ATP synthases.

Purified F-ATP synthase dimers of yeast mitochondria display Ca^{2+}-dependent channel activity with properties resembling those of the permeability transition pore (PTP) of mammals. After treatment with the Ca^{2+} ionophore ETH129, which allows electrophoretic Ca^{2+} uptake, isolated yeast mitochondria undergo inner membrane permeabilization due to PTP opening. Yeast mutant strains Δ*TIM11* and Δ*ATP20* (lacking the e and g F-ATP synthase subunits, respectively, which are necessary for dimer formation) display a striking resistance to PTP opening. These results show that the yeast PTP originates from F-ATP synthase and indicate that dimerization is required for pore formation *in situ*.

Mitochondria from a variety of sources can undergo an inner membrane permeability increase, the permeability transition (PT),[4] due to opening of a high conductance channel, the PT pore (PTP) (1). The PTP coincides with the mitochondrial megachannel (MMC) defined by patch clamp studies in mitoplasts (2–5). In mammals, PTP opening requires matrix Ca^{2+} and is favored by oxidative stress and P_i, inhibited by adenine nucleotides and Mg^{2+}, and antagonized by cyclosporin A (CsA) through its interaction with matrix cyclophilin (CyP)D (6, 7). The mammalian PTP is today recognized to play a role in cell death in a variety of disease paradigms (8).

Inner membrane permeability pathways have been described in yeast (9) and in *Drosophila melanogaster* (10), but whether these coincide with the mammalian PTP remains an open question (11–14). The issue is particularly complex in the case of yeast, where multiple conductance pathways may exist including an uncoupling protein-independent permeability activated by ATP (15–17). Furthermore, the yeast PTP (yPTP) is inhibited rather than activated by P_i and insensitive to CsA (9), and due to the lack of a mitochondrial Ca^{2+} uniporter, its Ca^{2+} dependence has been more difficult to assess (18), although the Ca^{2+} content of *Saccharomyces cerevisiae* mitochondria is close to that of rat liver mitochondria (19). The problem of the Ca^{2+} dependence was solved by the Shinohara group (20), who showed that yeast mitochondria incubated with optimized substrate and P_i concentrations readily undergo a Ca^{2+}-dependent PT upon treatment with ETH129, a Ca^{2+} ionophore that allows electrophoretic Ca^{2+} transport into the matrix of energized mitochondria. We recently demonstrated that dimers of mammalian F-ATP synthase reconstituted into planar bilayers give rise to Ca^{2+}-activated currents with conductances ranging up to 1.3 nS in 150 mM KCl that closely match those displayed by the MMC-PTP (21). Here we have tested whether gel-purified F-ATP synthase dimers of *S. cerevisiae* form channels when reconstituted in lipid bilayers, and whether dimerization of the F-ATP synthase is necessary for PTP formation in intact mitochondria.

EXPERIMENTAL PROCEDURES

Yeast Strains and Materials—The *S. cerevisiae* strains BY4743 (4741/4742), as well as the mutants Δ*CPR3* (MATa, *his3Δ1*, *leu2Δ0*, *met5Δ0*, *ura3Δ0*), Δ*TIM11* (MATa, *his3Δ1*, *leu2Δ0*, *met5Δ0*, *ura3Δ0*), and Δ*ATP20* (MATα, *his3Δ1*, *leu2Δ0*, *lys2Δ0*, *ura3Δ0*), were purchased from Thermo Scientific. Δ*TIM11*Δ*ATP20* mutants were obtained by mating the Δ*TIM11* and Δ*ATP20* strains and selecting the formed diploid by growth on synthetic defined (0.67% nitrogen base without amino acids, 2% dextrose) selective medium containing the

* This work was supported in part by Associazione Italiana per la Ricerca sul Cancro (AIRC) Grants IG13392 (to P. B.) and IG11814 (to I. S.), Progetti di Ricerca di Interesse Nazionale Programs 20107Z8XBW (to P. B.) and 2010CSJX4F (to I. S.), National Institutes of Health/Public Health Service Grant 1R01GM069883 (to M. F. and P. B.), a Consiglio Nazionale delle Ricerche (CNR) Project of Special Interest on Aging (to M. Z.), and the University of Padova Progetti Strategici di Ateneo "Models of Mitochondrial Diseases" (to P. B.).
◆ This article was selected as a Paper of the Week.
[1] Both authors contributed equally to this work.
[2] This work is in partial fulfillment of the requirements for a Ph.D. at the University of Padova.
[3] To whom correspondence should be addressed: Dept. of Biomedical Sciences, University of Padova, Via Ugo Bassi 58/B, I-35121 Padova, Italy. Fax: 39-049-827-6049; E-mail: bernardi@bio.unipd.it.

[4] The abbreviations used are: PT, permeability transition; PTP, permeability transition pore; yPTP, yeast permeability transition pore; BN-PAGE, blue native polyacrylamide gel electrophoresis; CRC, Ca^{2+} retention capacity; $Cu(OP)_2$, copper-*o*-phenanthroline; CsA, cyclosporin A; CyPD, cyclophilin D; MMC, mitochondrial megachannel; PhAsO, phenylarsine oxide; Tricine, *N*-[2-hydroxy-1,1-bis(hydroxymethyl)ethyl]glycine; Bis-Tris, 2-(bis(2-hydroxyethyl)amino)-2-(hydroxymethyl)propane-1,3-diol; S, siemens.

required nutritional supplements except methionine and lysine. Diploids were then induced to sporulate in 1% potassium acetate, tetrads were dissected, and haploids were analyzed with semiquantitative PCR to detect null mutants for *TIM11* and *ATP20* genes. Digitonin was from Sigma, and ETH129 was from Sigma-Aldrich Japan and was dissolved in methanol. NADH, disodium salt was purchased from Roche Applied Science.

Yeast Culture and Mitochondria Isolation—Yeast cells were cultured aerobically in 50 ml of 1% yeast extract, 1% bacto-polypeptone medium containing 2% glucose at 30 °C. When it reached an optical density of 2 at 600 nm, the culture was added to 800 ml of bacto-polypeptone medium supplemented with 2% galactose and incubated for 20 h at 30 °C under rotation at 180 rpm, yielding about 4.0 g of yeast cells. Yeast mitochondria were isolated as described (20) with the following modifications. Briefly, cells were washed, incubated for 15 min at 37 °C in a 0.1 M Tris-SO_4 buffer (pH 9.4) supplemented with 10 mM dithiothreitol (DTT), and washed once with 1.2 M sorbitol, 20 mM P_i, pH 7.4. Yeast cells were then suspended in the same buffer and incubated for 45 min at 30 °C with 0.4 mg/g of cells of Zymolyase 100T to form spheroplasts. The latter were washed once with sorbitol buffer and homogenized in 0.6 M Mannitol, 10 mM Tris-HCl, pH 7.4, and 0.1 mM EDTA-Tris with a Potter homogenizer. The homogenate was centrifuged for 5 min at 2,000 × *g*, and the supernatant was collected and centrifuged for 10 min at 12,000 × *g*. The resulting mitochondrial pellet was suspended in mannitol buffer, and protein concentration was determined from the A_{280} of SDS-solubilized mitochondria (14).

Mitochondrial Calcium Retention Capacity—Mitochondrial Ca^{2+} uptake was measured with Calcium Green-5N (Molecular Probes) fluorescence using a Fluoroskan Ascent FL (Thermo Electron) plate reader at a mitochondrial concentration of 0.5 mg × ml^{-1}. Mitochondria were incubated as specified in the figure legends.

Gel Electrophoresis and Western Blotting—Mitochondria were suspended at 10 mg/ml in 150 mM potassium acetate, 30 mM HEPES, 10% glycerol, 1 mM phenylmethylsulfonyl fluoride and solubilized with 1.5% (w/v) digitonin. After centrifugation at 100,000 × *g* with a Beckman TL-100 rotor for 25 min at 4 °C, supernatants were collected, supplemented with 50 mg/ml Coomassie Blue and 5 M aminocaproic acid, and quickly loaded onto a blue native polyacrylamide 3–12% gradient gel (BN-PAGE, Invitrogen). Electrophoresis was carried out at 150 V for 20 min and at 250 V for 2 h followed by gel staining with 0.25 mg/ml Coomassie Blue, 10% acetic acid or used for in-gel activity staining to detect bands corresponding to ATP synthase. Activity was monitored in 270 mM glycine, 35 mM Tris, pH 7.4, 15 mM $MgSO_4$, 8 mM ATP, Tris-buffered to pH 7.4, and 2 mg/ml $Pb(NO_3)_2$. Bands corresponding to monomeric and dimeric forms of ATP synthase were cut from the gels, and protein complexes were eluted overnight by incubation at 4 °C in 25 mM Tricine, 15 mM $MgSO_4$, 8 mM ATP, 7.5 mM Bis-Tris, 1% (w/v) *n*-heptyl β-D-thioglucopyranoside, pH 7.0. Samples were then centrifuged at 20,000 × *g* for 10 min at 4 °C, and supernatants were used for bilayer experiments. For cross-linking experiments, mitochondria were incubated 20 min at room temperature at 1 mg/ml in 250 mM sucrose, 2 mM P_i, and 2 mM $CuCl_2$. Five millimolar *N*-ethylmaleimide and 5 mM EDTA were then added to block the cross-linking reaction, and the incubations were transferred on ice for 10 min followed by centrifugation and preparation for BN-PAGE as described above. Total yeast mitochondria lysates and bands corresponding to dimers of F-ATP synthase cut out of BN-PAGE gels were subjected to SDS-PAGE followed by silver staining or transfer to nitrocellulose for Western blot analysis. Antibodies were polyclonal rabbit anti-ATP synthase γ subunit (a gift from Marie-France Giraud, Bordeaux, France), anti-Tom20 and anti-Tim54 (a gift from Nikolaus Pfanner, Freiburg, Germany).

Electrophysiology—Planar lipid bilayer experiments were performed as described in Ref. 31. Briefly, bilayers of 150–200 picofarads of capacitance were prepared using purified soybean asolectin. The standard experimental medium was 150 mM KCl, 10 mM Hepes, pH 7.5. All reported voltages refer to the *cis* chamber, zero being assigned to the *trans* (grounded) side. Currents are considered as positive when carried by cations flowing from the *cis* to the *trans* compartment. Freshly prepared F-ATP synthase dimers were added to the *cis* side. No current was observed when PTP activators were added to the membrane in the absence of F-ATP synthase dimers ($n = 2$).

RESULTS AND DISCUSSION

Properties of the Ca^{2+}-dependent Permeability Transition of Yeast Mitochondria—We used ETH129 to allow Ca^{2+} uptake by energized yeast mitochondria (20) and monitored the propensity of the yPTP to open based on the Ca^{2+} retention capacity (CRC), *i.e.* the maximal Ca^{2+} load retained by mitochondria before onset of the PT (22). In keeping with previous observations (20), (i) energized yeast mitochondria were able to accumulate Ca^{2+} provided as a train of pulses (Fig. 1*A*) until onset of the PT, which causes depolarization followed by Ca^{2+} release; and (ii) increasing concentrations of P_i increased the matrix Ca^{2+} load necessary to open the yPTP (Fig. 1, *A* and *B*), possibly following formation of matrix P_i-Ca^{2+} complexes. As in mammalian mitochondria, Mg^{2+}-ADP increased the CRC, an effect consistent with yPTP inhibition (Fig. 1*C*). The CRC was not affected by decavanadate (results not shown), which inhibits the ATP-induced, voltage-dependent anion channel (VDAC)-dependent yeast permeability pathway (23, 24).

The mammalian PTP is modulated by two classes of redox-sensitive thiols whose oxidation increases the pore sensitivity to Ca^{2+}, *i.e.* (i) matrix thiols that react with phenylarsine oxide (PhAsO) and can be oxidized by diamide (25); and (ii) external thiols that can be oxidized by copper-*o*-phenanthroline ($Cu(OP)_2$) (26). The threshold Ca^{2+} load required for yPTP opening was moderately affected by PhAsO (Fig. 1*D*), whereas it was very sensitive to diamide (Fig. 1*E*) and to $Cu(OP)_2$ (Fig. 1*F*). These experiments indicate that the yeast PTP is affected by the redox state of thiol groups as also suggested by a previous study (18).

CsA desensitizes the mammalian pore to Ca^{2+} through matrix CyPD, a peptidyl-prolyl *cis-trans* isomerase that behaves as a PTP inducer (27, 28). Through studies of CyPD-null mitochondria, it became clear that CyPD is a modulator but not an obligatory constituent of the PTP and that a PT can occur in the

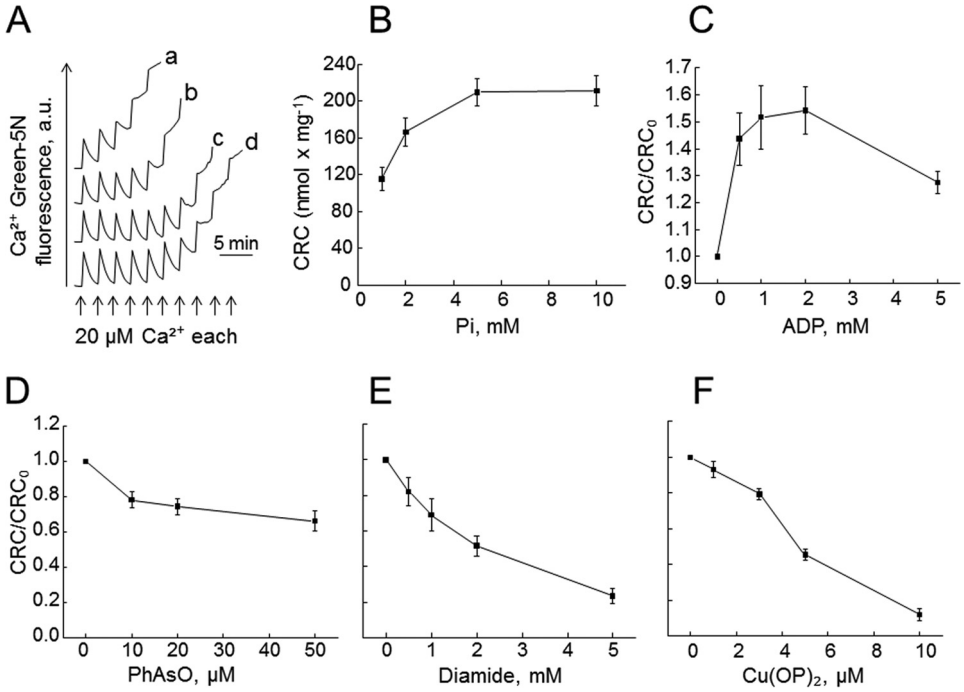

FIGURE 1. **Properties of the permeability transition of yeast mitochondria.** The incubation medium contained 250 mM sucrose, 10 mM Tris-MOPS, 1 mM NADH, 10 μM EGTA-Tris, 5 μM ETH129, 1 μM Calcium Green-5N, final pH 7.4, 0.5 mg/ml bovine serum albumin, and 0.1 mg of mitochondria in a final volume of 0.2 ml. *A*, the medium was supplemented with 1 mM (*trace a*), 2 mM (*trace b*), 5 mM (*trace c*), or 10 mM P_i (*trace d*), and where indicated, Ca^{2+} was added. Traces shown are representative of 13 independent experiments. *a.u.*, arbitrary units. *B*, experimental conditions as in *panel A* with the indicated P_i concentrations. Values on the ordinate refer to the amount of Ca^{2+} accumulated prior to the precipitous release that follows the PT ($n = 13 \pm$ S.E.). *C*, the experimental conditions were as in *panel A* with 2 mM P_i, and the medium was supplemented with 2 mM $MgCl_2$, 1 μM oligomycin, and the stated concentrations of ADP ($n = 8 \pm$ S.E.). *D–F*, the experimental conditions were as in *panel A* with 2 mM P_i, and the medium was supplemented with the stated concentrations of PhAsO (*D*), diamide (*E*), or $Cu(OP)_2$ (*F*). For *panels D–F*, *n* (± S.E.) was 6, 4, and 7, respectively.

absence of CyPD, or in the presence of CsA, albeit at higher matrix Ca^{2+} loads (8). Yeast mitochondria possess a matrix CyP (CPR3), which facilitates folding of imported proteins in the matrix and is sensitive to CsA (29); however, the yPTP is not affected by CsA (9), as also confirmed in the CRC assay (Fig. 2*A*, compare *traces a* and *b*). These findings suggest either that CPR3 does not interact with the pore or that CsA does not interfere with CPR3 binding. To resolve this issue, we tested the CRC of Δ*CPR3* mutants, which displayed a lower rate and slightly lower extent of Ca^{2+} accumulation (Fig. 2*A*, *trace c*), indicating that CPR3 does not sensitize the yPTP to Ca^{2+}, at variance from the effects of CyPD in mammalian mitochondria (30). The small decrease of CRC in the mutants (Fig. 2*B*) may be due to slower protein import and defective respiratory chain assembly and/or function (31). It was recently established that rotenone is a good inhibitor of the PTP in mammalian mitochondria lacking CyPD, possibly because of decreased production of reactive oxygen species through inhibition of reverse electron flow (32). Rotenone did not affect the yPTP (Fig. 2*A*, *trace d*), in keeping with the lack of a rotenone-sensitive, energy-conserving complex I and with the lack of "off-site" effects. Taken together, the above results suggest that, despite the lack of a fast Ca^{2+} uptake system (19), *S. cerevisiae* mitochondria can undergo a Ca^{2+}-induced PT, which displays some similarities with the mammalian PT (sensitization by matrix Ca^{2+} and oxidative stress, inhibition by Mg^{2+}-ADP), but also some differences (inhibition by phosphate and lack of sensitivity to CPR3 and rotenone).

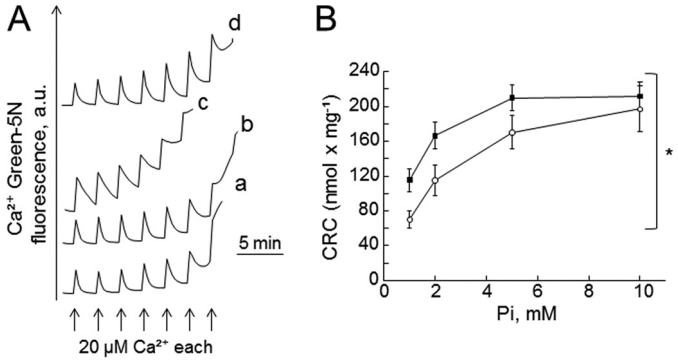

FIGURE 2. ***CPR3* deletion does not affect the yeast permeability transition.** *A*, the experimental conditions were as in Fig. 1 with 2 mM P_i; 0.8 μM CsA was added in *trace b* only, and 2 μM rotenone was added in *trace d* only. Where indicated, Ca^{2+} was added to wild-type (*traces a*, *b*, and *d*) or Δ*CPR3* (*trace c*) mitochondria (traces are representative of three independent experiments). *B*, the experimental conditions were as in Fig. 1 with P_i as indicated ($n = 4 \pm$ S.E.). *Closed symbols*, wild-type mitochondria; *open symbols*, Δ*CPR3* mitochondria. Two-way analysis of variance test was performed, *, $p < 0.05$.

Purified F-ATP Synthase Dimers Possess Channel Activity—To test whether yeast F-ATP synthase dimers can form channels similar to those found in mammals (21), we separated mitochondrial protein extracts by BN-PAGE, identified dimers by in-gel activity staining, and eluted them for incorporation into a planar asolectin membrane (see Fig. 4*A* for an example of the dimer used). The addition of 1–10 pmol of the dimers to the bilayers in symmetrical 150 mM KCl did not elicit current activity unless Ca^{2+}, PhAsO, and $Cu(OP)_2$ were also added (Fig. 3*A*). We observed a clear activity in 12 out of 14 reconstitutions, with

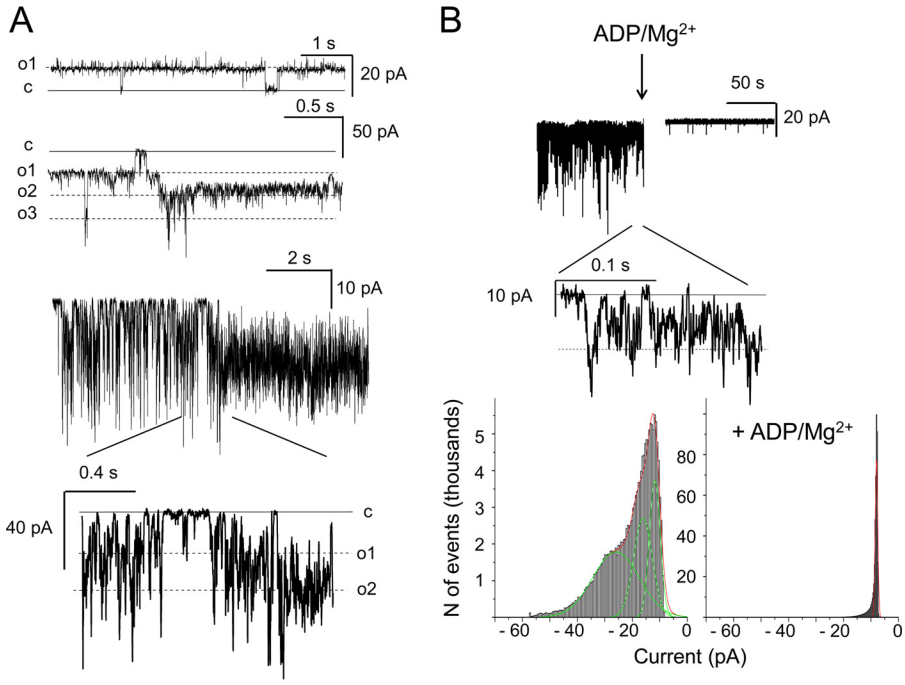

FIGURE 3. **F-ATP synthase dimers reconstituted in planar lipid bilayers display Ca^{2+}-induced currents.** Dimers were excised (see Fig. 4*A*, wild-type) and eluted for planar bilayer experiments. *A*, *upper part*, representative current traces recorded at +80 and −100 mV (*cis*) (*upper* and *lower traces*, conductance (g) = 125 and 250 pS) upon incorporation of purified dimeric F-ATP synthase following the addition of 3 mM Ca^{2+} (added to the *trans* side) plus 0.1 mM PhAsO and 20 μM $Cu(OP)_2$ (added to both sides). *Lower part*, typical, most often observed channel kinetics (see also expanded portion of the recording obtained at −60 mV (*cis*); g = 250 pS). *a.u.*, arbitrary units. *B*, *top*, effect of 2 mM ADP plus 1.6 mM Mg^{2+} added to the *trans* side on channel activity (−60 mV, g = 250 pS); current trace before and immediately after the addition of the modulators is shown. *Bottom*, amplitude histograms obtained from the same experiment before (*left panel*) and after (*right panel*) the addition of ADP/Mg^{2+}. Gaussian fitting (*green lines*) was obtained using the Origin 6.1 Program Set.

channel unit conductance usually ranging between 250 and 300 pS (multiples of this unit conductance were often observed; in one case 1000 pS was reached). This conductance is compatible with the values exhibited by a channel observed in mitoplasts from a porin-less yeast strain, which was insensitive to CsA, ADP, or protons and in which the combination of ADP and Mg^{2+} was not tested (33). The activity studied here was characterized by rapid oscillations between closed and open states (flickering), which is typical of the mammalian MMC-PTP, and by variable kinetics. A typical flickering behavior is illustrated in the bottom part of Fig. 3*A*. As is the case for the mammalian F-ATP synthase (21) and for the MMC-PTP measured in mitoplasts (4), the addition of Mg^{2+}-ADP induced a clear-cut inhibition of the channel in five out of six experiments (total inhibition was observed in two cases, and partial inhibition was observed in three cases). The representative experiment of Fig. 3*B* shows activity recorded before and immediately after the addition of Mg^{2+}-ADP in one case of full inhibition, which is illustrated in the corresponding amplitude histograms (Fig. 3*B*). Taken together, these data provide evidence that under conditions of oxidative stress, yeast F-ATP synthase can form Ca^{2+}-activated channels with features resembling the MMC-PTP (although with lower conductance). It should be noted that the dimer preparation did not contain Tom20 or Tim54 (Fig. 4*A*) and therefore that channel activity cannot be due to the twin pore translocase (34).

Dimerization of F-ATP Synthase Is Required for PTP Formation—Dimers of F-ATP synthase are the "building blocks" of long rows of oligomers located deep into the cristae, which contribute to formation of membrane curvature and to maintenance of proper cristae shape and mitochondrial morphology (35–42). Mammalian F-ATP synthase dimers also appear to be the units from which the PTP forms in a process that is highly favored by Ca^{2+} and oxidative stress (21), events that are required for channel formation (8, 21). To test the hypothesis that yPTP formation requires the presence of F-ATP synthase dimers, we studied mutants lacking subunits involved in dimerization/oligomerization of the enzyme, *i.e.* subunit e (TIM11) and subunit g (ATP20) (35, 43–45). Strains lacking these subunits display balloon-shaped cristae with ATP synthase monomers distributed randomly in the membrane (39). The Δ*TIM11*, Δ*ATP20*, and Δ*TIM11*Δ*ATP20* mutants lacked dimers when analyzed by BN-PAGE, whereas the monomeric F-ATP synthase was assembled and active (Fig. 4*A*), consistent with their ability to grow on non-fermentable carbon sources, and developed a normal membrane potential upon energization with NADH (results not shown). CRC assays with ETH129 demonstrated that mitochondria from Δ*TIM11*, Δ*ATP20*, and Δ*TIM11*Δ*ATP20* strains take up a larger Ca^{2+} load than wild-type strains (Fig. 4*B*), with a doubling of the CRC (Fig. 4*C*).

Dimers may transiently form also in Δ*TIM11* and Δ*ATP20* strains (46), a finding that could explain why Ca^{2+} release is eventually observed also in the "dimerization-less" mutants. Consistent with this possibility, we did detect dimers in BN-PAGE after treatment with $CuCl_2$ (Fig. 4*D*), which promotes formation of disulfide bridges between adjacent cysteine residues of the monomers (45, 47, 48). Not all of the monomers dimerized after $CuCl_2$ treatment (Fig. 4*D*), suggesting that cysteine oxidation stabilizes pre-existing dimers that are otherwise

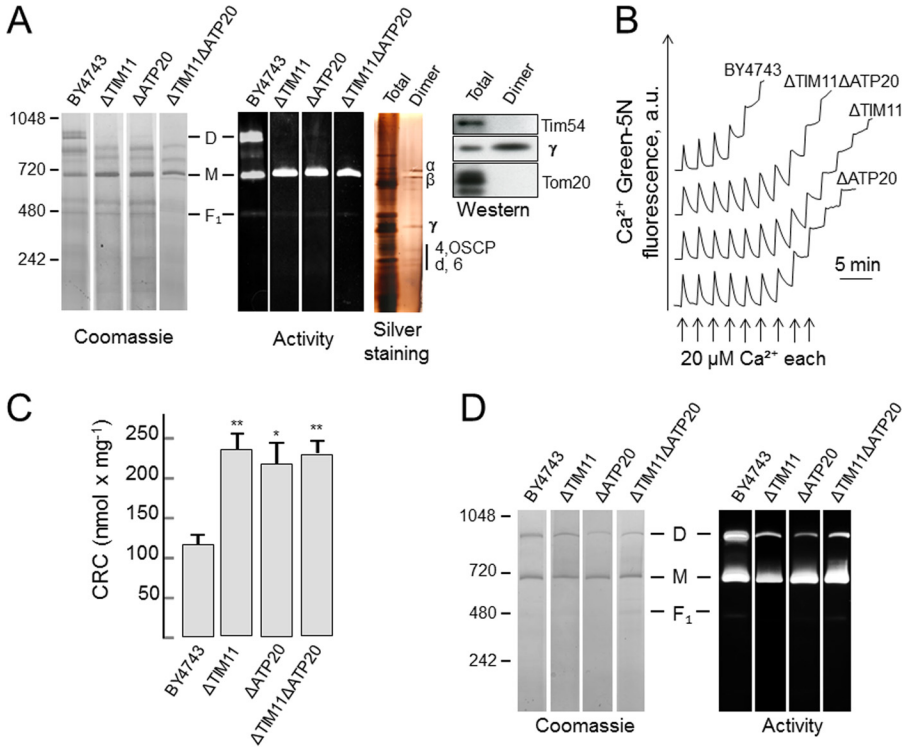

FIGURE 4. **Δ*TIM11*, Δ*ATP20*, and Δ*TIM11*Δ*ATP20* mutants lacking subunits involved in dimerization of F-ATP synthase are resistant to PTP opening.** *A*, mitochondrial protein extracts were separated with BN-PAGE and stained with Coomassie blue (lanes labeled *Coomassie*) or subjected to in-gel activity staining (lanes labeled *Activity*) to identify bands of F-ATP synthase dimers (*D*) and monomers (*M*) (note also a faint band corresponding to F_1 (F^1)). The gel region corresponding to the dimers of the BY4743 strain was cut out and subjected to SDS-PAGE together with a mitochondrial extract from the same strain followed by silver staining (lanes labeled *Silver staining*) or blotting and probing with the indicated antibodies (lanes labeled *Western*). OSCP, oligomycin sensitivity-conferring protein. *B*, the experimental conditions were as in Fig. 1 with 1 mM P_i. Where indicated, Ca^{2+} was added to wild type, Δ*TIM11*Δ*ATP20*, Δ*TIM11*, or Δ*ATP20* mutants (traces are representative of 13, 6, 7, and 6 independent experiments for the corresponding genotypes). *C*, experimental conditions as in *A* with 1 mM P_i. One-way analysis of variance test was performed to analyze CRC differences between BY4743 and mutants, *, $p < 0.01$, **, $p < 0.001$. *D*, BN-PAGE (*left lanes*) and activity staining (*right lanes*) of mitochondria with the indicated genotypes after treatment with 2 mM $CuCl_2$.

dissociated by detergent treatment, but does not *induce* cross-linking of monomers.

In summary, our data provide the first demonstration that yeast F-ATP synthase dimers form high conductance channels analogous to the mammalian MMC-PTP, and thus that channel formation is a conserved feature of F-ATP synthases; show that yeast mitochondria can undergo a *bona fide* PT activated by oxidative stress; and indicate that dimers of F-ATP synthase are required for PTP formation *in situ* (21). Our findings do not exclude the existence of other permeability pathways that may involve the voltage-dependent anion channel (23, 24), nor the possible regulation of yPTP by outer mitochondrial membrane proteins (8). We think that it will now be possible to unravel the many open questions about the structure and function of the PTP (8) with the powerful methods of yeast genetics.

Acknowledgments—We thank Marie-France Giraud and Nikolaus Pfanner for the generous gift of antibodies and Raffaele Lopreiato for advice on the preparation of mutants.

REFERENCES

1. Hunter, D. R., Haworth, R. A., and Southard, J. H. (1976) Relationship between configuration, function, and permeability in calcium-treated mitochondria. *J. Biol. Chem.* **251,** 5069–5077
2. Kinnally, K. W., Campo, M. L., and Tedeschi, H. (1989) Mitochondrial channel activity studied by patch-clamping mitoplasts. *J. Bioenerg. Biomembr.* **21,** 497–506
3. Petronilli, V., Szabó, I., and Zoratti, M. (1989) The inner mitochondrial membrane contains ion-conducting channels similar to those found in bacteria. *FEBS Lett.* **259,** 137–143
4. Szabó, I., Bernardi, P., and Zoratti, M. (1992) Modulation of the mitochondrial megachannel by divalent cations and protons. *J. Biol. Chem.* **267,** 2940–2946
5. Szabó, I., and Zoratti, M. (1992) The mitochondrial megachannel is the permeability transition pore. *J. Bioenerg. Biomembr.* **24,** 111–117
6. Fournier, N., Ducet, G., and Crevat, A. (1987) Action of cyclosporine on mitochondrial calcium fluxes. *J. Bioenerg. Biomembr.* **19,** 297–303
7. Crompton, M., Ellinger, H., and Costi, A. (1988) Inhibition by cyclosporin A of a Ca^{2+}-dependent pore in heart mitochondria activated by inorganic phosphate and oxidative stress. *Biochem. J.* **255,** 357–360
8. Bernardi, P. (2013) The mitochondrial permeability transition pore: A mystery solved? *Front. Physiol.* **4,** 95
9. Jung, D. W., Bradshaw, P. C., and Pfeiffer, D. R. (1997) Properties of a cyclosporin-insensitive permeability transition pore in yeast mitochondria. *J. Biol. Chem.* **272,** 21104–21112
10. von Stockum, S., Basso, E., Petronilli, V., Sabatelli, P., Forte, M. A., and Bernardi, P. (2011) Properties of Ca^{2+} transport in mitochondria of *Drosophila melanogaster*. *J. Biol. Chem.* **286,** 41163–41170
11. Manon, S., Roucou, X., Guérin, M., Rigoulet, M., and Guérin, B. (1998) Characterization of the yeast mitochondria unselective channel: a counterpart to the mammalian permeability transition pore? *J. Bioenerg. Biomembr.* **30,** 419–429
12. Azzolin, L., von Stockum, S., Basso, E., Petronilli, V., Forte, M. A., and Bernardi, P. (2010) The mitochondrial permeability transition from yeast to mammals. *FEBS Lett.* **584,** 2504–2509
13. Uribe-Carvajal, S., Luévano-Martínez, L. A., Guerrero-Castillo, S., Ca-

brera-Orefice, A., Corona-de-la-Peña, N. A., and Gutiérrez-Aguilar, M. (2011) Mitochondrial unselective channels throughout the eukaryotic domain. *Mitochondrion* **11,** 382–390
14. Bradshaw, P. C., and Pfeiffer, D. R. (2013) Characterization of the respiration-induced yeast mitochondrial permeability transition pore. *Yeast* **30,** 471–483
15. Prieto, S., Bouillaud, F., Ricquier, D., and Rial, E. (1992) Activation by ATP of a proton-conducting pathway in yeast mitochondria. *Eur. J. Biochem.* **208,** 487–491
16. Prieto, S., Bouillaud, F., and Rial, E. (1995) The mechanism for the ATP-induced uncoupling of respiration in mitochondria of the yeast *Saccharomyces cerevisiae*. *Biochem. J.* **307,** 657–661
17. Prieto, S., Bouillaud, F., and Rial, E. (1996) The nature and regulation of the ATP-induced anion permeability in *Saccharomyces cerevisiae* mitochondria. *Arch. Biochem. Biophys.* **334,** 43–49
18. Kowaltowski, A. J., Vercesi, A. E., Rhee, S. G., and Netto, L. E. (2000) Catalases and thioredoxin peroxidase protect *Saccharomyces cerevisiae* against Ca^{2+}-induced mitochondrial membrane permeabilization and cell death. *FEBS Lett.* **473,** 177–182
19. Carafoli, E., and Lehninger, A. L. (1971) A survey of the interaction of calcium ions with mitochondria from different tissues and species. *Biochem. J.* **122,** 681–690
20. Yamada, A., Yamamoto, T., Yoshimura, Y., Gouda, S., Kawashima, S., Yamazaki, N., Yamashita, K., Kataoka, M., Nagata, T., Terada, H., Pfeiffer, D. R., and Shinohara, Y. (2009) Ca^{2+}-induced permeability transition can be observed even in yeast mitochondria under optimized experimental conditions. *Biochim. Biophys. Acta* **1787,** 1486–1491
21. Giorgio, V., von Stockum, S., Antoniel, M., Fabbro, A., Fogolari, F., Forte, M., Glick, G. D., Petronilli, V., Zoratti, M., Szabó, I., Lippe, G., and Bernardi, P. (2013) Dimers of mitochondrial ATP synthase form the permeability transition pore. *Proc. Natl. Acad. Sci. U.S.A.* **110,** 5887–5892
22. Fontaine, E., Ichas, F., and Bernardi, P. (1998) A ubiquinone-binding site regulates the mitochondrial permeability transition pore. *J. Biol. Chem.* **273,** 25734–25740
23. Roucou, X., Manon, S., and Guérin, M. (1997) Conditions allowing different states of ATP- and GDP-induced permeability in mitochondria from different strains of *Saccharomyces cerevisiae*. *Biochim. Biophys. Acta* **1324,** 120–132
24. Gutiérrez-Aguilar, M., Pérez-Vázquez, V., Bunoust, O., Manon, S., Rigoulet, M., and Uribe, S. (2007) In yeast, Ca^{2+} and octylguanidine interact with porin (VDAC) preventing the mitochondrial permeability transition. *Biochim. Biophys. Acta* **1767,** 1245–1251
25. Petronilli, V., Costantini, P., Scorrano, L., Colonna, R., Passamonti, S., and Bernardi, P. (1994) The voltage sensor of the mitochondrial permeability transition pore is tuned by the oxidation-reduction state of vicinal thiols: increase of the gating potential by oxidants and its reversal by reducing agents. *J. Biol. Chem.* **269,** 16638–16642
26. Costantini, P., Colonna, R., and Bernardi, P. (1998) Induction of the mitochondrial permeability transition by *N*-ethylmaleimide depends on secondary oxidation of critical thiol groups: potentiation by copper-*ortho*-phenanthroline without dimerization of the adenine nucleotide translocase. *Biochim. Biophys. Acta* **1365,** 385–392
27. Halestrap, A. P., and Davidson, A. M. (1990) Inhibition of Ca^{2+}-induced large-amplitude swelling of liver and heart mitochondria by cyclosporin is probably caused by the inhibitor binding to mitochondrial-matrix peptidyl-prolyl *cis-trans* isomerase and preventing it interacting with the adenine nucleotide translocase. *Biochem. J.* **268,** 153–160
28. Woodfield, K. Y., Price, N. T., and Halestrap, A. P. (1997) cDNA cloning of rat mitochondrial cyclophilin. *Biochim. Biophys. Acta* **1351,** 27–30
29. Matouschek, A., Rospert, S., Schmid, K., Glick, B. S., and Schatz, G. (1995) Cyclophilin catalyzes protein folding in yeast mitochondria. *Proc. Natl. Acad. Sci. U.S.A.* **92,** 6319–6323
30. Basso, E., Fante, L., Fowlkes, J., Petronilli, V., Forte, M. A., and Bernardi, P. (2005) Properties of the permeability transition pore in mitochondria devoid of Cyclophilin D. *J. Biol. Chem.* **280,** 18558–18561
31. Rassow, J., Mohrs, K., Koidl, S., Barthelmess, I. B., Pfanner, N., and Tropschug, M. (1995) Cyclophilin 20 is involved in mitochondrial protein folding in cooperation with molecular chaperones Hsp70 and Hsp60. *Mol. Cell. Biol.* **15,** 2654–2662
32. Li, B., Chauvin, C., De Paulis, D., De Oliveira, F., Gharib, A., Vial, G., Lablanche, S., Leverve, X., Bernardi, P., Ovize, M., and Fontaine, E. (2012) Inhibition of complex I regulates the mitochondrial permeability transition through a phosphate-sensitive inhibitory site masked by cyclophilin D. *Biochim. Biophys. Acta* **1817,** 1628–1634
33. Szabó, I., Báthori, G., Wolff, D., Starc, T., Cola, C., and Zoratti, M. (1995) The high-conductance channel of porin-less yeast mitochondria. *Biochim. Biophys. Acta* **1235,** 115–125
34. Rehling, P., Model, K., Brandner, K., Kovermann, P., Sickmann, A., Meyer, H. E., Kühlbrandt, W., Wagner, R., Truscott, K. N., and Pfanner, N. (2003) Protein insertion into the mitochondrial inner membrane by a twin-pore translocase. *Science* **299,** 1747–1751
35. Paumard, P., Vaillier, J., Coulary, B., Schaeffer, J., Soubannier, V., Mueller, D. M., Brèthes, D., di Rago, J.-P., and Velours, J. (2002) The ATP synthase is involved in generating mitochondrial cristae morphology. *EMBO J.* **21,** 221–230
36. Dudkina, N. V., Sunderhaus, S., Braun, H. P., and Boekema, E. J. (2006) Characterization of dimeric ATP synthase and cristae membrane ultrastructure from *Saccharomyces* and *Polytomella* mitochondria. *FEBS Lett.* **580,** 3427–3432
37. Strauss, M., Hofhaus, G., Schröder, R. R., and Kühlbrandt, W. (2008) Dimer ribbons of ATP synthase shape the inner mitochondrial membrane. *EMBO J.* **27,** 1154–1160
38. Thomas, D., Bron, P., Weimann, T., Dautant, A., Giraud, M. F., Paumard, P., Salin, B., Cavalier, A., Velours, J., and Brèthes, D. (2008) Supramolecular organization of the yeast F_1F^o-ATP synthase. *Biol. Cell* **100,** 591–601
39. Davies, K. M., Anselmi, C., Wittig, I., Faraldo-Gómez, J. D., and Kühlbrandt, W. (2012) Structure of the yeast F_1F_o-ATP synthase dimer and its role in shaping the mitochondrial cristae. *Proc. Natl. Acad. Sci. U.S.A.* **109,** 13602–13607
40. Davies, K. M., Strauss, M., Daum, B., Kief, J. H., Osiewacz, H. D., Rycovska, A., Zickermann, V., and Kühlbrandt, W. (2011) Macromolecular organization of ATP synthase and complex I in whole mitochondria. *Proc. Natl. Acad. Sci. U.S.A.* **108,** 14121–14126
41. Baker, L. A., Watt, I. N., Runswick, M. J., Walker, J. E., and Rubinstein, J. L. (2012) Arrangement of subunits in intact mammalian mitochondrial ATP synthase determined by cryo-EM. *Proc. Natl. Acad. Sci. U.S.A.* **109,** 11675–11680
42. Daum, B., Walter, A., Horst, A., Osiewacz, H. D., and Kühlbrandt, W. (2013) Age-dependent dissociation of ATP synthase dimers and loss of inner-membrane cristae in mitochondria. *Proc. Natl. Acad. Sci. U.S.A.* **110,** 15301–15306
43. Arnold, I., Pfeiffer, K., Neupert, W., Stuart, R. A., and Schägger, H. (1998) Yeast mitochondrial F_1F_0-ATP synthase exists as a dimer: identification of three dimer-specific subunits. *EMBO J.* **17,** 7170–7178
44. Wittig, I., Velours, J., Stuart, R., and Schägger, H. (2008) Characterization of domain interfaces in monomeric and dimeric ATP synthase. *Mol. Cell. Proteomics* **7,** 995–1004
45. Habersetzer, J., Ziani, W., Larrieu, I., Stines-Chaumeil, C., Giraud, M. F., Brèthes, D., Dautant, A., and Paumard, P. (2013) ATP synthase oligomerization: from the enzyme models to the mitochondrial morphology. *Int. J. Biochem. Cell Biol.* **45,** 99–105
46. Gavin, P. D., Prescott, M., and Devenish, R. J. (2005) F_1F_0-ATP synthase complex interactions *in vivo* can occur in the absence of the dimer specific subunit e. *J. Bioenerg. Biomembr.* **37,** 55–66
47. Fronzes, R., Weimann, T., Vaillier, J., Velours, J., and Brèthes, D. (2006) The peripheral stalk participates in the yeast ATP synthase dimerization independently of e and g subunits. *Biochemistry* **45,** 6715–6723
48. Velours, J., Stines-Chaumeil, C., Habersetzer, J., Chaignepain, S., Dautant, A., and Brèthes, D. (2011) Evidence of the proximity of ATP synthase subunits 6 (*a*) in the inner mitochondrial membrane and in the supramolecular forms of *Saccharomyces cerevisiae* ATP synthase. *J. Biol. Chem.* **286,** 35477–35484

Channel Formation by Yeast F-ATP Synthase and the Role of Dimerization in the Mitochondrial Permeability Transition

Michela Carraro, Valentina Giorgio, Justina Sileikyte, Geppo Sartori, Michael Forte, Giovanna Lippe, Mario Zoratti, Ildikò Szabò and Paolo Bernardi

J. Biol. Chem. 2014, 289:15980-15985.
doi: 10.1074/jbc.C114.559633 originally published online May 1, 2014

Elsevier Editorial System(tm) for Cell
Calcium

Manuscript Draft

Manuscript Number:

Title: Calcium and reactive oxygen species in regulation of the mitochondrial permeability transition and of programmed cell death in yeast

Article Type: SI:signaling and ROS

Keywords: Yeast Mitochondria; Programmed cell death; Ca2+; Reactive oxygen species; Permeability transition
F-ATP synthase

Corresponding Author: Prof. Paolo Bernardi, MD

Corresponding Author's Institution: University of Padova
First Author: Michela Carraro

Order of Authors: Michela Carraro; Paolo Bernardi, MD

Abstract: Mitochondria-dependent programmed cell death (PCD) in yeast shares many features with the intrinsic apoptotic pathway of mammals. With many stimuli, increased cytosolic [Ca2+] and ROS generation are the triggering signals that lead to mitochondrial permeabilization and release of proapoptotic factors, which initiates yeast PCD. While in mammals the permeability transition pore (PTP), a high-conductance inner membrane channel activated by increased matrix Ca2+ and oxidative stress, is recognized as part of this signaling cascade, whether a similar process occurs in yeast is still debated. The potential role of the PTP in yeast PCD has generally been overlooked because yeast mitochondria lack the Ca2+ uniporter, which in mammals allows rapid equilibration of cytosolic Ca2+ with the matrix. In this short review we discuss the nature of the yeast permeability transition and reevaluate its potential role in the effector phase of yeast PCD triggered by Ca2+ and oxidative stress.

Cell Calcium Special Issue *ROS in Ca^{2+} Signaling and Disease*

(Indu Ambudkar and Shmuel Muallem, Editors)

Calcium and reactive oxygen species in regulation of the mitochondrial permeability transition and of programmed cell death in yeast

Michela Carraro and Paolo Bernardi*

Department of Biomedical Sciences and CNR Neuroscience Institute

University of Padova, Italy

*Correspondence to:

Paolo Bernardi
Department of Biomedical Sciences
University of Padova
Via Ugo Bassi 58/B
I-35121 Padova, Italy
bernardi@bio.unipd.it

ABSTRACT

Mitochondria-dependent programmed cell death (PCD) in yeast shares many features with the intrinsic apoptotic pathway of mammals. With many stimuli, increased cytosolic [Ca^{2+}] and ROS generation are the triggering signals that lead to mitochondrial permeabilization and release of proapoptotic factors, which initiates yeast PCD. While in mammals the permeability transition pore (PTP), a high-conductance inner membrane channel activated by increased matrix Ca^{2+} and oxidative stress, is recognized as part of this signaling cascade, whether a similar process occurs in yeast is still debated. The potential role of the PTP in yeast PCD has generally been overlooked because yeast mitochondria lack the Ca^{2+} uniporter, which in mammals allows rapid equilibration of cytosolic Ca^{2+} with the matrix. In this short review we discuss the nature of the yeast permeability transition and reevaluate its potential role in the effector phase of yeast PCD triggered by Ca^{2+} and oxidative stress.

Keywords:

Yeast Mitochondria; Programmed cell death; Ca^{2+}; Reactive oxygen species; Permeability transition

F-ATP synthase

1. Mitochondria and yeast programmed cell death

Occurrence of programmed cell death (PCD) in yeast and its role in population dynamics and aging is increasingly understood [1,2]. Remarkably, many of the signaling events of the mammalian intrinsic (mitochondrial) pathway to apoptosis take place in yeast [3]. These include increase of intracellular [Ca^{2+}] and reactive oxygen species (ROS), which are causally involved in yeast PCD induced by oxidative stress itself [4], acetic acid [5-7], pheromone or amiodarone [8,9], ethanol [10] and osmotic [11] or ER stress [12]. As in mammals, increased intracellular [Ca^{2+}] precedes the surge of ROS levels, cristae remodeling, mitochondrial depolarization, ATP depletion, matrix swelling and outer membrane permeabilization eventually leading to release of cytochrome *c* and other proapoptotic proteins [1-3]. In yeast, the link between increased intracellular [Ca^{2+}]/ROS and outer mitochondrial membrane (OMM) permeabilization remains puzzling because yeast does not possess a mitochondrial Ca^{2+} uniporter (MCU) [13-15], which in mammals mediates rapid equilibration of Ca^{2+} across the inner mitochondrial membrane (IMM) [16,17]. Matrix Ca^{2+} in turn is essential for opening of the permeability transition pore (PTP), an IMM high-conductance channel that can form under conditions of oxidative stress and mediates a permeability increase (the permeability transition, PT) causing many of the above-mentioned mitochondrial events of PCD in mammals [18]. The defining features of the mammalian pore are high conductance, up to 1.3 nS [19,20], which allows permeation of solutes up to about 1.5 kDa in mass [21]; absolute requirement for matrix Ca^{2+} [21]; inhibition by Mg^{2+} and adenine nucleotides [22]; inhibition (desensitization to Ca^{2+}) by cyclosporin A (CsA) [23,24], an effect exerted through matrix cyclophilin (CyP) D [25]; and requirement for inducing factors such as oxidants and Pi [26] (Table I). Whether a bona fide PTP exists in yeast, and whether it plays a role in yeast PCD, has been the matter of debate [27],

2. The mitochondrial permeability transition pore in yeast

Before discussing the features of the yeast PTP, we would like to mention that yeast mitochondria appear to possess multiple dissipative pathways, a situation that is further complicated by strain-specific

differences. These include an ATP-dependent H^+-conductive pathway [28,29] and a variety of both selective [30-33] and unselective channels [34-39].

To the best of our knowledge the first evidence that yeast mitochondria may possess a PTP-like channel was obtained in studies of Pi transport in an industrial baker's yeast strain, Yeast Foam [34]. Mitochondria suspended in a K^+-based medium showed respiration-dependent large-amplitude swelling insensitive to mersalyl (and thus independent of the Pi carrier) and fully inhibited by antimycin A [34]. Subsequent studies demonstrated that a similar pathway was also present in laboratory yeast strains, where it allowed solute permeation with a cutoff of about 1.5 kDa [36,40-43]. At variance from the mammalian PTP, the yeast PTP (i) was unaffected by matrix Ca^{2+} even when uptake of the cation was made possible by the ionophore ETH129 [40]; (ii) was insensitive to Mg^{2+} and ADP [40]; (iii) was insensitive to CsA [40] in spite of the presence of a CsA-sensitive matrix CyP [44,45]; and (iv) was inhibited rather than induced by Pi [40,46]. A PT could be detected in strains lacking VDAC or the adenine nucleotide translocator (ANT), both of which were considered to be essential components of the PTP in mammals (see [27] for a thorough discussion), but the demonstration of a CsA-sensitive PTP in mammalian mitochondria lacking ANT [47] and VDACs [48,49] has refuted the paradigm that these proteins are essential for the PT [18].

Many apparent discrepancies with the mammalian PTP have been resolved in recent years. The Ca^{2+}-dependence of the yeast PTP has now been demonstrated beyond doubt in protocols where Ca^{2+} uptake was permitted by addition of the ionophore ETH129 and the concentration of Pi was optimized to prevent its inhibitory effect on the pore, which would otherwise mask the inducing effects of Ca^{2+} itself [50]. Lack of inhibition by Mg^{2+}/ADP may depend on the experimental conditions because of the presence of additional permeability pathways in yeast mitochondria, one of which is activated by ATP [28-30]. Finally, it is now clear that PTP opening can occur in the absence of CyPD also in mammalian mitochondria, as demonstrated both after genetic ablation of CyPD [51-55] and in cells and tissues where CyPD is expressed at low levels [56], conditions under which pore opening is obviously insensitive to CsA. The recent demonstration that after treatment with Ca^{2+} and oxidants F-ATP synthase forms channels with the

features expected of the PTP in *B. taurus* [57], *H. sapiens* [58], *S. cerevisiae* [59] and *D. melanogaster* [60] now provides a unifying frame to address its role(s) in pathophysiology across species [18].

Table I summarizes the channel properties of F-ATP synthases in *S. cerevisiae, D. melanogaster* and *B. taurus* (as determined by electrophysiology) [57,59,60] and the matching properties of their PTPs as determined in isolated mitochondria. It can be appreciated that a unique conductance is a feature of each species. A solute exclusion size of about 1.5 kDa has been defined for the PTP of isolated mitochondria of mammals [61,62] and yeast [40]. The size of the *D. melanogaster* species has not been defined precisely, but it appears to be considerably smaller because Drosophila mitochondria do not swell in sucrose-based media after opening of the PTP [63]. Swelling was not observed even in KCl-based media, suggesting that the low-conductance Drosophila channel is selective for Ca^{2+} and H^{+} [60,63]. Inspection of Table I reveals that conserved general features are (i) the requirement for matrix Ca^{2+} and facilitation by oxidants, which affect the pore at discrete sites [64,65]; and (ii) inhibition by Mg^{2+} (which competes with Ca^{2+} for a matrix binding site) and adenine nucleotides [22]. The inducing effect of Pi—a unique feature of the mammalian pore—has always been puzzling because Pi decreases matrix free [Ca^{2+}] [66] and would thus be expected to inhibit rather than promote PTP opening. The finding that Pi inhibits the PTP in *S. cerevisiae* [40,50,59] and *D. melanogaster* [63] suggests that stimulation of PTP opening by Pi in mammals may be due to a specific mechanism that evolved only later in evolution [18].

In mammals Pi increases CyPD binding to the OSCP subunit of the F-ATP synthase resulting in increased sensitivity of the PTP to Ca^{2+} [57,67]. We have proposed that CyPD binding, which is reversed by CsA [57,68], induces a conformational change favoring access of Ca^{2+} to the catalytic site of F-ATP synthase (which is usually occupied by Mg^{2+}) resulting in a conformational change that is transmitted to the intramembrane portion of the enzyme through the rigid lateral stalk. The conformational change would eventually cause PTP opening at the interface between two F-ATP synthase monomers in a process involving the dimerizations subunits e and g [18,59]. In keeping with this suggestion, in the absence of CyPD (or in the presence of CsA) low concentrations of Pi inhibit the PTP also in mammalian mitochondria [69].

The PTP of *S. cerevisiae* is insensitive to CsA despite the presence of a matrix CyP, Cpr3 [70]. We have shown that genetic ablation of *CPR3* does not affect the PTP, suggesting that Cpr3 does not interact with F-ATP synthase in yeast [59]. We could not detect a matrix CyP in *D. melanogaster*, whose genome potentially encodes several isoforms including one with a putative mitochondrial targeting sequence [71], but expression of the human species in mitochondria did sensitize the PTP to Ca^{2+} [60]. In summary, the key PTP-forming features of F-ATP synthases may have appeared early in evolution, before the regulatory interactions of matrix CyPD developed. The reader is referred to a recent extensive review for further details on the mechanistic and species-specific features of the PTP [18].

3. Calcium homeostasis in yeast

Ca^{2+} ions are fundamental regulators of a wide variety of processes in all eukaryotic cells. Ca^{2+} signaling is triggered by activation of either ion channels or G protein-coupled receptors and affects reactions that range from modulation of enzyme activities to motility, regulation of ion channels and gene transcription. Yeast is no exception, and maintains a tight control of intracellular Ca^{2+} homeostasis through an integrated array of transport systems [72-74]. In addition to cell growth, Ca^{2+}controls mating between *MATα* and *MATα* cells that secrete specific pheromones able to increase its cytosolic concentration, leading to cellular changes required for agglutination [75]. A key role of Ca^{2+} signaling has also been attributed to the response to an alkaline environment [76] as well as to hypotonic shock through the activation of MAP kinases [77]. Cytosolic free [Ca^{2+}] in yeast is finely regulated and maintained at low levels (50-200 nM) through Ca^{2+} storage in several compartments, i.e. vacuole, endoplasmic reticulum (ER), Golgi apparatus [72-74] and possibly mitochondria. Extracellular Ca^{2+}influx mainly occurs through the plasma membrane voltage-gated Ca^{2+} channel, also referred to as Cch1/Mid1 complex, that is activated by several stimuli such as depolarization, hypotonic shock, pheromone stimulation and unfolded protein response [75,78,79]. Following influx Ca^{2+} binds calmodulin, creating a complex able to activate calcineurin and thus to promote transcription of specific sets of genes required for cell proliferation and for the response to pheromone [80,81]. The signal is terminated by Ca^{2+} sequestration in the vacuole–the major Ca^{2+} store–through the

Ca^{2+} ATPase Pmc1 [72] and the high capacity, low-affinity Ca^{2+}/H^{+} exchanger Vcx1 [82], which may link Ca^{2+} homeostasis to regulation of intracellular pH. A contribution of ER/Golgi as alternative Ca^{2+} storage sites has also been recently proposed [83].

4. Mitochondria and Ca^{2+} homeostasis

In mammals, mitochondria play a crucial role in cytosolic Ca^{2+} homeostasis through an array of transport systems [84]. In energized mitochondria the inner membrane MCU complex (which is inhibited by lanthanides [85] and ruthenium red [86]) mediates rapid Ca^{2+} uptake down the cation electrochemical gradient [87]. With a membrane potential of 180 mV (negative inside) the equilibrium Ca^{2+} accumulation is 10^6, which for a cytosolic [Ca^{2+}] of 100 nM would correspond to a matrix [Ca^{2+}] of 100 mM. Thermodynamic equilibration is never attained, however, due to the existence of the $3Na^{+}/Ca^{2+}$ exchanger and of a putative $3H^{+}/Ca^{2+}$ exchanger that extrude Ca^{2+} and thus prevent massive accumulation of Ca^{2+} and Pi (see [88] for a recent review).

Yeast mitochondria do not possess an MCU complex [87] and therefore their potential role in Ca^{2+} homeostasis is usually not given much consideration. However, also in yeast the Ca^{2+} electrochemical gradient favors Ca^{2+} accumulation with the same predicted equilibrium distribution as that of mammalian mitochondria. To quote the original conclusions of Carafoli and Lehninger "We consider it likely that all mitochondria, whatever the cell type, possess the electrochemical capacity for moving Ca^{2+} across the membrane. This capacity cannot be expressed, however, unless a pathway for trans-membrane movement of Ca^{2+} is available, either through the occurrence of a specific Ca^{2+} carrier system or through simple physical permeability of the mitochondrial membrane to Ca^{2+}" [14]. We contend that the driving force is so large that Ca^{2+} uptake could be relevant even if it occured through a leak pathway rather than through a specific transport system. Consistently (i) *S. cerevisae* mitochondria have a Ca^{2+} content of 8-9 ngatoms/mg protein, which is close to that of rat liver mitochondria [14]; (ii) addition of EGTA or Ca^{2+} led to relevant changes of mitochondrial matrix free Ca^{2+} measured with a trapped fluorescent indicator, and mitochondrial Ca^{2+} release could be elicited by antimycin A or uncouplers [89]; and (iii) electrophoretic Ca^{2+}

uptake coupled to H^+ ejection can be easily measured in isolated *S. cerevisiae* and *C. utilis* mitochondria when the cation is added at concentrations of 1-10 mM [15]. It is of note that respiration-driven uptake is observed with Ca^{2+}, Sr^{2+} and Mn^{2+} but not with Mg^{2+} [15], suggesting that cation accumulation could be taking place through a low-affinity system whose discrimination for the transported species is strikingly similar to that of the MCU [84]. It is also interesting to recall that yeast mitochondria are endowed with a very effective $2H^+/Ca^{2+}$ antiporter activated by fatty acids that mediates mitochondrial Ca^{2+} release [90]. Like in mammals, the antiporter could prevent excessive mitochondrial Ca^{2+} accumulation but also allow rapid mobilization of the matrix Ca^{2+} pool following activation of phospholipases and perhaps other relevant pathophysiological stimuli.

In contrast to the general assumption that yeast mitochondria lack a specific Ca^{2+} transport system machinery, a high-capacity Ca^{2+} uptake system driven by the membrane potential and stimulated by polyamines and ADP has been described in the yeast *E. magnusii* [91,92]. Rather than acting as an inhibitor, and at variance from the mammalian MCU, ruthenium red affected Ca^{2+} transport only marginally or even stimulated it under specific conditions [93]. Taken together, these findings suggest that a specific Ca^{2+} transport system may exist also in yeast mitochondria, and that this putative system could be expressed at varying levels in different yeast strains. Occurrence of Ca^{2+} uptake in *S. cerevisiae* mitochondria combined with the sensitivity of the PTP to oxidative stress may provide the missing link between combined increase of intracellular [Ca^{2+}] and ROS, common triggers of yeast PCD [1-12], and activation of the intrinsic pathway of apoptosis.

5. Ca^{2+} and the permeability transition in yeast programmed cell death

As already mentioned, yeast PCD is increasingly recognized as a physiologically relevant event that has intriguing analogies with mammalian apoptosis, which are particularly striking for the mitochondrial pathway [1]. The major mitochondrial changes occurring in yeast apoptosis include cristae remodeling, increased ROS production, matrix swelling and cytochrome *c* release which are often preceded by increased cytsolic [Ca^{2+}] [1-3]. It is remarkable that the mechanistic basis for these changes has not been

fully clarified yet, and it is legitimate to wonder whether the striking analogies with the matching consequences of PTP opening in mammals are just a coincidence, or rather underscore occurrence of a *bona fide* PT as also suggested in a relevant study of yeast spheroblasts [94].

An important advance, linking yeast PCD to the Bcl-2 inhibitable Bax/Bak pathway for OMM permeabilization of mammals, was identification of Ybh3p, a yeast protein possessing a functional Bcl-2 homology domain 3 [95]. Upon treatment with lethal stimuli Ybh3p translocates to mitochondria and triggers apoptosis, which is accompanied by mitochondrial depolarization and release of cytochrome *c* and other proapoptotic proteins in a process that involves the Pi carrier Mir1p and the core subunit of ubiquinol-cytochrome *c* oxidoreductase Cor1p [95]. The mechanism(s) through which Ybh3p translocation causes the mitochondrial changes and intermembrane protein release, and whether the PTP could have been involved, remains unclear particularly because the site of integration of Ybh3p—whether the IMM or the OMM—was not defined. It is interesting, however, that the stimulus used to trigger apoptosis was acetic acid, which causes increased ROS production [6] and may therefore require a functional respiratory chain and thus Cor1p . The requirement for Mir1p, on the other hand, may depend on the Pi-requirement for mitochondrial Ca^{2+} uptake which is stimulated up to 8-fold by Pi [15]. In this respect it is very intriguing that cell death induced by acetic acid was greatly reduced in ρ_0 cells (where no mitochondrial respiration hence ROS production takes place) and in *ATP10* mutants (which cannot assemble the F-ATP synthase) [6]. The latter finding acquires a new meaning in the light of the demonstration that yeast F-ATP synthase forms channels with the features of the yeast PTP when subjected to oxidative stress in the presence of Ca^{2+} [59].

One of the most relevant studies on the involvement of mitochondria in yeast PCD was performed using the pheromone α factor or amiodarone, agents known to induce an increase of cytosolic [Ca^{2+}] and cell death with superimposable features. Cell death occurred by apoptosis and required a functional respiratory chain, as ρ_0 cells were extremely resistant; and was linked to ROS formation, as it could be protected by antioxidants and by low concentrations of the protonophore FCCP [9]. Amiodarone has complex effects on respiration in intact yeast cells, but consistently increased mitochondrial respiration and

ROS production which preceded mitochondral depolarization. The Authors suggest that increased respiration was caused by Ca^{2+}-dependent stimulation of NADH dehydrogenase from the intermembrane space, sequentially causing an increase of membrane potential and of ROS production, followed by IMM permeabilization and cell death [9]. We suspect (i) that ROS-dependent depolarization in this and other paradigms was caused by PTP opening induced by oxidative stress and (ii) that this event could be a final common pathway in a variety of forms of yeast PCD. This hypothesis has so far been hard to test due to the lack of a structure for the PTP and to the insensitivity of the yeast PT to CsA. We have already found that genetic ablation of the e and/or g subunits, whose presence is important for F-ATP synthase dimerization [96], confers at least partial resistance to PTP opening [59]. Identification of the cysteine residues responsible for the sensitizing effects of oxidative stress and the availability of novel, CyP-independent PTP inhibitors [97-99] should soon allow a stringent test of this hypothesis.

6. Summary and conclusions

In spite of the absence of the MCU, yeast mitochondria accumulate enough Ca^{2+} to undergo the PT when cells are challenged by stimuli that cause yeast PCD, which is accompanied by oxidative stress and increased cytosolic [Ca^{2+}]. Once PTP opening occurs, cytosolic and matrix Ca^{2+} equilibrate stabilizing the PTP in the open conformation, which is followed by osmotic swelling of the matrix, OMM damage and release of intermembrane proteins causing cell death. PTP formation by the F-ATP synthase provides a unifying framework for future studies and should allow to assess whether the transition of the energy-conserving complex into an energy-dissipating device plays a role in yeast PCD.

Acknowledgements

This work is in partial fulfillment of the requirements for the PhD of Michela Carraro at the University of Padova. Research in our laboratory is supported by Associazione Italiana Ricerca sul Cancro (AIRC) IG 17067, Italian Ministry for University and Research (MIUR) FIRB RBAP11S8C3 and PRIN

20107Z8XBW, Telethon Italy GGP14037 and GPP14187, and the National Institutes of Health – Public Health Service (USA) R01GM069883.

References

1. C. Pereira, R.D. Silva, L. Saraiva, B. Johansson, M.J. Sousa, M. Côrte-Real, Mitochondria-dependent apoptosis in yeast, Biochim. Biophys. Acta 1783 (2008) 1286-1302.
2. M. Côrte-Real, F. Madeo, Yeast programed cell death and aging, Front. Oncol. 3 (2013) 283.
3. N. Guaragnella, M. Zdralevic, L. Antonacci, S. Passarella, E. Marra, S. Giannattasio, The role of mitochondria in yeast programmed cell death, Front. Oncol. 2 (2012) 70.
4. F. Madeo, E. Fröhlich, M. Ligr, M. Grey, S.J. Sigrist, D.H. Wolf, K.U. Fröhlich, Oxygen stress: a regulator of apoptosis in yeast, J. Cell Biol. 145 (1999) 757-767.
5. P. Ludovico, M.J. Sousa, M.T. Silva, C. Leão, M. Côrte-Real, *Saccharomyces cerevisiae* commits to a programmed cell death process in response to acetic acid, Microbiology 147 (2001) 2409-2415.
6. P. Ludovico, F. Rodrigues, A. Almeida, M.T. Silva, A. Barrientos, M. Côrte-Real, Cytochrome c release and mitochondria involvement in programmed cell death induced by acetic acid in *Saccharomyces cerevisiae*, Mol. Biol. Cell 13 (2002) 2598-2606.
7. P. Ludovico, F. Sansonetty, M.T. Silva, M. Côrte-Real, Acetic acid induces a programmed cell death process in the food spoilage yeast *Zygosaccharomyces bailii*, FEMS Yeast Res. 3 (2003) 91-96.
8. F.F. Severin, A.A. Hyman, Pheromone induces programmed cell death in *S. cerevisiae*, Curr. Biol. 12 (2002) R233-R235.
9. A.I. Pozniakovsky, D.A. Knorre, O.V. Markova, A.A. Hyman, V.P. Skulachev, F.F. Severin, Role of mitochondria in the pheromone- and amiodarone-induced programmed death of yeast, J. Cell Biol. 168 (2005) 257-269.
10. H. Kitagaki, Y. Araki, K. Funato, H. Shimoi, Ethanol-induced death in yeast exhibits features of apoptosis mediated by mitochondrial fission pathway, FEBS Lett. 581 (2007) 2935-2942.

11. G.H. Huh, B. Damsz, T.K. Matsumoto, M.P. Reddy, A.M. Rus, J.I. Ibeas, M.L. Narasimhan, R.A. Bressan, P.M. Hasegawa, Salt causes ion disequilibrium-induced programmed cell death in yeast and plants, Plant J. 29 (2002) 649-659.

12. K. Kajiwara, T. Muneoka, Y. Watanabe, T. Karashima, H. Kitagaki, K. Funato, Perturbation of sphingolipid metabolism induces endoplasmic reticulum stress-mediated mitochondrial apoptosis in budding yeast, Mol. Microbiol. 86 (2012) 1246-1261.

13. E. Carafoli, W.X. Balcavage, A.L. Lehninger, J.R. Mattoon, Ca^{2+} metabolism in yeast cells and mitochondria, Biochim. Biophys. Acta 205 (1970) 18-26.

14. E. Carafoli, A.L. Lehninger, A survey of the interaction of calcium ions with mitochondria from different tissues and species, Biochem. J. 122 (1971) 681-690.

15. W.X. Balcavage, J.L. Lloyd, J.R. Mattoon, T. Ohnishi, A. Scarpa, Cation movements and respiratory response in yeast mitochondria treated with high Ca^{2+} concentrations, Biochim. Biophys. Acta 305 (1973) 41-51.

16. J.M. Baughman, F. Perocchi, H.S. Girgis, M. Plovanich, C.A. Belcher-Timme, Y. Sancak, X.R. Bao, L. Strittmatter, O. Goldberger, R.L. Bogorad, V. Koteliansky, V.K. Mootha, Integrative genomics identifies MCU as an essential component of the mitochondrial calcium uniporter, Nature 476 (2011) 341-345.

17. D. De Stefani, A. Raffaello, E. Teardo, I. Szabó, R. Rizzuto, A forty-kilodalton protein of the inner membrane is the mitochondrial calcium uniporter, Nature 476 (2011) 336-340.

18. P. Bernardi, A. Rasola, M. Forte, G. Lippe, The Mitochondrial Permeability Transition Pore: Channel Formation by F-ATP Synthase, Integration in Signal Transduction, and Role in Pathophysiology, Physiol. Rev. 95 (2015) 1111-1155.

19. K.W. Kinnally, M.L. Campo, H. Tedeschi, Mitochondrial channel activity studied by patch-clamping mitoplasts, J. Bioenerg. Biomembr. 21 (1989) 497-506.

20. V. Petronilli, I. Szabó, M. Zoratti, The inner mitochondrial membrane contains ion-conducting channels similar to those found in bacteria, FEBS Lett. 259 (1989) 137-143.

21. R.A. Haworth, D.R. Hunter, The Ca^{2+}-induced membrane transition in mitochondria. II. Nature of the Ca^{2+} trigger site, Arch. Biochem. Biophys. 195 (1979) 460-467.

22. D.R. Hunter, R.A. Haworth, The Ca^{2+}-induced membrane transition in mitochondria. I. The protective mechanisms, Arch. Biochem. Biophys. 195 (1979) 453-459.

23. M. Crompton, H. Ellinger, A. Costi, Inhibition by cyclosporin A of a Ca^{2+}-dependent pore in heart mitochondria activated by inorganic phosphate and oxidative stress, Biochem. J. 255 (1988) 357-360.

24. K.M. Broekemeier, M.E. Dempsey, D.R. Pfeiffer, Cyclosporin A is a potent inhibitor of the inner membrane permeability transition in liver mitochondria, J. Biol. Chem. 264 (1989) 7826-7830.

25. A.P. Halestrap, A.M. Davidson, Inhibition of Ca^{2+}-induced large-amplitude swelling of liver and heart mitochondria by cyclosporin is probably caused by the inhibitor binding to mitochondrial-matrix peptidyl-prolyl *cis-trans* isomerase and preventing it interacting with the adenine nucleotide translocase, Biochem. J. 268 (1990) 153-160.

26. D.R. Hunter, R.A. Haworth, J.H. Southard, Relationship between configuration, function, and permeability in calcium-treated mitochondria, J. Biol. Chem. 251 (1976) 5069-5077.

27. S. Manon, X. Roucou, M. Guerin, M. Rigoulet, B. Guerin, Characterization of the yeast mitochondria unselective channel: a counterpart to the mammalian permeability transition pore?, J Bioenerg. Biomembr. 30 (1998) 419-429.

28. S. Prieto, F. Bouillaud, D. Ricquier, E. Rial, Activation by ATP of a proton-conducting pathway in yeast mitochondria, Eur. J. Biochem. 208 (1992) 487-491.

29. S. Prieto, F. Bouillaud, E. Rial, The mechanism for the ATP-induced uncoupling of respiration in mitochondria of the yeast *Saccharomyces cerevisiae*, Biochem. J. 307 (Pt 3) (1995) 657-661.

30. S. Prieto, F. Bouillaud, E. Rial, The nature and regulation of the ATP-induced anion permeability in *Saccharomyces cerevisiae* mitochondria, Arch. Biochem. Biophys. 334 (1996) 43-49.

31. S. Manon, M. Guerin, Evidence for three different electrophoretic pathways in yeast mitochondria: ion specificity and inhibitor sensitivity, J. Bioenerg. Biomembr. 25 (1993) 671-678.

32. X. Roucou, S. Manon, M. Guérin, ATP opens an electrophoretic potassium transport pathway in respiring yeast mitochondria, FEBS Lett. 364 (1995) 161-164.

33. X. Roucou, S. Manon, M. Guérin, Conditions allowing different states of ATP- and GDP-induced permeability in mitochondria from different strains of S*accharomyces cerevisiae*, Biochim. Biophys. Acta 1324 (1997) 120-132.

34. G. de Chateaubodeau, M. Guérin, B. Guérin, Studies on anionic transport in yeast mitochondria and promitochondria. Swelling in ammonium phosphate, glutamate, succinate and fumarate solutions, FEBS Lett. 46 (1974) 184-187.

35. B. Guérin, O. Bunoust, V. Rouqueys, M. Rigoulet, ATP-induced unspecific channel in yeast mitochondria, J. Biol. Chem. 269 (1994) 25406-25410.

36. V. Perez-Vazquez, A. Saavedra-Molina, S. Uribe, In *Saccharomyces cerevisiae*, cations control the fate of the energy derived from oxidative metabolism through the opening and closing of the yeast mitochondrial unselective channel, J. Bioenerg. Biomembr. 35 (2003) 231-241.

37. M. Gutierrez-Aguilar, V. Perez-Vazquez, O. Bunoust, S. Manon, M. Rigoulet, S. Uribe, In yeast, Ca^{2+} and octylguanidine interact with porin (VDAC) preventing the mitochondrial permeability transition, Biochim. Biophys. Acta 1767 (2007) 1245-1251.

38. M. Gutierrez-Aguilar, X. Perez-Martinez, E. Chavez, S. Uribe-Carvajal, In *Saccharomyces cerevisiae*, the phosphate carrier is a component of the mitochondrial unselective channel, Arch. Biochem. Biophys. 494 (2010) 184-191.

39. S. Uribe-Carvajal, L.A. Luévano-Martìnez, S. Guerrero-Castillo, A. Cabrera-Orefice, N.A. Corona-de-la-Peña, M. Gutiérrez-Aguilar, Mitochondrial Unselective Channels throughout the eukaryotic domain, Mitochondrion 11 (2011) 382-390.

40. D.W. Jung, P.C. Bradshaw, D.R. Pfeiffer, Properties of a cyclosporin-insensitive permeability transition pore in yeast mitochondria, J. Biol. Chem. 272 (1997) 21104-21112.

41. S. Manon, Dependence of yeast mitochondrial unselective channel activity on the respiratory chain, Biochimica et Biophysica Acta (BBA) - Bioenergetics 1410 (1999) 85-90.

42. M.V. Kovaleva, E.I. Sukhanova, T.A. Trendeleva, M.V. Zyl'kova, L.A. Ural'skaya, K.M. Popova, N.E. Saris, R.A. Zvyagilskaya, Induction of a non-specific permeability transition in mitochondria from *Yarrowia lipolytica* and *Dipodascus* (*Endomyces*) *magnusii* yeasts, J. Bioenerg. Biomembr. 41 (2009) 239-249.

43. P. Bradshaw, D.R. Pfeiffer, Characterization of the respiration-induced yeast mitochondrial permeability transition pore, Yeast 30 (2013) 471-483.

44. M. Tropschug, I.B. Barthelmess, W. Neupert, Sensitivity to cyclosporin A is mediated by cyclophilin in *Neurospora crassa* and *Saccharomyces cerevisiae*, Nature 342 (1989) 953-955.

45. J. Rassow, K. Mohrs, S. Koidl, I.B. Barthelmess, N. Pfanner, M. Tropschug, Cyclophilin 20 is involved in mitochondrial protein folding in cooperation with molecular chaperones Hsp70 and Hsp60, Mol. Cell Biol. 15 (1995) 2654-2662.

46. J. Velours, M. Rigoulet, B. Guerin, Protection of yeast mitochondrial structure by phosphate and other H^+-donating anions, FEBS Lett. 81 (1977) 18-22.

47. J.E. Kokoszka, K.G. Waymire, S.E. Levy, J.E. Sligh, J. Cai, D.P. Jones, G.R. MacGregor, D.C. Wallace, The ADP/ATP translocator is not essential for the mitochondrial permeability transition pore, Nature 427 (2004) 461-465.

48. A. Krauskopf, O. Eriksson, W.J. Craigen, M.A. Forte, P. Bernardi, Properties of the permeability transition in *VDAC1*$^{-/-}$ mitochondria, Biochim. Biophys. Acta 1757 (2006) 590-595.

49. C.P. Baines, R.A. Kaiser, T. Sheiko, W.J. Craigen, J.D. Molkentin, Voltage-dependent anion channels are dispensable for mitochondrial-dependent cell death, Nat. Cell Biol. 9 (2007) 550-555.

50. A. Yamada, T. Yamamoto, Y. Yoshimura, S. Gouda, S. Kawashima, N. Yamazaki, K. Yamashita, M. Kataoka, T. Nagata, H. Terada, D.R. Pfeiffer, Y. Shinohara, Ca^{2+}-induced permeability transition can be observed even in yeast mitochondria under optimized experimental conditions, Biochim. Biophys. Acta 1787 (2009) 1486-1491.

51. C.P. Baines, R.A. Kaiser, N.H. Purcell, N.S. Blair, H. Osinska, M.A. Hambleton, E.W. Brunskill, M.R. Sayen, R.A. Gottlieb, G.W. Dorn, J. Robbins, J.D. Molkentin, Loss of cyclophilin D reveals a critical role for mitochondrial permeability transition in cell death, Nature 434 (2005) 658-662.

52. E. Basso, L. Fante, J. Fowlkes, V. Petronilli, M.A. Forte, P. Bernardi, Properties of the permeability transition pore in mitochondria devoid of cyclophilin D, J. Biol. Chem. 280 (2005) 18558-18561.

53. T. Nakagawa, S. Shimizu, T. Watanabe, O. Yamaguchi, K. Otsu, H. Yamagata, H. Inohara, T. Kubo, Y. Tsujimoto, Cyclophilin D-dependent mitochondrial permeability transition regulates some necrotic but not apoptotic cell death, Nature 434 (2005) 652-658.

54. A.C. Schinzel, O. Takeuchi, Z. Huang, J.K. Fisher, Z. Zhou, J. Rubens, C. Hetz, N.N. Danial, M.A. Moskowitz, S.J. Korsmeyer, Cyclophilin D is a component of mitochondrial permeability transition and mediates neuronal cell death after focal cerebral ischemia, Proc. Natl. Acad. Sci. U. S. A. 102 (2005) 12005-12010.

55. U. De Marchi, E. Basso, I. Szabó, M. Zoratti, Electrophysiological characterization of the Cyclophilin D-deleted mitochondrial permeability transition pore, Mol. Membr. Biol. 23 (2006) 521-530.

56. B. Li, C. Chauvin, D. De Paulis, F. De Oliveira, A. Gharib, G. Vial, S. Lablanche, X. Leverve, P. Bernardi, M. Ovize, E. Fontaine, Inhibition of complex I regulates the mitochondrial permeability transition through a phosphate-sensitive inhibitory site masked by cyclophilin D, Biochim. Biophys. Acta 1817 (2012) 1628-1634.

57. V. Giorgio, S. von Stockum, M. Antoniel, A. Fabbro, F. Fogolari, M. Forte, G.D. Glick, V. Petronilli, M. Zoratti, I. Szabó, G. Lippe, P. Bernardi, Dimers of mitochondrial ATP synthase form the permeability transition pore, Proc. Natl. Acad. Sci. U. S. A. 110 (2013) 5887-5892.

58. K.N. Alavian, G. Beutner, E. Lazrove, S. Sacchetti, H.A. Park, P. Licznerski, H. Li, P. Nabili, K. Hockensmith, M. Graham, G.A. Porter, Jr., E.A. Jonas, An uncoupling channel within the c-subunit ring of the F_1F_O ATP synthase is the mitochondrial permeability transition pore, Proc. Natl. Acad. Sci. U. S. A. 111 (2014) 10580-10585.

59. M. Carraro, V. Giorgio, J. Šileikyte, G. Sartori, M. Forte, G. Lippe, M. Zoratti, I. Szabó, P. Bernardi, Channel Formation by Yeast F-ATP Synthase and the Role of Dimerization in the Mitochondrial Permeability Transition, J. Biol. Chem. 289 (2014) 15980-15985.

60. S. von Stockum, V. Giorgio, E. Trevisan, G. Lippe, G.D. Glick, M.A. Forte, C. Da-Rè, V. Checchetto, G. Mazzotta, R. Costa, I. Szabò, P. Bernardi, F-ATPase of *D. melanogaster* Forms 53 Picosiemen (53-pS) Channels Responsible for Mitochondrial Ca^{2+}-induced Ca^{2+} Release, J. Biol. Chem. 290 (2015) 4537-4544.

61. S. Massari, G.F. Azzone, The equivalent pore radius of intact and damaged mitochondria and the mechanism of active shrinkage, Biochim. Biophys. Acta 283 (1972) 23-29.

62. D.R. Hunter, R.A. Haworth, The Ca^{2+}-induced membrane transition in mitochondria. III. Transitional Ca^{2+} release, Arch. Biochem. Biophys. 195 (1979) 468-477.

63. S. von Stockum, E. Basso, V. Petronilli, P. Sabatelli, M.A. Forte, P. Bernardi, Properties of Ca^{2+} Transport in Mitochondria of *Drosophila melanogaster*, J. Biol. Chem. 286 (2011) 41163-41170.

64. M.C. Beatrice, D.L. Stiers, D.R. Pfeiffer, The role of glutathione in the retention of Ca^{2+} by liver mitochondria, J. Biol. Chem. 259 (1984) 1279-1287.

65. P. Costantini, B.V. Chernyak, V. Petronilli, P. Bernardi, Modulation of the mitochondrial permeability transition pore by pyridine nucleotides and dithiol oxidation at two separate sites, J. Biol. Chem. 271 (1996) 6746-6751.

66. F. Zoccarato, D.G. Nicholls, The role of phosphate in the regulation of the independent calcium-efflux pathway of liver mitochondria, Eur. J. Biochem. 127 (1982) 333-338.

67. V. Giorgio, E. Bisetto, M.E. Soriano, F. Dabbeni-Sala, E. Basso, V. Petronilli, M.A. Forte, P. Bernardi, G. Lippe, Cyclophilin D modulates mitochondrial F_0F_1-ATP synthase by interacting with the lateral stalk of the complex, J. Biol. Chem. 284 (2009) 33982-33988.

68. A. Nicolli, E. Basso, V. Petronilli, R.M. Wenger, P. Bernardi, Interactions of cyclophilin with the mitochondrial inner membrane and regulation of the permeability transition pore, a cyclosporin A-sensitive channel, J. Biol. Chem. 271 (1996) 2185-2192.

69. E. Basso, V. Petronilli, M.A. Forte, P. Bernardi, Phosphate is essential for inhibition of the mitochondrial permeability transition pore by cyclosporin A and by cyclophilin D ablation, J. Biol. Chem. 283 (2008) 26307-26311.

70. P. Wang, J. Heitman, The cyclophilins, Genome Biol. 6 (2005) 226.1-226.6.

71. T.J. Pemberton, J.E. Kay, Identification and Comparative Analysis of the Peptidyl-Prolyl *cis/trans* Isomerase Repertoires of *H. sapiens, D. melanogaster, C. elegans, S. cerevisiae* and *Sz. pombe*, Comp. Funct. Genomics 6 (2005) 277-300.

72. K.W. Cunningham, G.R. Fink, Ca^{2+} transport in *Saccharomyces cerevisiae*, J. Exp. Biol. 196 (1994) 157-166.

73. J. Cui, J.A. Kaandorp, O.O. Ositelu, V. Beaudry, A. Knight, Y.F. Nanfack, K.W. Cunningham, Simulating calcium influx and free calcium concentrations in yeast, Cell Calcium 45 (2009) 123-132.

74. M.S. Cyert, C.C. Philpott, Regulation of cation balance in *Saccharomyces cerevisiae*, Genetics 193 (2013) 677-713.

75. H. Iida, H. Nakamura, T. Ono, M.S. Okumura, Y. Anraku, MID1, a novel *Saccharomyces cerevisiae* gene encoding a plasma membrane protein, is required for Ca^{2+} influx and mating, Mol. Cell Biol. 14 (1994) 8259-8271.

76. R. Serrano, A. Ruiz, D. Bernal, J.R. Chambers, J. Arino, The transcriptional response to alkaline pH in *Saccharomyces cerevisiae*: evidence for calcium-mediated signalling, Mol. Microbiol. 46 (2002) 1319-1333.

77. A.F. Batiza, T. Schulz, P.H. Masson, Yeast respond to hypotonic shock with a calcium pulse, J. Biol. Chem. 271 (1996) 23357-23362.

78. M. Fischer, N. Schnell, J. Chattaway, P. Davies, G. Dixon, D. Sanders, The *Saccharomyces cerevisiae* CCH1 gene is involved in calcium influx and mating, FEBS Lett. 419 (1997) 259-262.

79. M. Bonilla, K.K. Nastase, K.W. Cunningham, Essential role of calcineurin in response to endoplasmic reticulum stress, EMBO J. 21 (2002) 2343-2353.

80. K.W. Cunningham, G.R. Fink, Calcineurin-dependent growth control in *Saccharomyces cerevisiae* mutants lacking PMC1, a homolog of plasma membrane Ca^{2+} ATPases, J Cell Biol 124 (1994) 351-363.

81. J.L. Withee, J. Mulholland, R. Jeng, M.S. Cyert, An essential role of the yeast pheromone-induced Ca^{2+} signal is to activate calcineurin, Mol. Biol. Cell 8 (1997) 263-277.

82. A. Miseta, R. Kellermayer, D.P. Aiello, L. Fu, D.M. Bedwell, The vacuolar Ca^{2+}/H^{+} exchanger Vcx1p/Hum1p tightly controls cytosolic Ca^{2+} levels in *S. cerevisiae*, FEBS Lett. 451 (1999) 132-136.

83. P. D'hooge, C. Coun, V. Van Eyck, L. Faes, R. Ghillebert, L. Mariaën, J. Winderickx, G. Callewaert, Ca^{2+} homeostasis in the budding yeast *Saccharomyces cerevisiae*: Impact of ER/Golgi Ca^{2+} storage, Cell Calcium 58 (2015) 226-235.

84. R. Rizzuto, D. De Stefani, A. Raffaello, C. Mammucari, Mitochondria as sensors and regulators of calcium signalling, Nat. Rev. Mol. Cell Biol. 13 (2012) 566-578.

85. L. Mela, Inhibition and activation of calcium transport in mitochondria. Effect of lanthanides and local anesthetic drugs, Biochemistry 8 (1969) 2481-2486.

86. F.D. Vasington, P. Gazzotti, R. Tiozzo, E. Carafoli, The effect of ruthenium red on Ca^{2+} transport and respiration in rat liver mitochondria, Biochim. Biophys. Acta 256 (1972) 43-54.

87. D. De Stefani, M. Patron, R. Rizzuto, Structure and function of the mitochondrial calcium uniporter complex, Biochim. Biophys. Acta 1853 (2015) 2006-2011.

88. P. Bernardi, S. von Stockum, The permeability transition pore as a Ca^{2+} release channel: New answers to an old question, Cell Calcium 52 (2012) 22-27.

89. S. Uribe, P. Rangel, J.P. Pardo, Interactions of calcium with yeast mitochondria, Cell Calcium 13 (1992) 211-217.

90. P.C. Bradshaw, D.W. Jung, D.R. Pfeiffer, Free fatty acids activate a vigorous Ca^{2+}:$2H^{+}$ antiport activity in yeast mitochondria, J. Biol. Chem. 276 (2001) 40502-40509.

91. T.V. Votyakova, E.N. Bazhenova, R.A. Zvjagilskaya, Yeast mitochondrial calcium uptake: regulation by polyamines and magnesium ions, J. Bioenerg. Biomembr. 25 (1993) 569-574.

92. E.N. Bazhenova, Y.I. Deryabina, O. Eriksson, R.A. Zvyagilskaya, N.E. Saris, Characterization of a high capacity calcium transport system in mitochondria of the yeast *Endomyces magnusii*, J Biol Chem. 273 (1998) 4372-4377.

93. E.N. Bazhenova, N.E. Saris, R.A. Zvyagilskaya, Stimulation of the yeast mitochondrial calcium uniporter by hypotonicity and by ruthenium red, Biochim. Biophys. Acta 1371 (1998) 96-100.

94. A.J. Kowaltowski, A.E. Vercesi, S.G. Rhee, L.E. Netto, Catalases and thioredoxin peroxidase protect *Saccharomyces cerevisiae* against Ca^{2+}-induced mitochondrial membrane permeabilization and cell death, FEBS Lett. 473 (2000) 177-182.

95. S. Büttner, D. Ruli, F.N. Vögtle, L. Galluzzi, B. Moitzi, T. Eisenberg, O. Kepp, L. Habernig, D. Carmona-Gutierrez, P. Rockenfeller, P. Laun, M. Breitenbach, C. Khoury, K.U. Fröhlich, G. Rechberger, C. Meisinger, G. Kroemer, F. Madeo, A yeast BH3-only protein mediates the mitochondrial pathway of apoptosis, EMBO J. 30 (2011) 2779-2792.

96. I. Arnold, K. Pfeiffer, W. Neupert, R.A. Stuart, H. Schägger, Yeast mitochondrial F_1F_0-ATP synthase exists as a dimer: identification of three dimer-specific subunits, EMBO J. 17 (1998) 7170-7178.

97. D. Fancelli, A. Abate, R. Amici, P. Bernardi, M. Ballarini, A. Cappa, G. Carenzi, A. Colombo, C. Contursi, F. Di Lisa, G. Dondio, S. Gagliardi, E. Milanesi, S. Minucci, G. Pain, P.G. Pelicci, A. Saccani, M. Storto, F. Thaler, M. Varasi, M. Villa, S. Plyte, Cinnamic Anilides as New Mitochondrial Permeability Transition Pore Inhibitors Endowed with Ischemia-Reperfusion Injury Protective Effect in Vivo, J. Med. Chem. 57 (2014) 5333-5347.

98. S. Roy, J. Šileikyte, M. Schiavone, B. Neuenswander, F. Argenton, J. Aubé, M.P. Hedrick, T.D.Y. Chung, M.A. Forte, P. Bernardi, F.J. Schoenen, Discovery, Synthesis, and Optimization of Diarylisoxazole-3-carboxamides as Potent Inhibitors of the Mitochondrial Permeability Transition Pore, ChemMedChem 10 (2015) 1655-1671.

99. S. Roy, Šileikyte, B. Neuenswander, M.P. Hedrick, T.D. Chung, J. Aubé, F.J. Schoenen, M.A. Forte, P. Bernardi, N-Phenylbenzamides as Potent Inhibitors of the Mitochondrial Permeability Transition Pore, ChemMedChem. in press (2015) .

***Graphical Abstract**